STUDY OF ANISOTROPIC FLOW AND ROTATIONAL DYNAMICS AT INTERMEDIATE ENERGIES

A THESIS

submitted to the

THAPAR INSTITUTE OF ENGINEERING AND TECHNOLOGY, PATIALA

for the degree of

DOCTOR OF PHILOSOPHY

IN THE FACULTY OF SCIENCE

By

Kamaldeep Kaur

Regn. No. 951312003

THAPAR INSTITUTE
OF ENGINEERING & TECHNOLOGY
(Deemed to be University)

SCHOOL OF PHYSICS AND MATERIALS SCIENCE

THAPAR INSTITUTE OF ENGINEERING AND TECHNOLOGY, PATIALA

PATIALA-147004, PUNJAB (INDIA)

JUNE 2019

Dedicated to

My Beloved Parents

THAPAR INSTITUTE
OF ENGINEERING & TECHNOLOGY
(Deemed to be University)

THAPAR INSTITUTE OF ENGINEERING AND TECHNOLOGY, PATIALA

CANDIDATE'S DECLARATION

I hereby certify that the work which is being presented in this thesis entitled "**STUDY OF ANISOTROPIC FLOW AND ROTATIONAL DYNAMICS AT INTERMEDIATE ENERGIES**" is partial fulfillment of the requirements for the award of degree of Doctor of Philosophy and submitted in the School of Physics and Materials Science, Thapar Institute of Engineering and Technology, Patiala, is an authentic record of my own work carried out during a period from July 2013 to June 2018 under the supervision of **Dr. Suneel Kumar**, Associate Professor, Department of Physics, Central University of Haryana, Jant-Pali Mahendergarh, Haryana (India). The matter presented in this thesis has not been submitted by me in part or full for the award of any other degree in any other university or institute.

(Kamaldeep Kaur)
(Roll No. 951312003)

This is to certify that the above statement made by the candidate is correct to the best of our knowledge.

Supervisor
S Kumar
26/6/2019
(Dr. Suneel Kumar)
Associate Professor
Department of Physics
Central University of Haryana
Jant-Pali Mahendergarh, Haryana (India)

Acknowledgements

In the first place, I am grateful to God, for providing me this opportunity and granting me the capability to proceed successfully. My dream turns into reality because of the never ending blessings of God, who always guide and light my way in my study. The thesis appears in its current form due to the assistance and guidance of several people. I would like to thank everyone who directly or indirectly helped me in making this goal achievable and will always remain deeply beholden to them.

Firstly, from the core of my heart, I would like to thank my esteemed supervisor Dr. Suneel Kumar, Associate Professor, Department of Physics, Central University of Haryana, Mahendergarh, Haryana (India), for grooming me as a Ph.D. student, dynamic guidance, consistent support, valuable and innovative suggestions. I am truly grateful to him for his support and invaluable supervision.

I would like to express my sincere gratitude to Prof. Prakash Gopalan, Director, Thapar Institute of Engineering and Technology and Shri Gurbinder Singh, Registrar, Thapar Institute of Engineering and Technology, Patiala for their help and moral support. Thanks to Prof. Rafat Siddique, Dean, Research and sponsored projects for providing best possible facilities.

I am also thankful to Dr. O. P. Pandey, Professor and Head, School of Physics and Materials Science, Thapar Institute of Engineering and Technology, Patiala for encouraging me to accomplish this task, providing the possible research facilities and all the necessary facilities in the department.

I extend my sincere thanks to Prof. Kulbir Singh, for motivating me to pursue Ph.D and for consistent moral support. I would also like to acknowledge the valuable suggestions of the members of the doctoral committee, Dr. Manoj K. Sharma, Dr. Alka Upadhyay and Dr. A. K. Lal. My sincere thanks also goes to all the faculty and staff of the SPMS for their kind support and motivation. Centre of Information and Technology Management (CITM) has also been helpful for providing the super-computing facility.

I highly appreciate my lab mates Dr. Mandeep Kaur, Amandeep, Sangeeta, Rubina and Jagroop and many other research scholars from Thapar Institute of Engineering and Technology, for their pleasant company and for making this experience an enjoyable

and memorable one.

I acknowledge with thanks the co-operation and encouragement extended by Dr. R. K. Puri, Professor, Panjab University, Chandigarh for his fruitful discussions and novel views.

This institute have blessed me with a bunch of wonderful lifelong friends. On a more personal note, I would like to express gratitude to my dearest friends Dr. Gurvinder Kaur, Ms. Navjot Kaur and Dr. Kirandeep Sandhu. They have been my source of positivity in every situation throughout this journey and made my time here more enjoyable. This journey of Ph.D. will be incomplete without mentioning you both Shoaib and Neeraj, who met me by chance, but have taught me the beautiful lessons of true friendship. I will always miss those enchanting and refreshing hours of long lunch and evening tea breaks. Thank you for being with me and inspire me in the most stressful and frustrating time of my Ph.D.

Special note of thanks to my wonderful friend Dr. Deepshikha Moudgill for always supporting me in my hardest times. She took every responsibility during the final period of my Ph.D. and make every positive effort to accomplish it. I always owe to you for help, support and guidance.

I really have no words to express my gratitude towards my parents (Sh. Gulzar Singh and Smt. Kuldeep Kaur). Everything that I have achieved till date and what I am today is because of your unconditional love, strongest support and encouragement. I am indebted to my parents for their time, efforts and sacrifices. They have been eagerly waiting for the completion of this stage, with a mixed feeling of hope and anxiety. By completing this doctorate degree, I have fulfill my papa's dream. Thank you papa for strong belief in me and giving me a chance to prove myself. I am glad that I could live up to your dreams and make you proud of me. This work is dedicated to you for your love and trust in me.

I am lucky enough to have always blessed by my guardian angels, my nanaji and naniji (Late S. Sadhu Singh and Late Sdn. Mohinder Kaur). Although, you both are not with me today, but I know that you are always showering your love and blessing on me and happy to see me succeeded.

Lastly, I want to thank two most important persons of my life, my younger siblings and my best friends (Mr. Paramdeep Singh and Ms. Ravneet Kaur). I am grateful to god for blessing me with world's best brother and sister. You both are my strength and pillars of my life. I owe so much to both of you for filling my life with unconditional love, happiness and laughter. The stress of the frustrating hours of my doctorate degree got relieved after spending time with you in the evening. Thank you again for always supporting and guiding me in every difficult situation.

The regular financial assistance from teaching associateship from Thapar Institute of Engineering and Technology is gratefully acknowledged. I have learned many new insights of applied physics and gained good teaching experience from this T.A. ship that will be helpful for me in future.

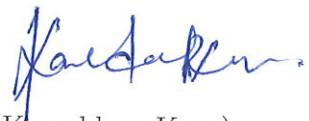

Patiala
June, 2019

(Kamaldeep Kaur)
(Roll No. 951312003)

List of Publications :

A. Journals :

1. On the rapidity distribution of nucleons participating in elliptical flow at intermediate energies.
   Kamaldeep Kaur and Suneel Kumar,
   Mod. Phys. Lett. A **32**, 1750001 (2017).
   DOI:10.1142/S0217732317500018 [Impact factor=1.338].

2. On the study of rotational effects in mass asymmetric colliding nuclei at intermediate energies.
   Kamaldeep Kaur and Suneel Kumar,
   Nuclear Physics A **973**, 149 (2018).
   DOI:10.1016/j.nuclphysa.2018.03.003 [Impact factor=1.916].

3. On scaling of nuclear flow in mass asymmetric heavy ion reactions.
   Kamaldeep Kaur and Suneel Kumar,
   Nuclear Physics A **980**, 91 (2018).
   DOI:10.1016/j.nuclphysa.2018.10.026 [Impact factor=1.916].

B. Symposia/Workshops/Conferences:

4. Maxima in the production of fragments and their flow at certain geometry and energy.
   Kamaldeep Kaur
   Proc. of National Conference on Emerging Challenges in Nuclear and Many-body Physics, P-24, Page no. 30 (2014).

5. Effect of isospin degree of freedom on the distribution of nucleons in elliptical flow.
   Kamaldeep Kaur and Suneel Kumar,
   Proceedings of the DAE Symp. on Nucl. Phys. 59, 430 (2014).

6. Effect of isospin-dependent spatial and momentum constraints on flow.
   Kamaldeep Kaur, Mandeep Kaur and Suneel Kumar,
   Zakopane Conference on Nuclear Physics, p.193 Sep. (2014).

7. Phase space analysis of nuclear stopping due to fragments.
   Mandeep Kaur, Kamaldeep Kaur and Suneel Kumar,
   Proceedings of the DAE Symp. on Nucl. Phys. **59**, 444 (2014).

8. Effect of rapidity range on the scaling of transverse flow in asymmetric collisions.
   Kamaldeep Kaur and Suneel Kumar,
   Proceedings of the DAE Symp. on Nucl. Phys.**62**, 518 (2017).

9. On the study of angular velocity in mass asymmetry nuclei.
   Kamaldeep Kaur and Suneel Kumar,
   AIP Conference Proceedings **1953**, 140031 (2018).
   DOI:10.1063/1.5033206.

10. Investigation of nuclear stopping with system size at intermediate energies.
    Kamaldeep Kaur and Suneel Kumar,
    Proceedings of the DAE Symp. on Nucl. Phys.**63**, 704 (2018).

11. Effect of rotational flow on transition energy in mass asymmetric nuclear reactions.
    Kamaldeep Kaur and Suneel Kumar,
    AIP Conference Proceedings **2050**, 020013 (2018).
    DOI:10.1063/1.5083600.

Contents

ABSTRACT

The present study provides a deep insight on the different aspects of anisotropic flow and rotational dynamics of heavy ion reactions.

Initially, the general introduction of the nuclear physics has been discussed. In this thesis, the importance of isospin and rapidity in collective flow, scaling of flow of fragments and rotational features of heavy ion reactions at the intermediate energies region have been described extensively. The theoretical and experimental attempts on the anisotropic flow, scaling of different component of flow and rotational dynamics have also been discussed.

A brief survey of various primary models based on isospin degree of freedom explicitly in the literature has also been summarised to study the different aspects of heavy-ion collisions. The model which is used to carry out the present study i.e., Isospin-dependent Quantum Molecular Dynamics model (IQMD) model has been explained in detail. Also, the secondary models such as Minimum Spanning Tree (MST) and its updated versions MSTP have also been discussed.

Furthermore, the yield of nucleons participating in elliptic flow has been studied for the reactions of ${}^{197}_{79}Au + {}^{197}_{79}Au$, ${}^{150}_{60}Nd + {}^{150}_{60}Nd$, ${}^{124}_{50}Sn + {}^{124}_{50}Sn$, ${}^{96}_{44}Ru + {}^{96}_{44}Ru$, ${}^{78}_{36}Kr + {}^{78}_{36}Kr$, ${}^{48}_{20}Ca + {}^{48}_{20}Ca$ and ${}^{40}_{20}Ca + {}^{40}_{20}Ca$ for various impact parameter ranges over the intermediate energy region. It has been found that the peak of yield of nucleons/protons as a function of rapidity decreases with decrease in the mass of colliding nuclei. First and second both transition energies depend on the mass of the fragment. Rotational phenomenon of nucleons can be observed for nucleons participating in elliptic flow.

The rotational dynamics has been studied for different mass asymmetric systems ${}^{122}_{49}In + {}^{126}_{50}Sn$, ${}^{114}_{48}Cs + {}^{134}_{54}In$, ${}^{100}_{40}Mo + {}^{148}_{64}Gd$, ${}^{86}_{36}Kr + {}^{162}_{67}Ho$, ${}^{71}_{31}Ga + {}^{177}_{71}Lu$, ${}^{60}_{28}Ni + {}^{188}_{76}Os$ and ${}^{50}_{24}Cr + {}^{198}_{78}Pt$ for incident energies ranging between 40 MeV/nucleon and 400 MeV/nucleon for impact parameter range $0.25 < \hat{b} < 0.45$. Our calculations reveal that the time evolutions of rotational quantities for participant and spectator nuclear matter are different in mass asymmetric heavy ion reactions. Theoretical data of BUU

model's azimuthal distributions for free protons have been compared successfully with IQMD model calculations. The rotational flow of free protons with increasing incident energies has been observed. Elliptic flow (calculated from the fits of azimuthal distributions of free protons) dependence with energy has also been investigated.

In addition to this, scaling of anisotropic flow of fragments has been studied in mass asymmetric nuclear reactions ${}^{122}_{49}In+{}^{126}_{50}Sn$, ${}^{114}_{48}Cs+{}^{134}_{54}In$, ${}^{100}_{40}Mo+{}^{148}_{64}Gd$, ${}^{86}_{36}Kr+{}^{162}_{67}Ho$, ${}^{71}_{31}Ga+{}^{177}_{71}Lu$, ${}^{60}_{28}Ni+{}^{188}_{76}Os$, ${}^{50}_{24}Cr+{}^{198}_{78}Pt$ and ${}^{40}_{20}Ca+{}^{208}_{82}Pb$ for incident energies ranging between 50 MeV/nucleon and 400 MeV/nucleon for the range of impact parameter $0.25 < \hat{b} < 0.45$. Our findings have revealed that strength of flow depends on the fragment mass and mass asymmetry content of the reaction for a rapidity range. Rapidity constraints play a dominant role in the calculation of scaling of flow of fragments.

Lastly, the results of the thesis have been summarised along with the prospect for the extension of present work.

Chapter 1

Introduction

" Measure what is measurable, and make measurable what is not so"..... Galileo Galilei

1.1 Introduction

The onset of nuclear physics was followed by the invention of radioactivity in 1896 by Becquerel [1]. The occupancy of the nucleus in the core as the smallest fundamental part of an atom was first put forward by Rutherford in 1911 [2,3]. The nuclear science regards itself with the nuclear matter properties (comprised of the massive cores of the atoms and molecules) which accounts for the remarkable percentage of the universe. Nuclear matter exists basically within the nucleus i.e., protons and neutrons (which

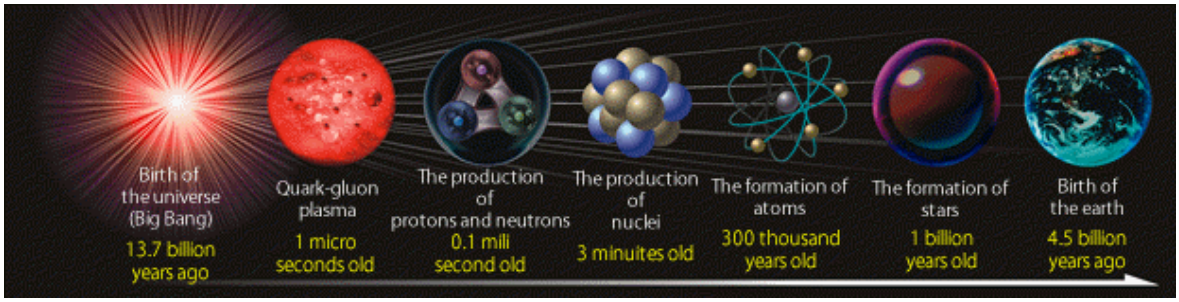

Figure 1.1: An illustration of time-scale from big-bang explosion evolution of earth [4].

play a dominant role in the nucleus formation), in neutron stars and in the matter that emerge from the Big Bang (shown in Fig. 1.1). Nuclear physicists have closely

examined the properties and structure of different phases of nuclear matter [5]. From the quarks and gluons which were present at the time of birth of any celestial body to the diverse ongoing nuclear reactions within the Sun which helps in operating different life cycles on earth.

Scientists have successfully established the understanding of the branch of nuclear physics to the nano-scopical scales. These scales are ordered in distinct levels which further develops their own subdisciplines like atom formation by primal nucleo-synthesis, condensation of galactic matter, cosmos nucleo-synthesis and solar system evolution etc. All these subdisciplines are closely related to each other as the galaxies are formed due to the density fluctuations in the early universe [6]. The shapes of the galaxies formed are determined by their initial mass and rotational speeds of proto-galaxies (cloud of gas). Slowly rotating proto-galaxies form spherical/elliptical galaxies, whereas highly rotating proto-galaxies took the shape of spiral galaxy like Milky-Way [6].

The basic questions that challenges today's nuclear physics has definitely led this field to extend its horizons. Nuclear physics has made its contribution in the invention of particle accelerator. The most predominant application of particle accelerators are the radiotherapy machines in hospitals for treatment of cancer.

In addition to this, the unpopular applications of nuclear physics in geographical sciences helped us to understand the Earth's ancient temperature by studying the ratio of oxygen isotopes in the ice cores from Antarctic and Greenland. This isotope tracking provides a deep insight in the flow of ocean currents and the geological evolution of earth as well as the happenings in the stellar systems [7].

Next sections will give an overview of heavy-ion reactions carried out at intermediate energies and associated phenomenon.

1.2 Heavy-Ion Collisions

The nuclear reactions involving collision of two nuclei having mass greater than ${}^{4}_{2}He$ (α particle) are known as heavy ion collisions. These collisions may be central, where these two ions collides at zero impact parameter or away from center (at non-zero impact parameter). The impact parameter and the beam direction constitutes the reaction

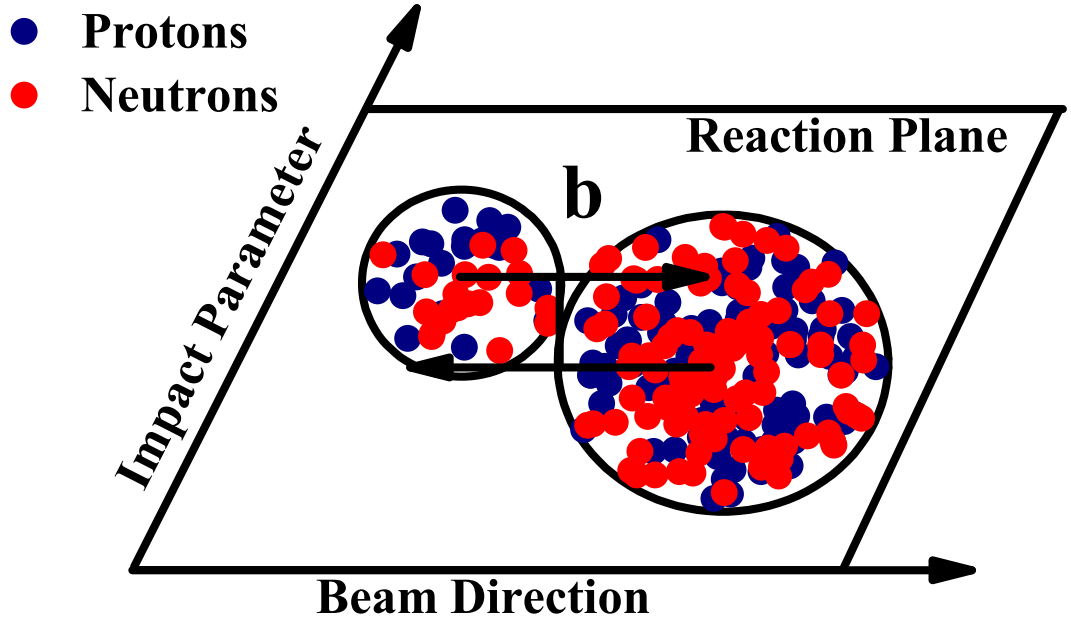

Figure 1.2: Representation of the reaction-plane for mass-asymmetric nuclear reaction.

plane shown in Fig. 1.2. In this Fig., a mass asymmetric nuclear reaction has been shown. Mass asymmetry of any reaction can be calculated by $\eta = \frac{A_T - A_P}{A_T + A_P}$, A_T and A_P are, respectively, the target and the projectile's masses [8]. Fig. 1.3 shows the different mass asymmetric reactions before the collision.

In heavy ion reaction, both ions initially approach each other then collides or just pass without any interaction. This process is controlled by the incident energy, sizes of colliding partners (mass asymmetry of the reaction) and impact parameter. At low incident energies (E $\leq$ 10 MeV/nucleon), heavy-ion reactions give the possibility to examine the different forms of nuclear potentials that have been used to understand the structure and stability of the nucleus, elastic and inelastic collisions, fusion-fission reactions, synthesis of heavy/superheavy elements, incomplete fusion and quasi fission

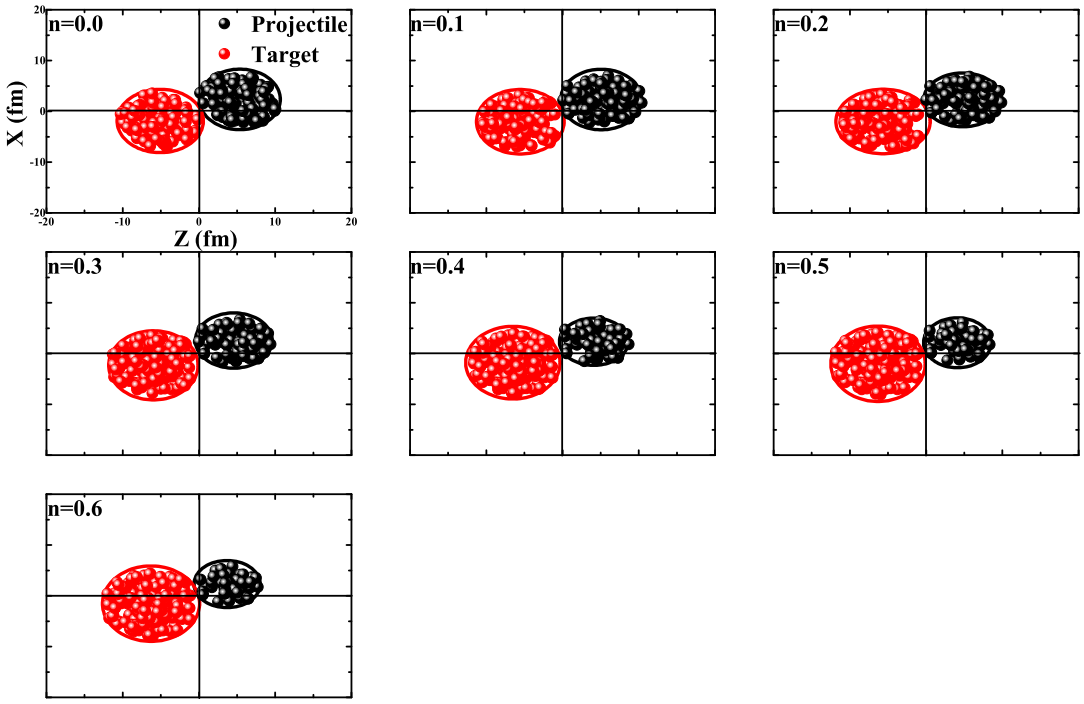

Figure 1.3: Representation of co-ordinate-space of projectile and target for nuclear reactions having different mass asymmetry.

etc [9–14].

However, the high incident energies (E > 2 GeV/nucleon) or relativistic heavy-ion collisions have very frequent and violent nucleon-nucleon collisions. These collisions are sufficient to break the nucleon's internal structure. This branch of nuclear physics mainly focus on the de-confinement of quark-gluon plasma and related phenomenon [15–18]. At relativistic energies, the colliding nuclei appears to be in disks form rather than spherical shapes due to length contraction. To understand the nuclear reactions that includes both nucleon-nucleon collisions and mean-field, the branch of nuclear physics at intermediate energies having energy range between 10 MeV/nucleon <E $\leq$ 2 GeV/nucleon is somehow useful [19].

This branch is mainly used to obtain crucial information regarding the nuclear matter under extreme conditions of temperature and pressure [20,21]. Here, the nuclear density is 2-3 times the normal nuclear matter density and involves several phenomenon like

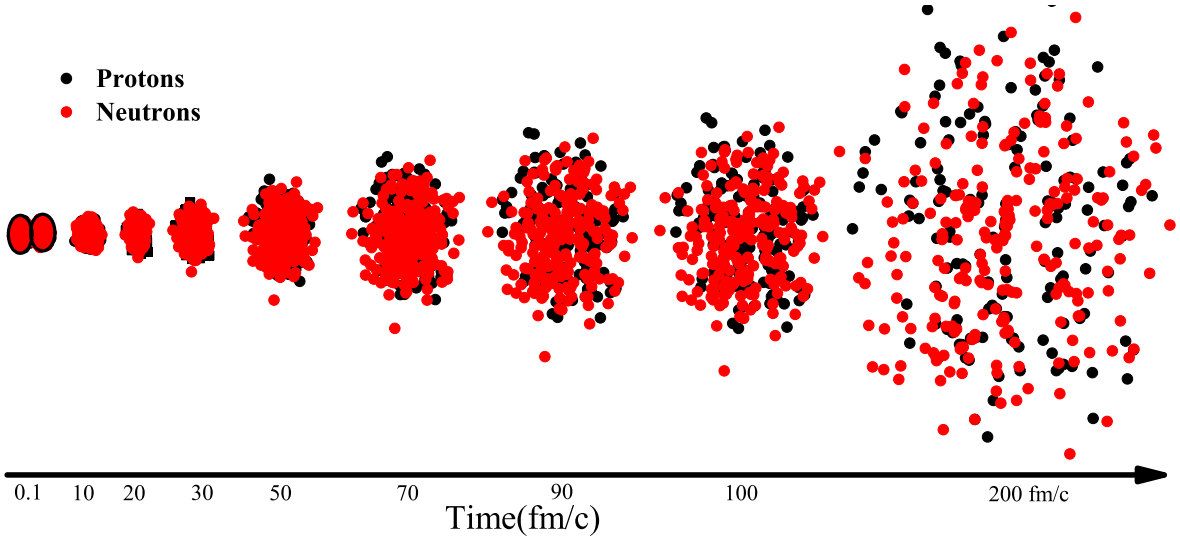

Figure 1.4: Time evolution of multifragmentation process.

multi-fragmentation, nuclear flow, collective flow and subthreshold particle production [22].

1.2.1 Multi-fragmentation

The process of shattering of the highly excited compressed nuclear matter (which has been formed by the collision of target and projectile nuclei) into fragments of different sizes is known as multi-fragmentation [23]. This phenomenon consisting of free nucleons having mass (A = 1), light mass fragments (2≤A≤4) and intermediate mass fragments (5≤A≤(A_{total})/3). Initially, two nuclei approaches each other faster or slower pace depending on the incident energy. The two nuclei then fully or partly merge or penetrate into each other depending on the impact parameter, incident energy and mass asymmetry of the nuclear reaction. Emission of fragments of different masses take place after the expansion of compressed nuclear matter.

Fig. 1.4 shows the time evolution of compressed matter formed by two similar sized colliding partners. At the freeze-out stage, the produced free nucleons/fragments do not interact with each other. At lower incident energies, the decay of compound nucleus occurs whereas at higher incident energies, the further decay of the produced

fragments takes place. The sizes and multiplicity of the emitted fragments depend on the incident energy, impact parameter, iso-spin content and mass of the colliding partners. The free nucleons and light mass fragments are produced in the central collisions because of high density achieved by the compressed matter formed by the maximum collisions between the nucleons. However, at peripheral impact parameters and for mass asymmetric nuclear collisions, the heavy fragments are formed in majority than the free nucleons or light mass fragments [24].

1.2.2 Collective Flow

Another process that takes place in the intermediate energy nuclear reactions is the flow of nucleons of the excited nuclear matter and its remnants called collective flow [25]. Nuclear flow is basically the transverse motion imparted to the emitted nucleons/fragments after the collision of projectile and target nuclei. Collective flow is associated with the pressure build-up during the collision of nuclei. Therefore it provides the important information about the expansion of the early universe and nuclear equation of state [EOS]. The compressed nuclear matter having very high pressure gradient, thus forces the movement of nucleons and fragments towards the regions of low pressure gradient. The emitted nucleons may emerged isotropically or an-isotropically depending on the incident reaction conditions.

Fig. 1.5, shows the anisotropic emission of nucleons from the highly compressed participant matter produced due to the non-central nuclear collisions. Only the excited participant zone is responsible for the collective flow. The nuclear flow comprised of nucleons is observed in a direction perpendicular to beam axis. The investigation of the anisotropy of nucleon's momentum distributions in the non-central collisions offers a great opportunity to grasp both the features and dynamics of the hot dense matter formed. The collective flow can be divided into radial [26], directed [27], elliptic [28], triangular and quadrangular flow [29, 30]. Out of all these parameters, only radial flow is observed to be emitted isotropically at the central nuclear collisions and remaining other components shows anisotropic emission. The detailed discussion of these parameters is in section 1.6.

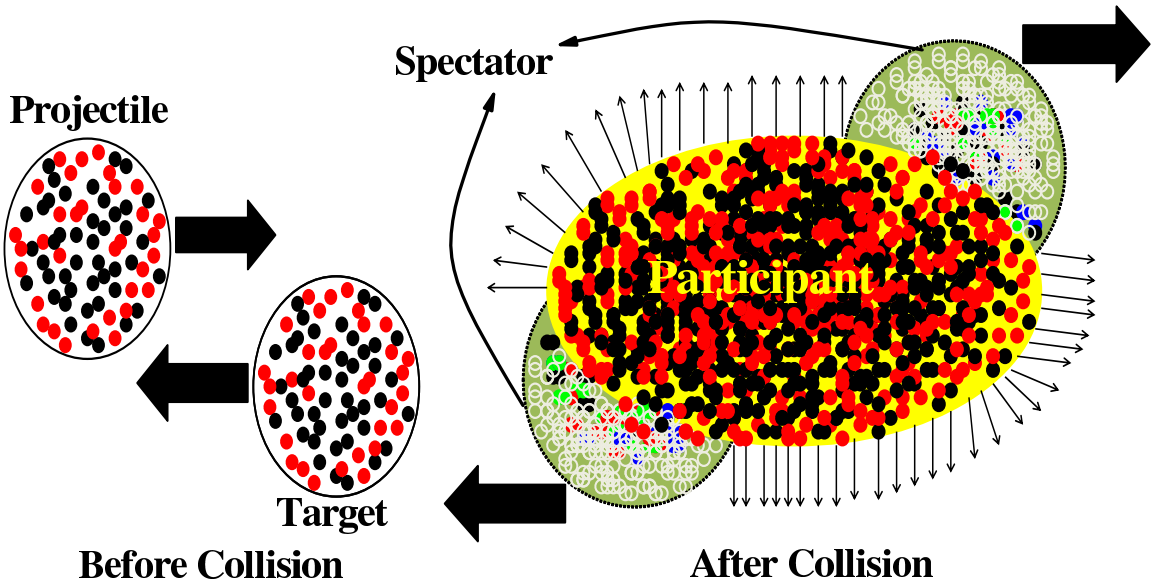

Figure 1.5: Anisotropic flow at non-central impact parameter.

Next section will provide a detailed discussion on phase-diagram of nuclear matter.

1.3 Phase-diagram of nuclear matter

There exists three different forms of nuclear matter under the influence of pressure and temperature, just like water. Water changes its state due to the variation of atmospheric pressure and temperature. It has different phases at every different value of pressure and temperature [31]. The phase diagram of nuclear matter (shown in Fig. 1.6) spreads over an infinite region of density and temperature. It represents quark-gluon plasma phase at extreme temperature and density to the condensed phase of nuclear matter, which lies in the neutron star's core (having high value of density) [22]. Between these two limits of temperature and density, there occur two remarkable transitions of phase: the nuclear liquid-gas phase transition and the quark hadron transition.

Nucleus is consisted of protons and neutrons, which are further comprised of quarks and gluons bounded by strong interactions described by quantum chromodynamics (QCD) [32]. At lower incident energies or for the normal state of nuclear matter,

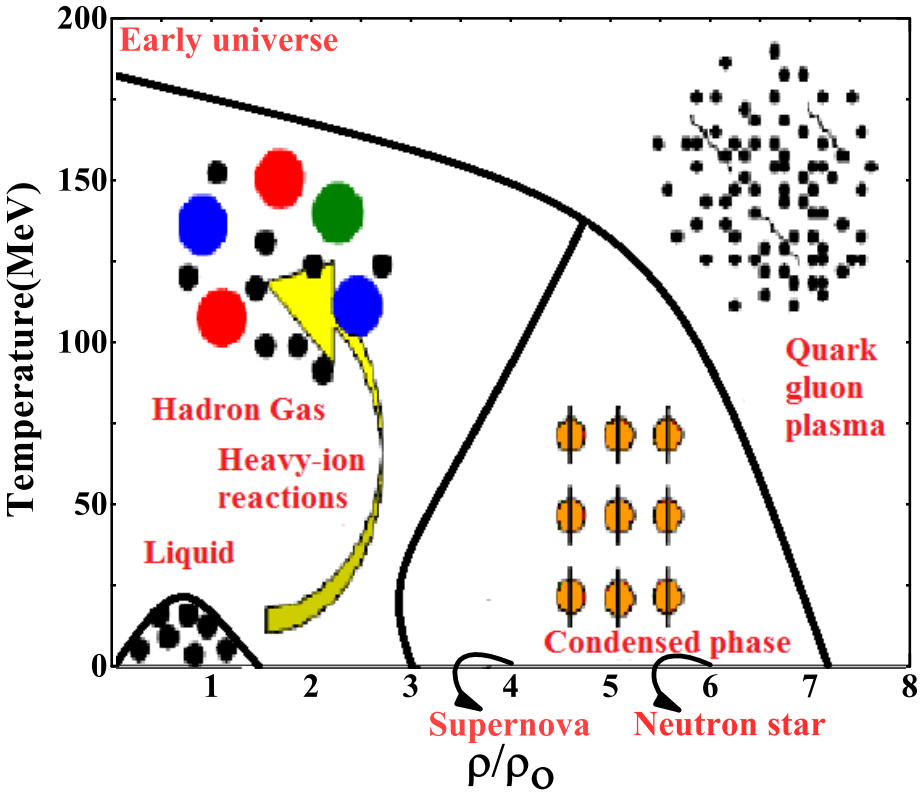

Figure 1.6: Phase-diagram of nuclear matter [22].

the nuclei shows liquid state and have normal density of 0.17 nucleons/fm^3. The nucleon-nucleon collisions can raise the temperature up to 100 MeV that can result in evaporation of nuclear matter. Similar to water, nuclear matter too have its latent heat of vaporisation. This forces the matter to undergo first order transition (liquid-gas phase) shown in lower left corner of Fig. 1.6 at temperature around 15 MeV.

Furthermore increase in the temperature and density is sufficient to break the nucleon's internal structure. The quarks, thus produced during this process are well confined. Due to this, it has never been achievable to isolate and get free quarks. This de-confined quark state of matter is called QGP [33]. These transitions are occurred at very high values of temperature and density (shown in right corner of Fig. 1.6). The existence of the curve at some constant value of density and temperature shows a sharp transition between the hadronic phase and QGP.

When a huge star having mass 8 times the mass of sun goes through a supernova explosion around density $\rho/\rho_0 = 4$ (as shown in Fig. 1.6). After the explosion, an iron nuclei's core (having the largest binding energy per particle) still remains behind. When the Fe core's mass exceeds the Chandrasekhar mass limit (having mass 1.44 the mass of sun) [34], the Fe core begins to collapse. The short-ranged nuclear repulsive forces are not sufficient to retain the colliding masses far away from each other [35]. This supernova explosion may leads to the neutron star's formation (very big assembly of neutrons) or black hole in the central part of the massive star due to the collapse of the gravitational core [36]. Some theoreticians anticipate that a massive neutron star could be of enormous density to generate a quark-gluon plasma [37].

In between the temperature and density range (around T = 100 MeV and ρ/ρ_0 = 2 - 3), the projectile and target does not stabilise. It depict the clear dynamics of the heavy ion reactions which provides the information about phenomenon like multi-fragmentation and collective flow. Out of these two observable, the anisotropic nuclear flow has been anticipated by hydrodynamical calculations [38, 39]. Flow of nucleonic matter in theoretical calculations and experimental observations is closely related to the present picture of the universe. This is originated by the big-bang explosion and the freeze-out state of the matter that formed during that explosion is our present universe [40, 41].

Isospin effects in heavy-ion nuclear reactions are also very crucial in the nuclear physics at intermediate energies. Next section will put a lime-light on this feature.

1.4 Isospin effects in heavy-ion collisions

New approaches in experimental research using radioactive beams with higher proton to neutron ratio have made it possible to generate not only nuclei having sufficient lifetime, but also temporary nuclear matter with considerable isospin asymmetry, compression and thermal excitation [42]. Iso-spin effects in heavy-ion collisions give the possibility to probe the intrinsic aspects of nuclear matter which lie in the region between iso-spin symmetric (having identical neutrons and protons number) and iso-spin asymmetric (having different number of neutrons and protons) nuclear matter. This

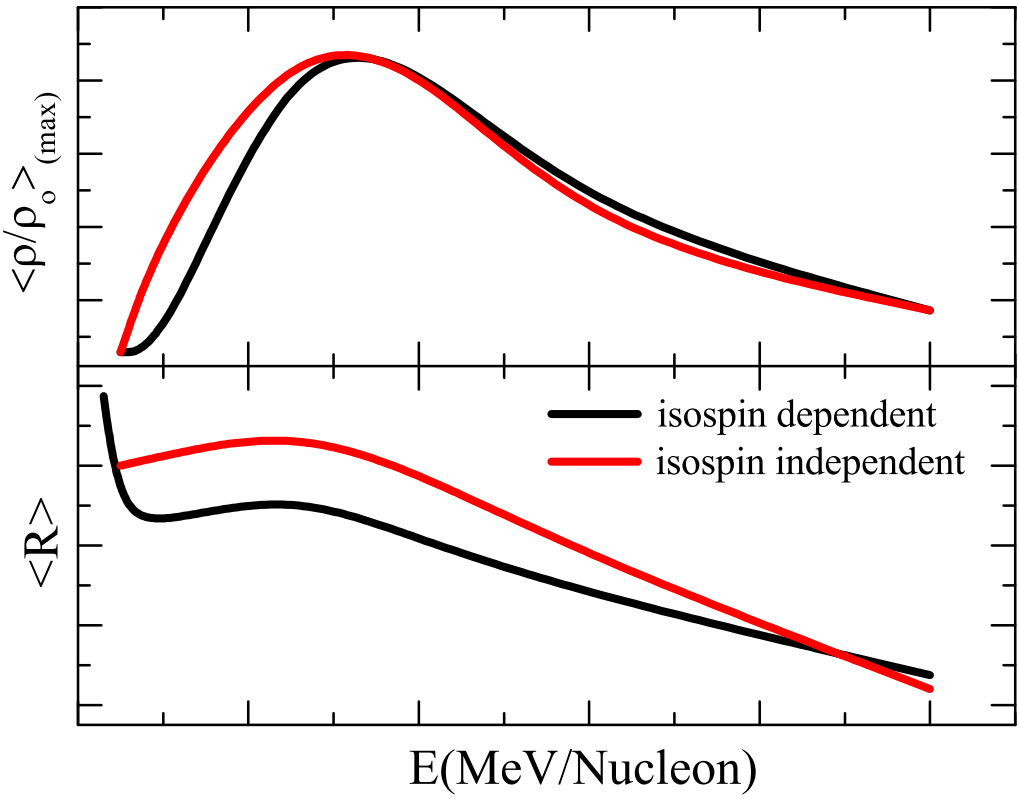

Figure 1.7: Role of iso-spin dependent and iso-spin independent cross-section in intermediate energies. Upper panel shows scaled density and lower panel shows anisotropy ratio/nuclear stopping.

study is somehow helpful in perceiving the explosion dynamics of supernova explosion and the neutron star's cooling [43].

In theoretical studies, different nucleon-nucleon cross-sections have been used for the calculations and found to be very successful. Many phenomena at intermediate energies are examined by varying the nuclear equation of state and in-medium nucleon-nucleon cross sections [21, 44, 45]. These studies lead to understand the isospin dependence of the nuclear collective flow [46] and balance energy, nuclear stopping, fragmentation as well as particle production [21, 44, 45]. Fig. 1.7, shows the effect of isospin dependent and isospin independent cross-section on scaled density and nuclear stopping [47].

In the mass empirical formula, the symmetry energy term is influenced by the isospin content of the nucleus. In Fig. 1.8, the lower and upper curves show the energy per

nucleon for isospin symmetric nuclear matter and pure neutron matter. All protons in a symmetric nuclear matter will be converted to neutrons at a particular value of density ρ by supplying the sufficient amount of energy (i.e., symmetry energy) in overcoming two extreme line's difference. The nuclear equation of state (NEOS) elaborates the fundamental properties of infinite nuclear matter at neutron-to-proton (N/Z) ratio away from the ground state nuclear matter. The isospin asymmetric nuclear matter's NEOS [48] is represented in parabolic form as [49]:

$$E_{sym}(\rho, \delta_A) \;=\; E_{sym}(\rho, 0) \;+\; E_{sym}(\rho)\delta_A^2 \;+\; O(\delta_A^4) \tag{1.1}$$

Where, $E_{sym}(\rho)$ and $E_{sym}(\rho, 0)$ are the energy per nucleon of normal nuclear mat-

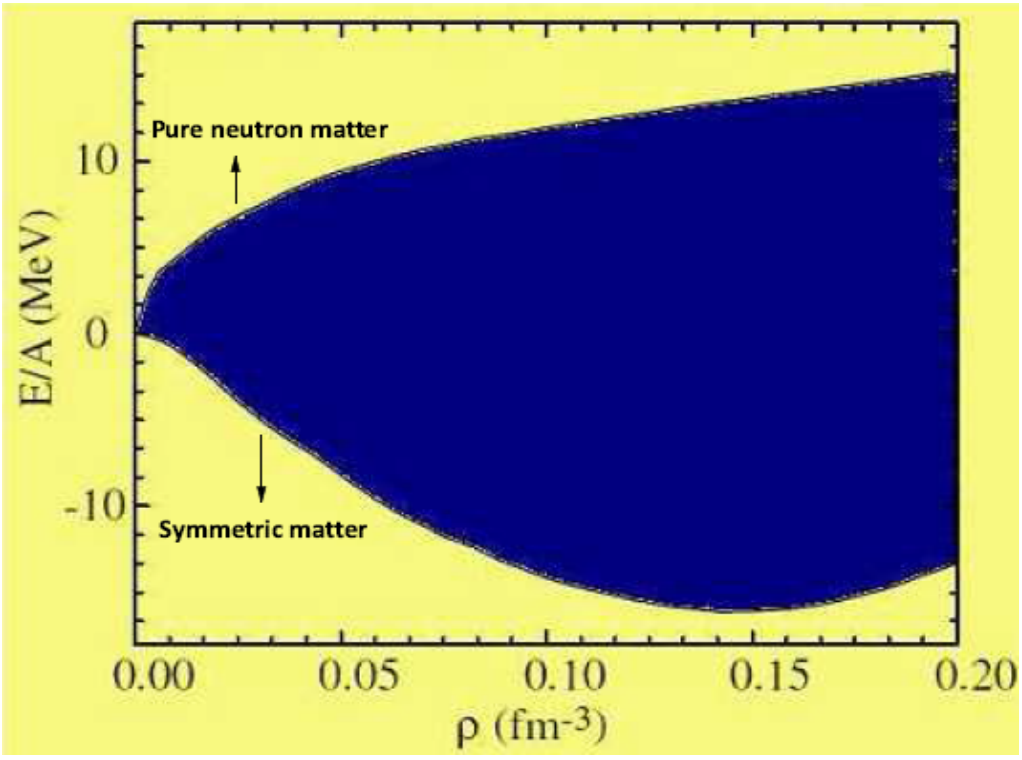

Figure 1.8: The density dependence of energy per nucleon for symmetric nuclear matter (lower curve) and pure neutron matter (upper curve). The symmetry energy is signified by shaded region [42].

ter and isospin symmetric nuclear matter respectively and $\delta_A = (\rho_n - \rho_p)/(\rho_n + \rho_p)$ represents the isospin asymmetry of nuclear matter. This equation has been used as

the empirical parabolic law for the equation of state of asymmetric nuclear matter and has been considered to be valid only at small isospin asymmetries (δ). However, many non-relativistic and relativistic calculations have shown that this isospin asymmetry is actually valid up to $\delta = 1$, at least for densities up to moderate values [49]. The density dependence of symmetry energy's parameterized form has been provided as [50, 51]:

$$E_{sym}(\rho) \;=\; E_{sym}(\rho_0)\left(\frac{\rho}{\rho_0}\right)^{\gamma}, \tag{1.2}$$

where, $E(\rho_0) = 32$ MeV is the symmetry energy varied in accordance with the normal nuclear matter density ($\rho_0 = 0.17 fm^{-3}$). The value of γ elaborates the rigidness or strength of symmetry energy at the values of densities elsewhere from ρ_0. Usually, two different values of density dependence of symmetry energy has been explored i.e., Stiff and Soft density dependent symmetry energy.

The entire work of this thesis is to explore the role of rapidity constraints on nuclear flow and rotational dynamics in nuclear reactions. The next section will give detailed description of rapidity.

1.5 Significance of rapidity

Rapidity is a variable commonly used to determine the particle's (nucleon's) kinematic conditions. The rapidity of any particle in motion is defined in accordance to its energy and momentum. Being a dimensionless quantity, it is correlated to the ratio of the positive or forward momentum of the particle to the negative or backward momentum of that particle. Rapidity of a particle is frame of reference dependent and is linked with the rapidity in another Lorentz frame of reference by an additive constant [52]. Mathematically rapidity is defined as [22]:

$$Y(i) = \frac{1}{2}\ln\frac{E(i) + P_z(i)c}{E(i) - P_z(i)c} \tag{1.3}$$

where $E(i)$ is the total energy and P_z is the longitudinal momentum of i^{th} particle. The significance of such a quantity can be interpreted as in relativistic high energy and intermediate energy reactions [53].

Rapidity constraints are helpful to interpret the impact of spectator-participant matter on the different harmonics of anisotropic nuclear flow. The fundamental concept

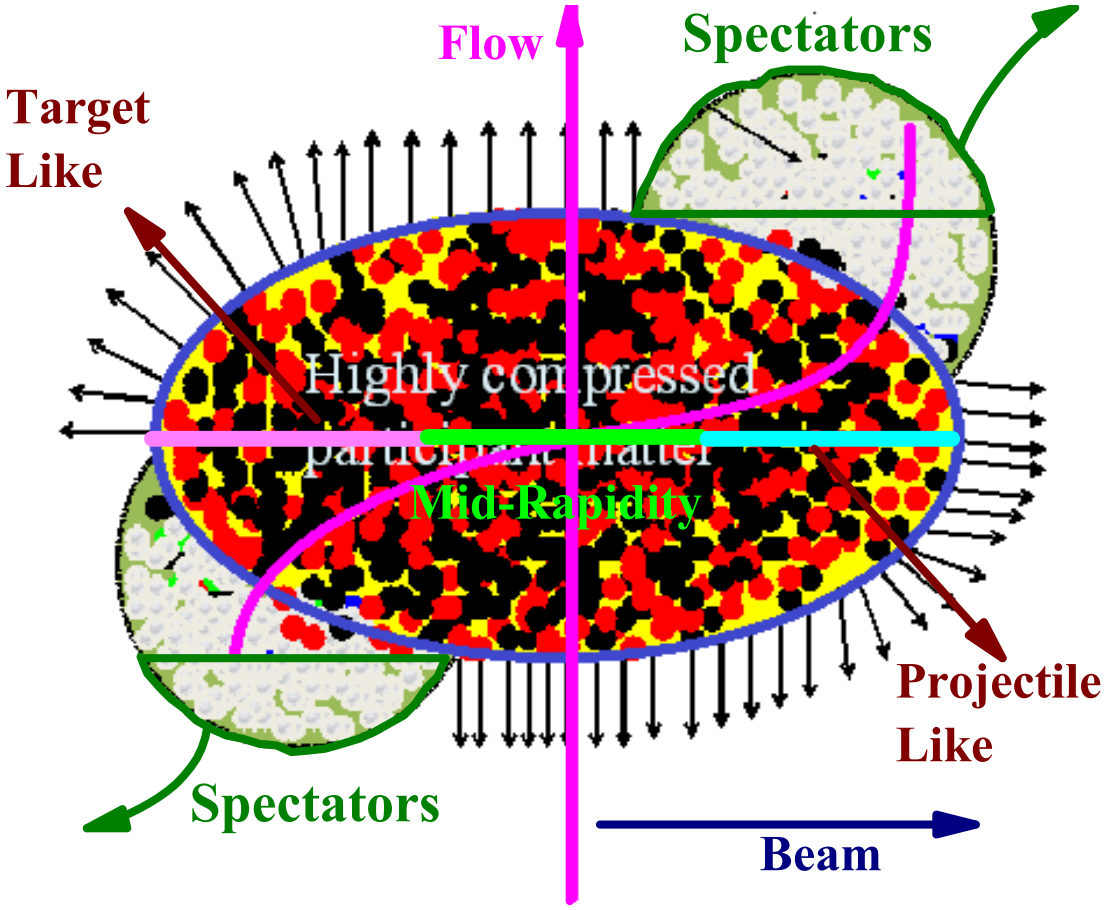

Figure 1.9: Representation of rapidity

of participant and spectators in reaction dynamics was first initiated by Bowman et al. [54]. This concept was carried forward by Westfall et al. [55] for the study of the nucleons which are pushed out mutually from the target and projectile to form a hot equilibrated fireball known as participant zone. The remaining non-interacted part thus formed by the colliding nuclei is known as spectator zone as shown in Fig. 1.9. If two symmetric mass nuclei collide head on then, one would observe a single maxima centered in the middle of rapidity region shown by the Gaussian shape [56], although there is a spreading of nucleons extending even to the edges of the rapidity (shown in Fig. 1.10). In Fig. 1.10, the highly compressed participant zone around the zero value of rapidity has been observed and the region around this zero-value ($|\frac{Y_{c.m.}}{Y_{beam}}| < 0.1$) is called mid-rapidity zone in the literature [57–60]. Very fascinating and crucial properties of the nuclear matter can be extracted from this zone. For example, the calculation

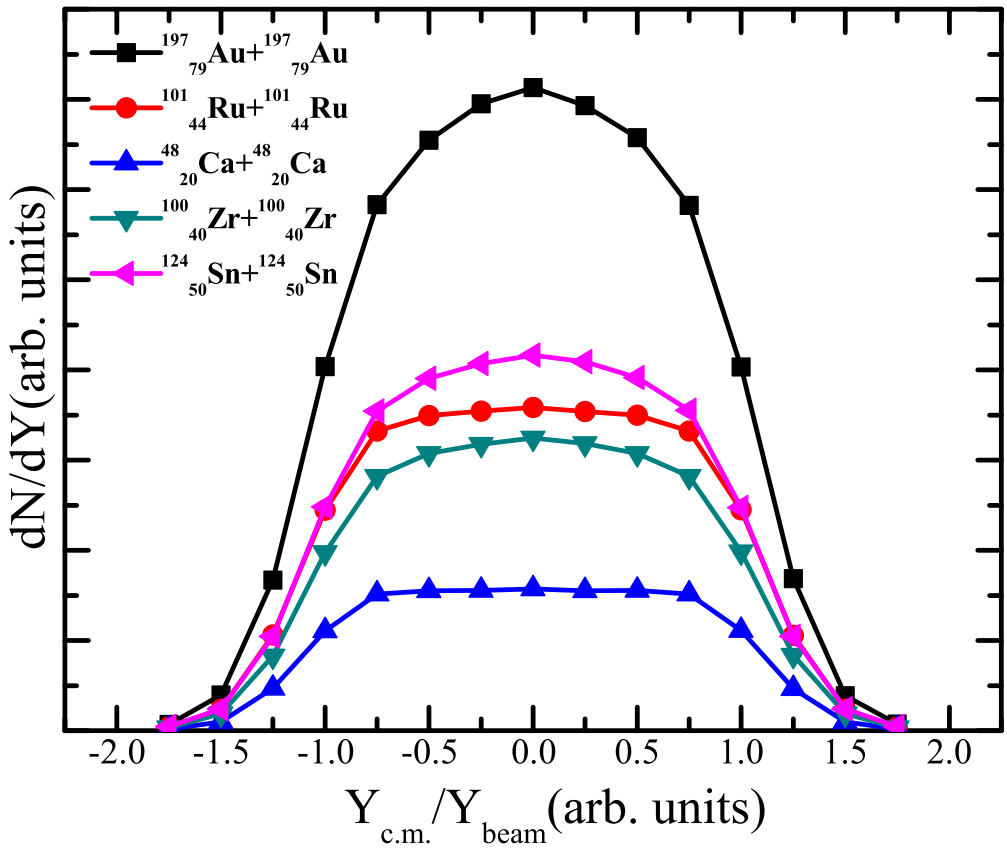

Figure 1.10: Representation of rapidity distribution of nucleons.

of balance energy associated with transverse flow and transition energy related to elliptic flow are carried out from the mid-rapidity region [61–63].

The emission of nucleons of spectator matter, which have not suffered any collision is distributed equally towards the both sides of mid-rapidity region. The region extending from $-1.75 \leq \frac{Y_{c.m.}}{Y_{beam}} \leq -0.1$ is known as target-like (T.L.) spectator region and the region from $0.1 \leq \frac{Y_{c.m.}}{Y_{beam}} \leq 1.75$ is called projectile-like (P.L.) spectator region. However, for the mass asymmetric nuclear reactions or for the collision of symmetric masses away from the central collisions, the single central peak as a function of rapidity will split into two peaks. Furthermore increase in the impact parameter leads to three peaks, two at the ends (at P.L. and T.L.) and one in the center (mid-rapidity) [54].

The region of participant zone keeps on shifting with the enhancement in mass asymmetry of the reaction as well as the T.L. and P.L. zones too are shifted depending upon

the mass asymmetry content of the reaction. Therefore, in mass asymmetric nuclear reactions, the mid-rapidity region, P.L. and T.L. regions are being calculated on the basis of equal contribution of participating nucleons from target and projectile nuclei. The significance of different rapidity zones have been explored [8, 63, 64]. The mid-rapidity intervals alter with the mass asymmetry of the reaction. A table displaying these rapidity ranges for different mass asymmetric nuclear reactions has been shown in chapter 4.

Rapidity is somehow inaccessible for the measurement of highly relativistic particles, because one will require both the total momentum and the energy of the particle. At larger values of the rapidity in actual practice, it is tough to calculate the total momentum vector of a particle, where the component of momentum is very large. However, there is a quantity called pseudorapidity (η), which is almost identical to the rapidity and have made it easier to measure rapidity for highly energetic particles [65, 66]. In hadron colliders such as the LHC (Large Hadron collider) [67], pseudo-rapidity is particularly beneficial. Several theoretical studies has also been carried out on this parameter at relativistic energy ranges [65, 66].

After discussing the rapidity thoroughly, it will be interesting to study nuclear flow and its components in detail in the next section.

1.6 Nuclear flow

In order to explain the pseudo-macroscopic aspects of nuclear matter, it is mandatory to explore collective flow observable. Entirety, this reference can be explained as: the number of colliding partners display a general feature (e.g. the emission of nucleons/fragments with an average velocity or in a common direction or vice-versa). The definition of collective flow can be interpreted as: Any conventional feature of all the nucleons/fragments released in a heavy-ion nuclear reaction can be taken as a measure for the nuclear-matter's unrevealed phase space distribution. The appearance of the distribution depends entirely on the impact parameter.

For central collisions, the reaction volume is spherical in shape whereas, an almond shaped fireball is formed in non-central collisions. The pressure gradient is sufficient to

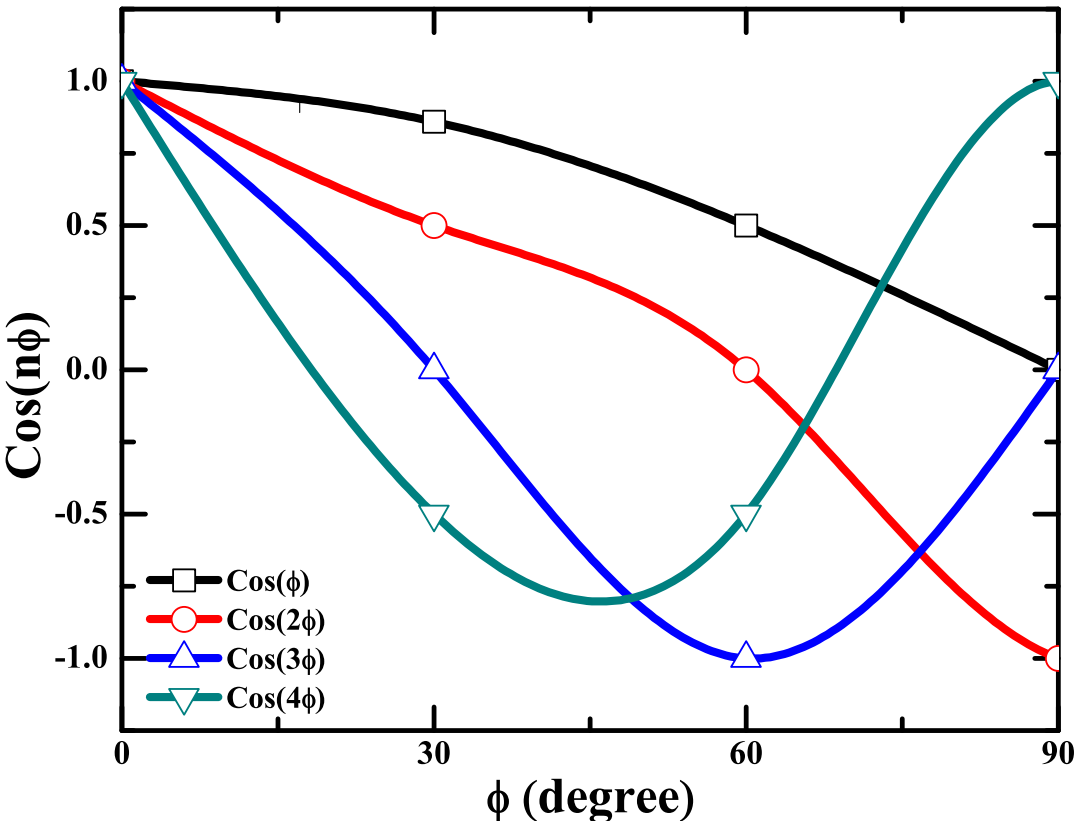

Figure 1.11: Representation of different harmonic coefficients with azimuthal angle.

translate an original spatial asymmetry to latter momentum anisotropy in non-central collisions. The anisotropic flow has been confirmed as a good probe to explore properties of dense matter as it can provide important knowledge about the Nuclear Equation of State (NEOS) [68]. Since the initial co-ordinate asymmetry decreases promptly with time, so collective flow can established only in the early phase of the nuclear reaction.

The collective flow is defined as the nth Fourier coefficient v_n of the invariant particle distribution [69]:

$$\frac{dN}{d\phi} \propto [1 + 2\sum_{n=1}^{\infty} v_n \cos(n\phi)] \tag{1.4}$$

where azimuthal angle (ϕ) is the angle between the reaction plane and the particle's transverse momentum. The order of flow can be represented by the coefficients of Fourier expansion.

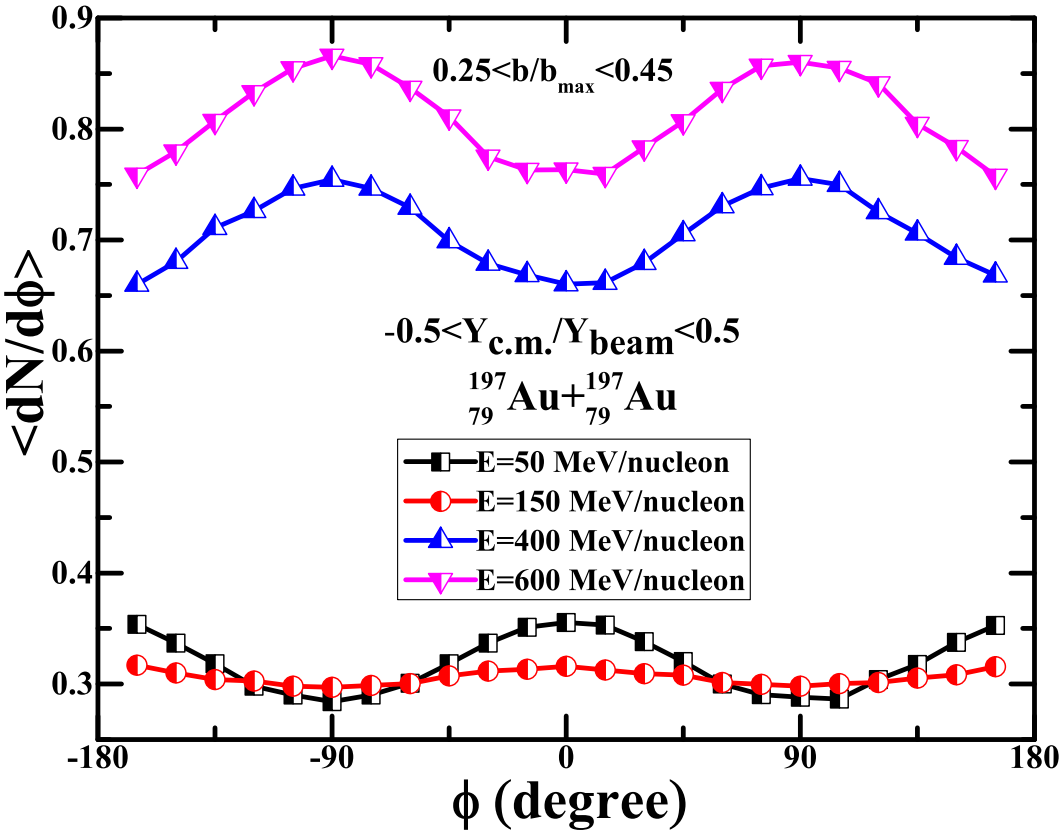

Figure 1.12: $dN/d\phi$ as a function of ϕ angle at different incident energies for the reaction of $^{197}_{79}Au +^{197}_{79} Au$

.

The azimuthal angle ϕ variation for different flow harmonics calculated theoretically has been shown in Fig. 1.11. The value of maxima of azimuthal distributions [70] at 0^0 shows with-in the plane emissions of nucleons or in-plane flow, whereas value maxima peaked at $\pm 90^0$ shows the out of the plane emissions of nucleons or squeeze-out flow as shown in Fig. 1.12. One can observe here that, for $^{197}_{79}Au+^{197}_{79}Au$ reaction, the transition energy lies around incident energy 150 MeV/nucleon and below this energy the flow is with-in the plane as can be seen at incident energy E = 50 MeV/nucleon, where the distribution of the nucleons is peaked at 0^0 . Whereas above these energies, the squeeze-out flow has been observed for the case of incident energies E = 400 MeV/nucleon and E = 600 MeV/nucleon.

All the different components of collective flow are discussed in detail in the succeeding

section.

1.7 Importance of different harmonics of flow

1.7.1 Directed Flow

The collective sideward flow of the emitted nucleons and fragments has been represented by first Fourier harmonic $< v_1 >$. It also provides important information from the beginning phase of the collisions [27]. In heavy-ion collisions, directed flow can be represented mathematically as [69]:

$$< v_1 > \; = \; \langle \cos\phi \rangle \; = \; \langle \frac{p_x}{p_t} \rangle \tag{1.5}$$

where projections of particle transverse momentum are represented parallel to the reaction plane by p_x and perpendicular by p_y. The total transverse momentum is defined by $p_t = \sqrt{p_x^2 + p_y^2}$.

The first experimental measurement of directed flow was achieved at the Bevalac in Berkeley, CA in the 1980s and had provided the evidence of a sidewards flow or side-splash of fragments by bounce-off of the projectile [71]. In such type of collisions, a dense and hot zone of compressed nuclear matter is formed. Only the nucleons/fragments which lie on the surface of denser zone, are likely to separate early. A simple representation of a non-central heavy-ion collision has been shown in Fig. 1.13 in order to illustrate the concept of directed flow. The initial interplay of the projectile and target is shown on the left-side. After the collision, projectile and target separates from each other, creating a quasi-target (QT) and quasi-projectile (QP) followed by emission of nucleons and fragments from the compressed zone.

The directed flow is provided by the movement of these emitted nucleons/fragments in the reaction plane, following the QP and QT. The incident energy of the reaction has an influential impact on the directed flow as shown in Fig. 1.13. If the beam energy is less than the balance energy (E_{bal}, where the nucleon-nucleon collisions balances mean-field effects) [72], of the system. The projectile and target rotate around each other. This results into the flow of nucleons/fragments within the plane. If the beam energy is greater than E_{bal}, then the projectile and target bounce-off and splash effect in the

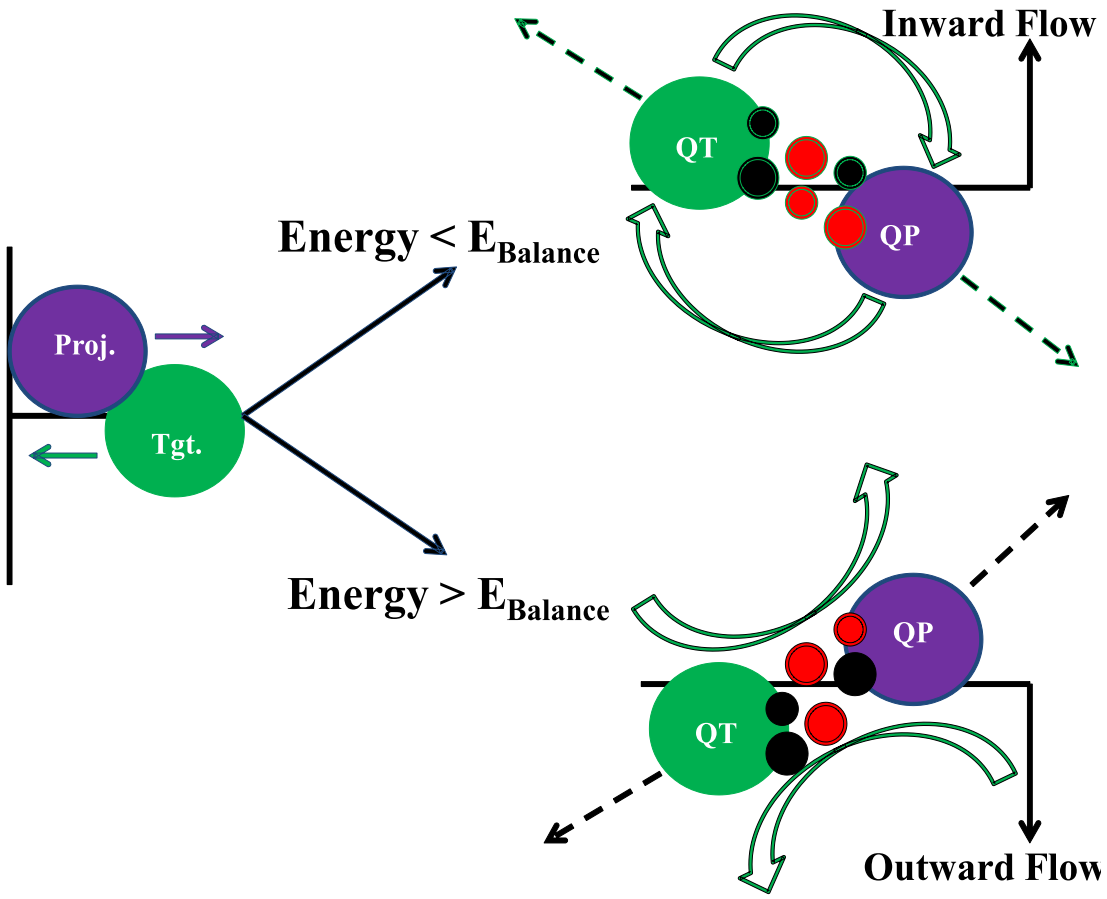

Figure 1.13: Representation of directed flow at different energies.

forward flow side is produced [61]. This process can be visualized as: when two nuclei collides, the density and pressure build up in the interaction zone increases. This leads to the compression of nuclear matter in the participant zone [73]. The participant zone depends on the impact parameter of the reaction. It is anisotropic for semi-central impact-parameter and disappears for central or peripheral impact-parameter due to non-uniformity or lack of needed participant zone respectively [74].

The magnitude and shape of directed flow has significance in research due to its sensitivity towards the equation of state (EOS) [75, 76]. The information can be extracted from the plot of flow against rapidity [77]. The graph when plotted at three different energies gives different picture of directed flow as:

(a)$E < E_{Balance}$ (at low incident energy) Here, the slope of curve comes out to be negative because the interactions between the nucleons are dominated by attractive mean fields, the nucleons are mainly scattered away from both the target and projectile side of the reaction plane to the negative angles. The rotational effects are observed due to these attractive interactions.

(b)$E > E_{Balance}$ (at high incident energy) Here, the slope of line comes out to be positive because the nucleons interactions are dominated by the repulsive nucleon-nucleon interactions and the nucleons are emitted to the positive angles. Due to repulsions, the side-splash effects between the nucleons take place.

(c)$E = E_{Balance}$ (at balance energy) At a particular incident energy, when both the repulsive and attractive interactions balance each other, the flow along the X-axis vanishes. The incident beam energy at which flow disappears is called as the energy of vanishing flow or balance energy [77]. At this energy, the azimuthal distribution of the emitted fragments (from both target and projectile side) with respect to the reaction plane do not exhibit peaks at 0^0 or 180^0.

The E_{bal} has been found to depend necessarily on the mass asymmetry of the reaction [78–82] as well as on the impact parameter of the reaction [80–83]. It has been reported that E_{bal} can be used as a probe to understand isospin dependance of nucleon-nucleon interactions [84].

The second harmonic is studied in detail in the next section.

1.7.2 Elliptic Flow

Azimuthal distribution of nucleon's momentum is denoted by second Fourier harmonic coefficient i.e., elliptic flow ($< v_2 >$). One can acquire the knowledge about equation of state and thermalization time using this harmonic of nuclear flow. Elliptic flow provides a strong evidence for the generation of dense and hot matter at a very early stage in the non-central collisions [85–87]. At non-central impact parameter, the expanded overlap region is basically almond-like in shape and does not acquire azimuthal isotropic distribution of nucleons as shown in Fig. 1.14. The initial geometrical asymmetry of the system results into anisotropic pressure gradients. These pressure gradients then lead to the anisotropy in momentum space. As, the spatial asymmetry declines immediately with time, so elliptic flow can emerge at a very early stage of the reaction. Mathematically, elliptic flow is represented as [69]:

$$< v_2 > \;=\; \langle \cos 2\phi \rangle \;=\; \langle \frac{p_x^2 - p_y^2}{p_t^2} \rangle \tag{1.6}$$

In Fig. 1.14, the two types of elliptic flow: in-plane flow and out-of-plane flow are shown. Here, in-plane flow represents the flow of nucleons with-in the plane with positive value of $< v_2 >$, whereas the negative value of $< v_2 >$ corresponds to the squeeze-out flow or out-of-plane of nucleons perpendicular to the reaction-plane [88]. This concept can be understood with the help of Fig. 1.15. This presents the clear picture of elliptic flow, here the shape of ϕ distribution (emitted nucleons) at mid-rapidity looks alike an ellipse with a major axis along the x-axis and minor axis along the y-axis. The major axis depicts the in-plane flow and minor axis points towards the squeeze-out flow. The azimuthal angle ϕ is the angle between the impact parameter axis and the reaction-plane. So, the $\phi = 0^0$ or 180^0 corresponds towards the positive (in-plane) flow and the $\phi = \pm 90^0$ signify towards the squeeze-out flow as shown in Fig. 1.12.

The elliptic flow is examined by the complex interplay due to expansion of hot compressed matter, rotation of participant matter and shadowing of spectator matter [57]. The elliptic flow or squeeze-out flow of the hot matter is basically the counter balancing of expanded hot matter and passing time of the spectator matter over the compressed

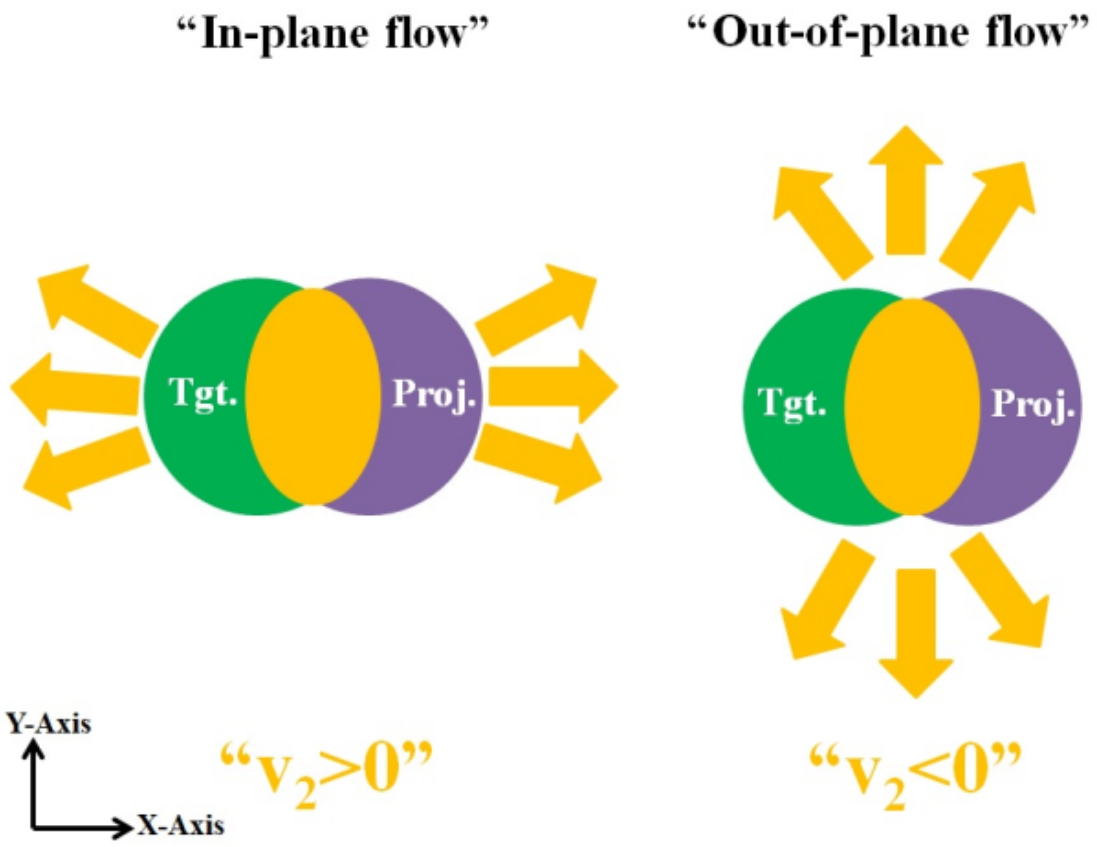

Figure 1.14: Representation of spatial anisotropy in elliptic flow.

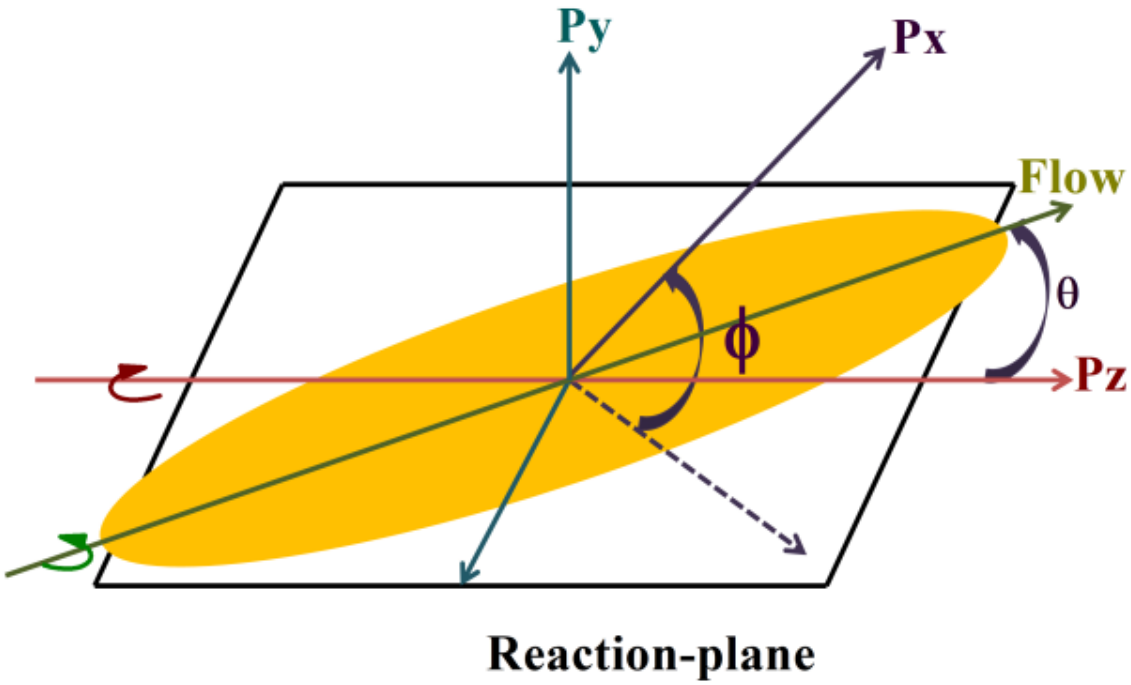

Figure 1.15: Representation of the azimuthal angle ϕ and flow angle θ.

participant zone. The flow of nucleons starts at this instant (cut off time of the spectator matter) due to the low pressure gradient outside the hot participant zone. Andronic et al. [57, 58], introduced a parameter t_{pass} ($t_{pass} = 2R/\gamma_s v_s$, where R = radius of nucleus at rest, v_s = spectator velocity in center-of-mass frame and γ_s = Lorentz factor), which depicts a close co-ordination between the expansion time of participant matter and spectator matter's (shadowing) passing time.

Due to these two similar time durations (i.e., participant's expansion time and spectator's passing time), the participant matter exhibit more squeeze-out and deflected out of the plane. In the incident energy span of 0.4 - 1.49 GeV/nucleon, t_{pass} decreases from time 30 to 16 fm/c indicating that the expansion becomes roughly 2 times rapid in high energy nuclear reactions. At later times, the participant nucleons are not blocked by the spectators because, the shadowing effect is not seen at this time during the process of participant matter's expansion.

The balancing of the attractive and repulsive interactions lead to the transition of the elliptic flow from in plane to out-of plane at a particular incident energy (about 100 MeV/nucleon, depending upon the combined mass and isospin content of the colliding partners). These transitions has prompted the researchers to carry out the exploration for collective flow. This study of elliptic flow can also put lime light on the various astrophysical aspects such as supernova explosion. Its worth mentioning that the mean field commands the dynamics at low incident energies. However, at higher energies role of mean field diminishes and nucleon-nucleon interactions becomes dominant. An in-depth inquiry of elliptic flow as a function of excitation energy can yield a useful piece of information regarding the nucleon-nucleon interactions.

Elliptic flow as a function of energy: The elliptic flow reduces to zero value at an exact value of incident energy while taking the transition from in-plane to out-of-plane or vice-versa. This particular value of energy is called $transition - energy$ (E_{Trans}) [89]. At low incident energies, the interactions among the nucleons are influenced by the attractive mean-field, which forces the projectile and target to form a rotating system [90]. The rotation of nuclear matter results into the centrifugal force,

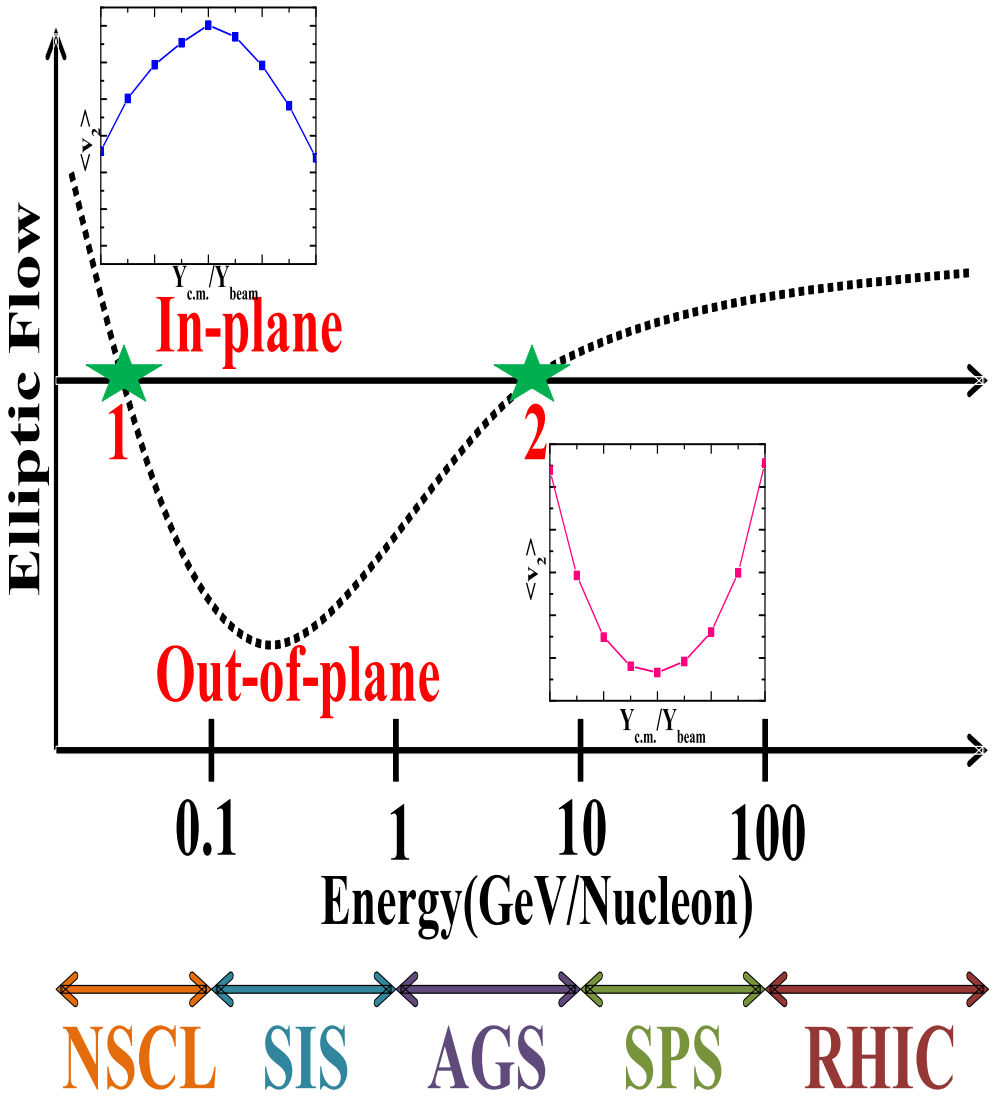

Figure 1.16: Variation of elliptic flow with energy.

which releases nucleons within the rotating plane, thus produces the in-plane elliptic flow [90,91]. The contributing nucleons due to the overlapping of target and projectile cannot flee the reaction-plane due to the existence of the spectator nucleons at high energies. This phenomenon consequences into the squeeze-out or out-of-plane elliptic flow [88]. The value of E_{Trans} depends on the impact parameter, mass of the colliding partners and mass asymmetry of the nuclear reaction etc [8, 57, 58, 88]. In addition to this, the transition energy can also be calculated by Fourier expansion series fitting of the azimuthal distributions of the rotational flow at different incident energies [8]. This is the best method to calculate E_{Trans} of the mass asymmetric nuclear reactions too.

Fig. 1.16 shows these two transitions of elliptic flow very clearly. First symbol of star 1 depicts the first transition from in-plane to out-of-plane (NSCL [0.1 GeV/nucleon] to SIS [1 GeV/nucleon]) and star 2 describes the second transition from out-of-plane to in-plane (SIS [1 GeV/nucleon] to AGS [11 GeV/nucleon]) [80]. The inset at low energy around E = 50 MeV/nucleon in the in-plane (below E_{Trans}) shows that, $< v_2 >$ of nucleons as a function of rapidity follows the positive value of v_2. Whereas, above the E_{Trans} at E = 400 MeV/nucleon in the out-of-plane shows the negative value of $< v_2 >$.

The detailed study of transition energy is helpful in the extraction of equation of state of the nuclear matter. Several experimental groups have produced an excellent amount of experimental data on transition energy using accelerators and synchrotrons like Diogene at Saturne, (Saclay Lab) France [92], EOS time projection chamber (TPC) at Lawrence Berkeley National Laboratory, Berkeley, California [93], Schwerionen synchrotron (SIS) at GSI, Germany [57, 94, 95], Super Proton Synchrotron (SPS) at CERN, Switzerland [96, 97], Berkeley at Bevalac, using the Plastic Ball/Wall Spectrometer [98, 99], Relativistic Heavy ion collider (RHIC) [100] at Brookhaven National Laboratory in New York, United States and Alternating Gradient Synchrotron (AGS) [101, 102].
The magnitude of elliptic flow presume the maximum value around 400 MeV/nucleon. At this energy, the sign of $< v_2 >$ points towards a reference for emission of nucleons in a direction perpendicular to reaction-plane. This change of sign reflects the

increasing pressure build up in the participant zone due to non-central collisions at ultra-relativistic energies [103, 104].

The second transition from out-of-plane to in-plane becomes important at relativistic energies. At higher incident energies around 10 GeV/nucleon, the spectators leave the interaction zone very rapidly. This kind of transition takes place at AGS, SIS upto RHIC energies. The primary goal of experiments at these energies is to create extremely dense and hot matter with partons as its fundamental components called the Quark-Gluon Plasma (QGP).

Next section will provide an overview on higher harmonics of flow.

1.7.3 Triangular flow and Quadrangular flow

The first measurement of these higher harmonics was reported by K. Aamodt et al. [29,30]. Triangular flow ($< v_3 >$) is the third harmonic coefficient of Fourier expansion. Indeed, because of the un-even shape, originating from the event by event variations of participating nucleons, it results into a triangle like shape that can be transformed into momentum space by hydrodynamical expansion. Spatial asymmetry's event-by-event fluctuations create extra odd harmonic symmetry planes, which are supposed to result into the triangular flow like odd harmonics.

The triangular flow is a good evident for calculating the system susceptibility to the original state fluctuations [29], as it is produced merely by event-by-event fluctuations in the initial arrangement of the colliding masses. In contrast with the elliptic flow, it is significantly less connected to the overall colliding range. Having a smaller magnitude, it is however, also difficult to measure accurately. $< v_3 >$ originated due to the collision of mass asymmetric nuclear reaction (e.g. C+Au) [105]. The collision ends in the shape of triangle like structure. Mathematically, it is represented as [69]:

$$< v_3 > \;=\; \langle \cos 3\phi \rangle \;=\; \langle \frac{p_x^3 - 3p_x p_y^2}{p_t^3} \rangle \tag{1.7}$$

A rectangular type deformed shape of amplitude $< v_4 >$ termed as quadrangular flow, which can be assumed as the overlapping of two perpendicular ellipses, could be non-zero for rapidity windows close to the center of mass, where both squeeze-out, emitting

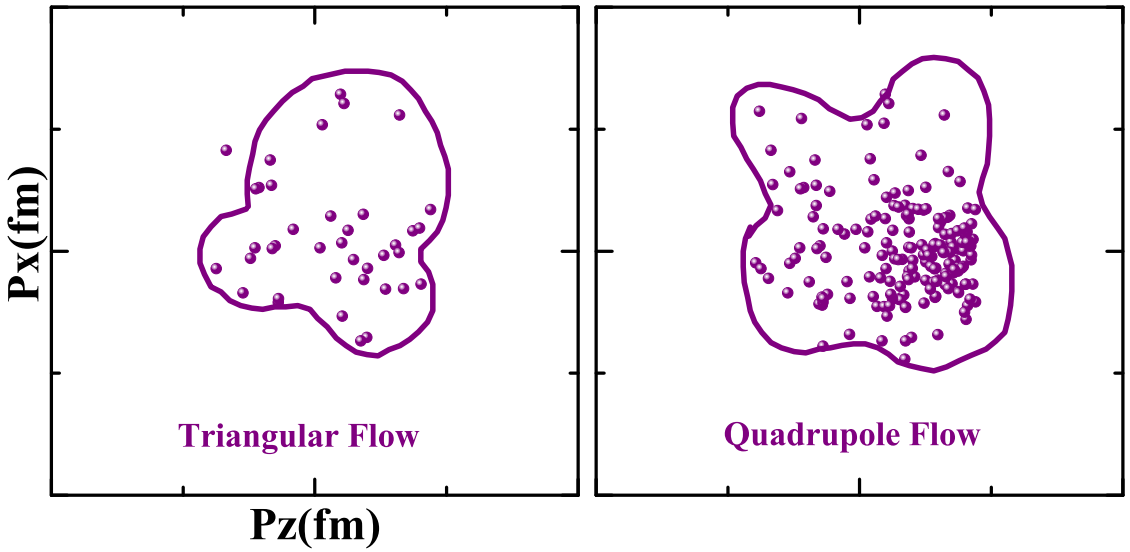

Figure 1.17: Representation of triangular and quadrangular flow.

preferentially more particles in the reaction plane's perpendicular direction and side-splash effects can be important. Mathematically, it is represented as [69]:

$$< v_4 > \;=\; \langle \cos 4\phi \rangle \;=\; \langle \frac{p_x^4 - 6p_x^2 p_y^2 + p_y^4}{p_t^4} \rangle \tag{1.8}$$

Originally, quadrangular flow $< v_4 >$ had been calculated with respect to the event plane of elliptic flow. These higher harmonics also divulge that the created QGP fireball strongly variate event by event, which ultimately changes into final state correlations of the produced nucleons after the collective expansion in high energy heavy ion collisions [106].

1.8 Rotational Dynamics

It has been witnessed that many things in the universe rotates around an axis like nucleons, electrons, earth, planets, stars and galaxies [107]. The cause of this rotation can be understood from the early phases of the universe, when the clouds of gas joins together to produce the stars [108]. These stars under the influence of strong gravitational interactions attract each other and forms massive bunches of stars. In the due course of time, these clusters amalgamate by the gravitational attractions and

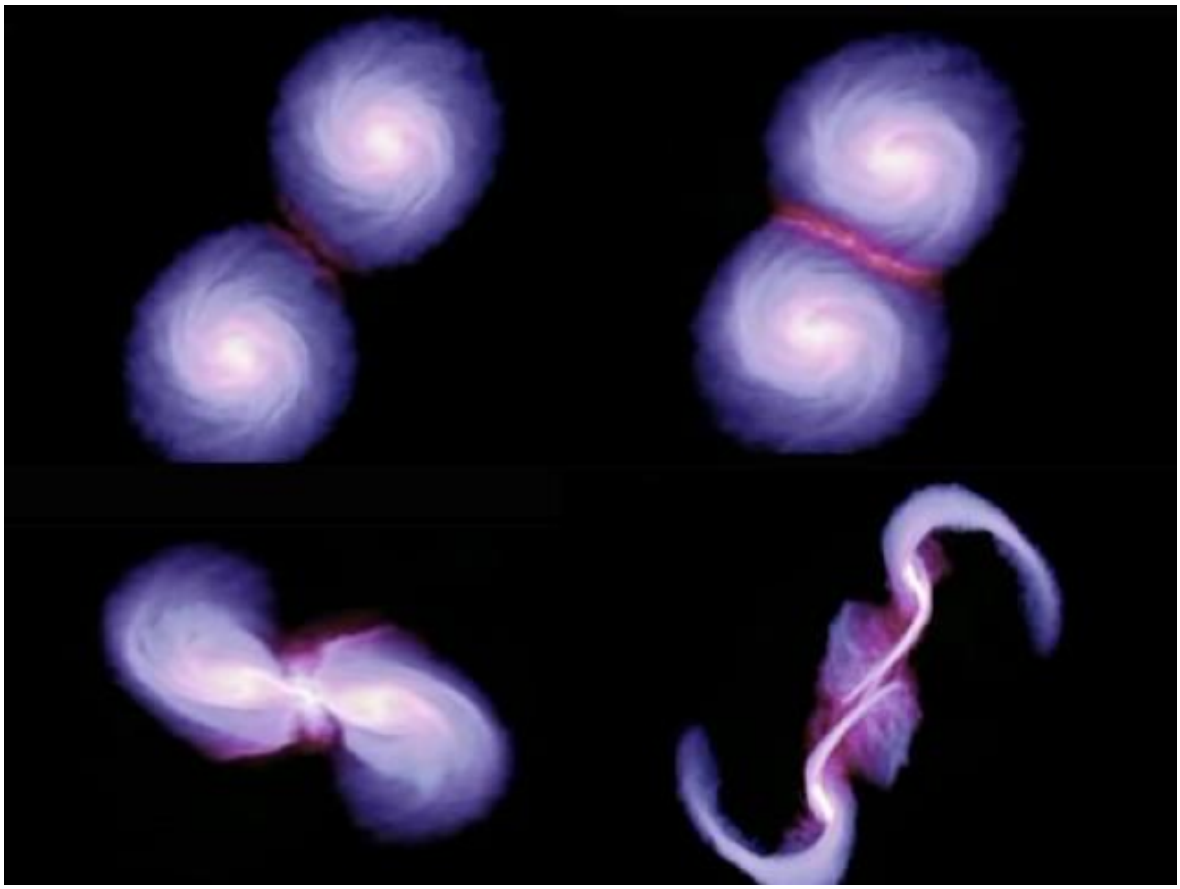

Figure 1.18: Representation of rotational dynamics in colliding galaxies [109].

all-together they initiate to rotate about a centre of mass. The angular speed of these combinations increases, which results into the compression of the group of stars into a flat disk with a lump at the centre [110].

The rotation or initial angular momentum of proto-galactic clouds (cloud of gas which is transform into a galaxy) i.e., the clouds having initial high value of angular momentum will end up attaining spiral shapes, having more young stars, more gas and blue in colour. The lower values of angular momentum or clouds with small rotational speed take the shape of spherical or elliptical galaxies, which are red in colour, have more old stars and lesser gaseous medium. Two spiral rotating galaxies collision results into an elliptical galaxy [6]. Density of the proto-galactic cloud decides the time of formation of galaxy and angular momentum provides the size of the disk. The origin of angular momentum in galaxies has been investigated by Peebles [111].

The rotation of galaxies has been studied by Jones [110] in which, it has been concluded that the angular momentum is low which has been derived from the orbital motion of merged galaxies. This spinning motion of galaxies continues even after their formation (different phases are shown in Fig. 1.18). Our Milky Way galaxy is among one of these rotating shapes and its entire disc comprised of stars, gas and dust is spinning at a speed of around 168 miles per second [109]. All the galaxies spins irrespective of their shape or size. Many studies are being carried out in the cosmology by Mather et. al., [109] which reveal that after the big-bang explosion, the galaxies were formed and then starts rotating. The collision of two rotating galaxies had produced the stars which were then converted into the planets like earth and the life of living beings was originated.

This type of study can be used as a motivation to the study the heavy ion reaction dynamics in nuclear physics. Mass symmetric and mass asymmetric nuclear reactions yields rotational effects in the participant and the spectator matter, which can be used for co-relating the rotational dynamics with splash off nuclei effects, squeeze-out effects and other collective flow effects in the intermediate energy range. Similar kind of study has been carried out by various theoreticians in literature [112–116].

The rotational dynamics in the nuclear reactions can be explored by analysing the average values of quantities i.e., <angular momentum/nucleon>, <moment of inertia/nucleon>, <angular velocity> and <rotational energy/nucleon> at the initial and freeze-out stage. Mathematically, these quantities about the axis normal to reaction plane ($y-axis$) can be expressed as follows [117],

$$L_y = \sum_i L_y(i) = \sum_i (z_i p_{xi} - x_i p_{zi}), \tag{1.9}$$

where L_y is the angular momentum, (x_i, z_i) are the position co-ordinates and (p_{xi}, p_{zi}) are the momentum co-ordinates of nucleons in the nucleus-nucleus (NN) center-of-mass frame (where the projectile and target have the same value of the linear momentum). All the nucleons which fall in the specific rapidity bin (see table 4.1) have been taken into consideration for the calculations.

The moment of inertia about the $(y-axis)$ [117]:

$$I_y = \sum_i I_y(i) = \sum_i m_i(r_i^2 - y_i^2), \tag{1.10}$$

where $r_i = \sqrt{x_i^2 + y_i^2 + z_i^2}$.

Similarly, the angular velocity around the $(y-axis)$ [117] :

$$w_y = L_y/I_y, \tag{1.11}$$

and the rotational energy [117],

$$E_{rot} = \frac{1}{2} I_y w_y^2 \tag{1.12}$$

This study can be helpful in many ways to theoreticians and experimentalists, as with the help of universal law of conservation of angular momentum, the angular velocity and moment of inertia of molecules/ions in atomic physics, galactic system's rotational energies and isotopes or radioactive elements separation by mass spectroscopy (by applying a electro-magnetic filter on the emitted fragments) can be measured easily.

The scaling between different components of flow is another interesting phenomenon to discuss. The following section will give an overview on this phenomenon.

1.9 Scaling of different flow harmonics: its origination and importance

Collective flow studies can be extended to identical particles. The nucleonic coalescence is the basic reason for the number-of-nucleon scaling [118]. While studying the anisotropic flow harmonics for different nucleons/fragments as a function of transverse-momentum, one visualises that the data points are ordered by the masses of the particles [119–122]. There is also a clear distinction between mesons and baryons at relativistic high energies. Scaling of flow coefficients by the quarks number, n_q (For mesons, $n_q = 2$ and for baryons, $n_q = 3$) removes this separation. Number of constituent-quark(NCQ)-scaling [123] for elliptic flow-transverse momentum dependence of unidentical mesons and baryons observed at RHIC was clarified by a quark coalescence model [124]. Since hadrons are simply integration of the constituent quarks, so flow

in the de-confined phase is directly changed into flow of the hadronic phase. A scaling law-inspired by constituent-quark coalescence or recombination models can account for the observed splitting between baryons and mesons [125].

When hadron generation is controlled by coalescence, the common curve formed after the recombination of quarks depicts the momentum-space anisotropy of constituent quarks before the hadron evolution [126]. Quark coalescence models assumes that in the intermediate transverse momentum range, particle production is influenced by recombining quarks: Two quarks travelling with the same momentum ends up as a meson with twice of the original quarks momentum, three quarks combines into a baryon with three times the quark momentum [127]. RHIC experimental data exhibited a scaling connection among $< v_n >$ and $< v_2 >$ as [127–129]: $v_n(p_t) \sim v_2^{n/2}(p_t)$. Denoting baryon flow by $v_{n,B}(p_t)$ and the meson flows by $v_{n,M}(p_t)$, it has been found that $v_{4,B}(p_t) = \frac{1}{3}v_{2,B}^2(p_t)$ for baryons and $v_{4,M}(p_t) = \frac{1}{4}v_{2,M}^2(p_t)$ for mesons, if quarks have no higher-order anisotropic flows.

At intermediate or low energies, this scaling phenomenon is replaced by the number-of-nucleon's scaling, where both $\frac{v_2}{A}$ verses $\frac{p_t}{A}$ and $\frac{v_1}{A}$ verses rapidity, for light nuclear fragments approximately merge on the single curve respectively. Before scaling or we can say without dividing these observable by its number-of-nucleon (A), the values of both $< v_1 >$ and $< v_2 >$ are different for different-mass clusters, indicating that there exists $< v_1 >$ and $< v_2 >$ scaling on the number-of-nucleon. If the scaling laws for baryons (NCQ = 3) and mesons (NCQ = 2) are assumed, then the above two equations are also valid for A = 3 and 2 nuclear clusters, respectively, then $< v_4/v_2^2 >$ for A = 3 and 2 clusters indeed provide the similar value of the $\frac{1}{2}$ as nucleons. So, the ratio $< v_4/v_2^2 >$ is approximately 1/2 independent of the values of transverse momentum [119–122].

The theoretical attempts to study nuclear flow and their scaling will be discussed in next section.

1.10 Theoretical literature review on flow, rotational dynamics and scaling

Several investigations have been carried out to study the different coefficients ($< v_1 >$, $< v_2 >$, $< v_3 >$ and $< v_4 >$) of anisotropic flow, their scaling and rotational phenomenon. The first harmonic coefficient of flow was studied theoretically by H. Stöcker et al. [27]. They predicted the directed flow for non-central collisions on the basis of fluid dynamical measurements. Using the time evolution of the Wigner function for ${}^{40}_{18}Ar + {}^{208}_{82}Pb$ at 770 MeV/nucleon with the help of the Vlasov-Uehling-Uhlenbeck theory and intermediate impact parameters, the sidewards flow of the participant matter and the bounce-off effect of the projectile fragments have been studied [130].

A transverse-momentum method has been used at 1.8 GeV/nucleon energy for ${}^{40}_{18}Ar + KCl$ reaction by P. Danielewicz et al. [131] to analyse charged-particle data for collective flow and predicted that collective effects are weaker than in the hydrodynamical model but considerably more in strength in the Cugnon cascade model [131]. Transverse momentum distributions are calculated with the help of Boltzmann equation for different nucleon-nucleon cross sections and nuclear equations of states by G.F. Bertsch [132]. Later on, many attempts has been carried out to study directed flow to understand many features like its dependence on equation of state at high energy [133]. Rapidity dependance of transverse flow for different reactions at high energies have been studied by A. Bonasera and L. P. Csernai [134]. At intermediate energies, transverse flow as a function of rapidity for different NEOS has been studied by G. Peilert et al. [75] and C. Gale et al. [76].

The outset of the transverse momentum distribution in heavy-ion collisions has been studied by B. Bl*ä*ttel et al. [135] and it has been found that their origin depends strongly on the rapidity constraints. In addition to this, the mass and impact-parameter dependence indicates that the peripheral collisions has been found to be useful to inquest the mean-field's momentum dependence [135]. Directed flow in the mid-rapidity zone for nucleons and pions at high energy ${}^{197}_{79}Au + {}^{197}_{79}Au$ collisions using RQMD Model [136] were studied by Snellings et al. [137].Wang further studied directed flow at interme-

diate energies for $^{197}_{79}Au +^{197}_{79} Au$ using different options in Ur-QMD and FOPI data is compared [138].

The introduction of E_{bal} in heavy-ion collisions has been studied by measuring the excitation function of the average in-plane transverse momentum at incident energies 50, 70, and 130 MeV/nucleon for the symmetric colliding system $^{139}_{57}La +^{139}_{57} La$ using Boltzmann-Uehling-Uhlenbeck equation by D. Krofcheck et al. [139]. Using a Boltzmann-Uehling-Uhlenbeck transport model, the dependance on in-medium cross section has been discussed by B. A. Li [140]. Using the framework of the quantum molecular dynamics model, in-medium cross section (G - matrix) and energy-dependent cross section, different nucleon-nucleon cross sections have been simulated and the impact parameter dependence of the disappearance of flow has been examined by Faessler et al., [141, 142]. Transverse flow and its disappearance has been studied involving masses between 24 and 394 at central collisions by A. D. Sood et al. [143] and found that the momentum-dependent interactions behaves differently in lighter colliding nuclei as compared to heavier colliding nuclei.

The role of isospin on E_{bal} and its mass dependence over the mass range on two different sets of isobaric systems with N/Z = 1 and 1.4 for central to peripheral colliding impact parameters has been investigated by S. Gautam [144] and is has been exhibited that the Coulomb interactions play a dominant role over isospin effects on E_{bal}. The symmetry energy influence the energy of vanishing flow is uniform for the input parameters [144]. Furthermore, different aspects of transverse flow are studied by many other groups [22, 145–160].

The second harmonic of flow(elliptic flow) was introduced theoretically by H. Sorge [28]. Later on, many theoreticians have investigated different aspects of elliptic flow. Stocker et al. [161] introduced the emission of nucleons from mid-rapidity zone in the direction perpendicular to the reaction plane. Introduction of the transition of nuclear matter emitted from in-plane to out of plane was brought forward by NAUTILUS Collaboration at GANIL in 1994 using $^{66}_{30}Zn +^{57}_{28} Ni$ reaction. Using the relativistic transport model (ART), excitation functions in central Au+Au collisions have been studied from SIS/GSI to AGS/Brookhaven [162]. Using a relativistic hadron transport model, in-

vestigation of the utility of the $< v_2 >$ excitation function as a inquest for onset of a possible quark-gluon-plasma phase transition and the stiffness of nuclear matter at alternating-gradient synchrotron energies ranging from 1 to 11 A GeV has been studied by P. Danielewicz et al. [163].

The approach and methods for inspecting $< v_2 >$ in relativistic nuclear collisions and the significance of the use of the azimuthal distribution's Fourier expansion has been presented by Poskanzer [164]. The study of $< v_2 >$ of proton at energies ranging between 30 and 100 MeV/nucleon in collisions of $^{48}_{20}Ca +^{48}_{20} Ca$ using isospin-dependent transport model has been carried out by Zheng et al [165] and revealed that with enhancement in incident energy, $< v_2 >$ shows a transition from positive flow to negative flow. The magnitude of $< v_2 >$ depends on both the nuclear equation of state (EOS) and the nucleon-nucleon scattering cross section.

Elliptic flow as a function of rapidity for different time-steps, energy and systems is investigated using RQMD model by Liu et al. [166]. It has been revealed that $< v_2 >$ for both $^{40}_{20}Ca +^{40}_{20} Ca$ and $^{112}_{50}Sn +^{112}_{50} Sn$ systems is not sensitive to EOS and study of the dependence of $< v_2 >$ on the fragment charge (mass) has been performed by Zhang et al. [59]. Using realistic dynamical cascade model, the systematic study of elliptic flow from SIS to RHIC energies has been carried out by Sahu et al. [167] and results with the data from PHOBOS and STAR collaborations at RHIC for elliptic flow of charged particles at mid-rapidity in $^{197}_{79}Au +^{197}_{79} Au$ collisions have also been checked. The systematic study of elliptic flow and the comparison with several experimental data is checked for p_t, rapidity, pseudo-rapidity dependance and for E_t [168].

$< v_2 >$ and E_t dependence on system size using improved quantum molecular dynamics model (ImQMD05) for $Z \leq 2$ particles at intermediate energies has been studied by Zhang and showed that a soft nuclear equation of state and incident energy dependent in-medium nucleon-nucleon cross-sections are required to explain the elliptic flow's excitation function at these energies [59]. Using the isospin-dependent quantum molecular dynamics (IQMD) model, the interplay among the participant and spectator matter in heavy-ion collisions has been explored by S. Kumar et al. [169] by exploring the effect of different rapidity constraints.

Influence of initial fluctuation effect on the elliptic flows for ^{197}Au +^{197} Au at 1 GeV/nucleon has been presented using IQMD model [170]. Y. Wang [138] studied the $< v_2 >$ of light particles (protons, He, neutrons, tritons and deuterons) in ^{197}Au+^{197}Au collisions at beam energies between 150 and 400 MeV/nucleon and the results has been compared with the experimental data(FOPI). Very recently, Using the iEBE-VISHNU hybrid model with AMPT initial conditions, the study has been carried out for the higher order flow harmonics of identified hadrons for $^{208}_{82}Pb$ +$^{208}_{82}$ Pb collisions at 2.76 TeV/nucleon and results has been compared with the ALICE measurements [171]. At the Relativistic Heavy Ion Collider(RHIC), the effect of an anisotropic escape mechanism on elliptic flow in $^{197}_{79}Au$ +$^{197}_{79}$ Au collisions in relativistic heavy-ion collisions at $\sqrt{S_{NN}}$ = 200 GeV and at $\sqrt{S_{NN}}$ = 2.76 TeV in $^{208}_{82}Pb$+$^{208}_{82}Pb$ collisions at Large Hadron Collider has been investigated by A. Jaiswal [172].

Higher harmonics has been investigated mainly in relativistic high energy heavy-ion collisions. Utilizing a transport + hydrodynamics hybrid model, investigation of the incident energy dependence of triangular flow $< v_3 >$ in $^{197}_{79}Au$+$^{197}_{79}$ Au collisions within the energy range $\sqrt{s_{NN}}$ = 5 to 200 GeV has been carried out by J. Auvinen et al., [173]. In ultra relativistic heavy-ion collisions, using viscous and ideal hydrodynamics transport theory, the study of triangular ($< v_3 >$) flow in contrast with the elliptic flow ($< v_2 >$), quadrangular flow ($< v_4 >$), pentagonal flow ($< v_5 >$) has been carried out with quantitative forecasts for $< v_3 >$ at LHC and RHIC as a function of centrality. Transverse momentum has also been examined [106]. Using a multi-phase transport model (AMPT), triangular flow investigation is carried out by Alver et al. [174].

Petersen predicted the foremost measurement of $< v_3 >$ using transport+hydrodynamics hybrid approach at $\sqrt{s_{NN}}$ = 200 A GeV in ^{197}Au+^{197}Au collisions and revealed that the $< v_3 >$ exhibits very less centrality dependence and its value is approximately near to elliptic flow in most central collisions. Furthermore, investigation of the rapidity and transverse momentum dependence of $< v_2 >$ and $< v_3 >$ for identified particles as well as charged particles has also been explored [175]. Many other theoreticians also studied higher harmonics and their dependance on various parameters using different theoretical models at high energies [176–180].

Mass asymmetric systems has been used to study the rotational dynamics and scaling of flow harmonics. Flow observable (directed and elliptic flow) has been studied in the literature to explore different aspects like balance energy or energy of vanishing flow [72, 130, 131]. S. Goyal studied the role of colliding geometry on balance energy of mass asymmetric systems [181]. V. Kaur et al. [182] reported the role of different equations of state as well as Coulomb interactions on the disappearance of transverse flow for various mass asymmetric reactions ${}^{56}_{26}Fe + {}^{96}_{44}Ru$, ${}^{50}_{24}Cr + {}^{102}_{44}Ru$, ${}^{40}_{20}Ca + {}^{112}_{50}Sn$, ${}^{32}_{16}S + {}^{120}_{50}Sn$, ${}^{28}_{14}Si + {}^{124}_{54}Xe$ and ${}^{16}_{8}O + {}^{136}_{54}Xe$. Elliptic flow transition from in-plane to out-of-plane for charged particles has been studied for various mass asymmetric systems ${}^{50}_{24}Cr + {}^{102}_{44}Ru$, ${}^{32}_{16}S + {}^{120}_{50}Sn$ and ${}^{16}_{8}O + {}^{136}_{54}Xe$ by V. Kaur et al. [183].

Y. G. Ma et al. has studied rotational behaviour using Boltzmann-Uehling-Uhlenbeck (BUU) model for mass asymmetric reaction ${}^{40}Ar + {}^{27}Al$ at impact-parameter, b = 4.5 fm [112]. The azimuthal distributions of protons has been calculated for different rapidity regions and fitted by Legendre polynomial. In addition to this, the in-plane flow and out-of-plane flow has been extracted by fitting coefficients from the mid-rapidity region. It has been concluded that these flow coefficients depend strongly on the nuclear equation of state and nucleon-nucleon cross-section [112]. Later on, the azimuthal correlations has been investigated for ${}^{40}Ar + {}^{27}Al$ reaction at incident energies between 36 MeV/nucleon and 100 MeV/nucleon and different impact-parameters using QMD model [113]. The energy at which rotational flow vanishes has been calculated using azimuthal correlation function [113].

The azimuthal correlation and azimuthal distribution of light charge particles have been studied for mass asymmetric reaction ${}^{84}Kr + {}^{27}Al$ at incident energy 10.6 MeV/nucleon by Shen et al. [114]. After that, the two-particle azimuthal correlations for deuteron, triton and alpha particles at mid-central collisions has been explored for reaction ${}^{84}Kr + {}^{27}Al$ at incident energies between 35 MeV/nucleon and 100 MeV/nucleon. Disappearance of rotational flow has also been calculated [115]. The isospin effect on rotational flow has been studied using IQMD model for ${}^{58}Fe + {}^{58}Fe$ and ${}^{58}NI + {}^{58}Ni$ reactions at 40 MeV/nucleon for mid-rapidity zone. The rotational quantities like angular momentum, moment of inertia, rotational energy and angular velocity of nucleons

have been calculated [115]. The nucleons are selected on the basis of their participation in mid-rapidity region. It has also been calculated that the neutron rich $^{58}Fe +^{58} Fe$ reaction shows stronger rotational collective flow. Meanwhile, it has also been indicated that the rotational flow is an impact-parameter dependent observable.

Scaling of different components of flow has been investigated theoretically by many theoretical groups. Few of them have been discussed here briefly: The foremost investigation on scaling at intermediate energies using IQMD model for $^{86}Kr +^{124} Sn$ at large centralities is by Y. G. Ma group. Number-of-nucleon scaling of the v_2 has been exhibited for the light mass fragments up to A = 4, and the ratio of $< v_4/v_2^2 >$ comes out to be a constant factor of 1/2 [119].

$< v_2 >$, $< v_2/A >$, $< v_4/A >$ and $< v_4/v_2^2 >$ has plotted as a function of P_t/A for different mass fragments (A = 2, 3 and 4), neutron and protons by varying the cross-sections and symmetry energy term. Also, $< v_4/v_2^2 >$ as a function of P_t gives a constant value of 0.5 independent of transverse momentum. It is shown that the increasing positive values for all cases with increasing P_t and phenomenon is same as RHIC results. The number-of-nucleon scaling for $< v_2 >$ occurs for light mass fragments at low value of P_t/A($< 0.2GeV/c$) similar to quark scaling of $< v_2 >$ vs P_t/n for different baryons and mesons observed at RHIC independent of the details of EOS and symmetry potential. Strength of v_2/A is sensitive to symmetry potential and EOS. Significant difference has been observed for n and p as compared to A = 2, 3 and 4 , because they encounter the effect of mean field (EOS) directly [120].

Y. G. Ma et al. [121], using IDQMD model simulated $^{40}Ca +^{40} Ca$, $^{86}Kr +^{58} Ni$ and $^{86}Kr +^{124} Sn$ reactions were simulated at incident energy E = 25 MeV/nucleon, impact parameter b = 4-6 fm, 6-10 fm and 7-11 fm for Hard EoS, Soft EoS with symmetry and without symmetry energy. It has been investigated that the number-of-nucleon scaling exists for $< v_1/A >$ for rapidity intervals. $< v_2/A >$ versus P_t/A for light mass fragments and showed that it originates from nucleonic coalescence. The scaled curves merge on each other but for P_t/A<0.25 GeV/c. This phenomenon is comparable to quarks scaling of $< v_2 >$ against P_t/n for baryons and mesons seen at RHIC and the constant factor for $< v_4/v_2^2 >$value does not depend on iso-spin dependent term, EoS

and P_t. The scaling laws for baryons (NCQ = 3) and mesons (NCQ = 2) are also valid for A = 3 and 2 nuclear clusters resp., then $< v_4/v_2^2 >$ for A = 3 and 2 clusters indeed provides the similar value of 1/2 as nucleons too.

After discussing various theoretical attempts to study nuclear flow, the next section will provide an overview on experimental facilities available to study nuclear flow and the various experimental attempts.

1.11 Experimental facilities available to study flow

Due to its attractive features, anisotropic flow harmonics have been experimentally measured by many collaborations. *Diogene* collaboration at *Saturne Synchrotron in Sachley (France)* [184, 185], *Plastic Ball/Wall at BEVALAC in Berkeley* group [71], *GANIL* facility used by *NAUTILUS* collaboration [186], *MINIBALL/ALADiN* Collaboration [57, 83], *STAR* collaboration at *NSCL, MSU(USA)* [187], *FOPI, ALADiN* collaboration at *GSI* [60] and *INDRA* collaboration at *GANIL* [188]. Out of them, brief summary of *FOPI* detector at *GSI/SIS* is given below [189]:

To investigate the properties of hot and dense nuclear matter, the FOPI detector system has been built at GSI/SIS (shown in Fig. 1.19). The accomplished system has been constructed in three stages which covers roughly the full 4π solid angle : (i) The forward plastic wall detector was completed in 1990 (an inner shell of 188 energy loss detectors and 764 scintillators) employed to measure the velocity and charge of all charged particles scattered with laboratory polar angles ranging between $1^o < \theta_{Lab} < 30^o$ over the full azimuth. (ii) Central Drift Chamber and the super-conducting solenoid was completed in 1992 within a widespread angular range of $30^o < \theta_{Lab} < 150^o$ enabled charged particles momentum determination. (iii) The plastic scintillator/Cherenkov Barrel and completed in 1995, is useful in velocity determination [189]. The illustration of production and flow of neutral strange particles for Ni+Ni collisions at 1.93 GeV/A is shown in Fig. 1.20.

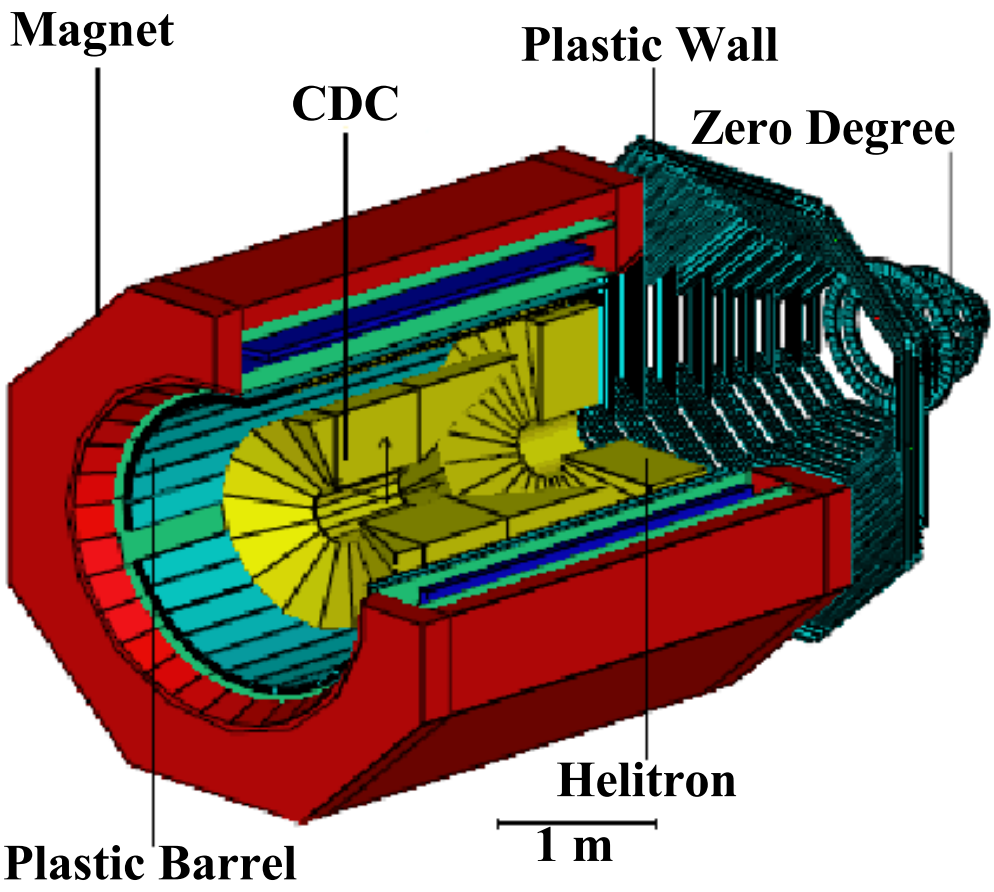

Figure 1.19: Schematic diagram of FOPI detector [190].

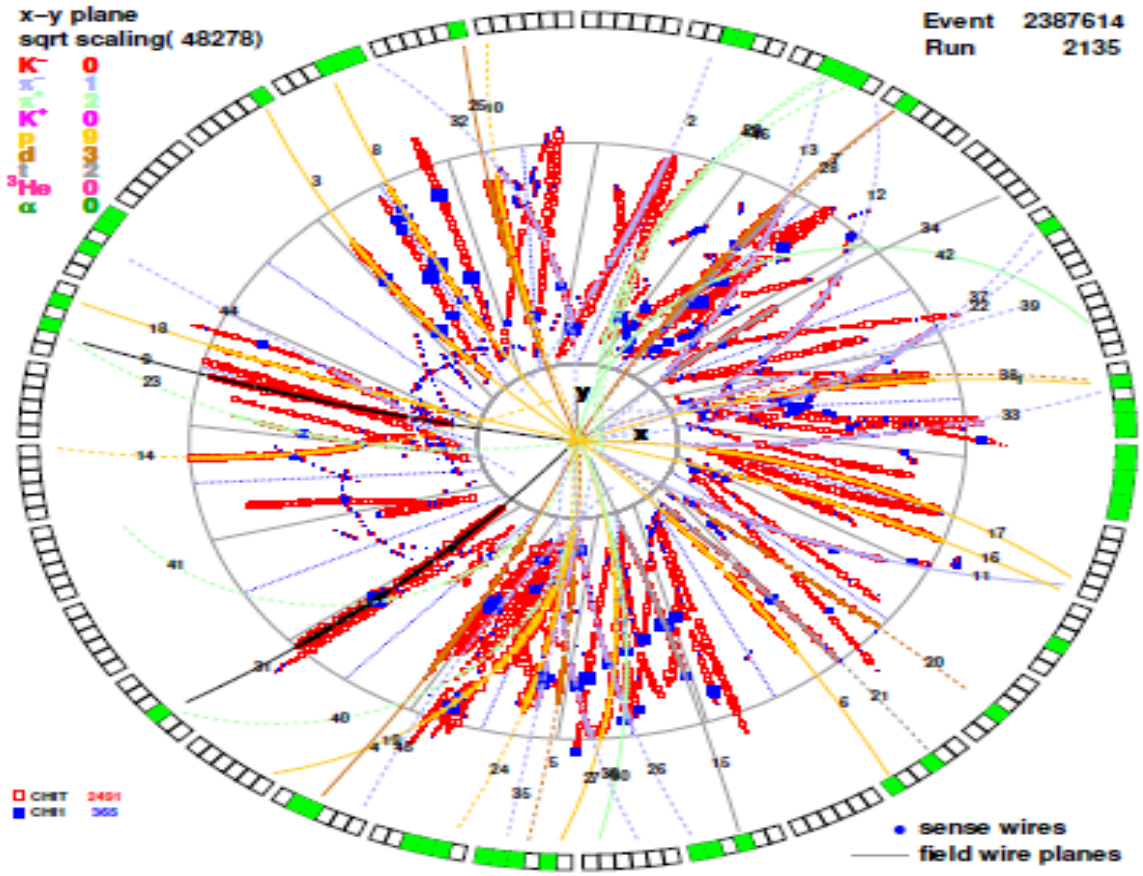

Figure 1.20: Cross-sectional view of central $^{58}_{28}Ni + ^{58}_{28}Ni$ collisions measured with CDC in transverse-plane [190].

1.12 Experimental Literature review on flow

Many experimental attempts have been made to study the process of collective flow. The very first experimental finding of directed flow has been made at the Bevalac with collisions of $^{93}_{41}Nb + ^{93}_{41}Nb$ and $^{40}_{20}Ca + ^{40}_{20}Ca$ at 400 MeV/nucleon with the Plastic Ball/Plastic Wall detector [71]. The Plastic Ball data revealed for first time the two different collective flow effects: the participant's side-splash and the bounce off in the fragmentation region [71]. To provide information on collective flow, experimental results on the formation of light particles (A $<$ 5) and intermediate mass fragments (6 $<$ A $<$ 18) have been produced by Harris et al. [191] for the reactions of $^{197}_{79}Au + ^{197}_{79}Au$ and $^{197}_{79}Au + ^{56}_{26}Fe$ at 200 MeV/nucleon [191].

Zheng et al., [192] constructed experimentally the reaction plane of high-multiplicity

$^{197}_{79}Au +^{197}_{79} Au$ collisions at incident energies between 75 and 650 MeV/nucleon which was decided by calculating the transverse velocity of charged fragments. It has been forecasted that the beginning of flow in high multiplicity $^{197}_{79}Au+^{197}_{79}Au$ collisions occurs at a low beam energy below 60 MeV/nucleon [192]. FOPI detector at SIS has provided experimental data for $^{197}_{79}Au +^{197}_{79} Au$ collisions at 400 MeV/nucleon for different rapidity intervals [193]. By the collision of Pb beam with a Pb target at the semi-central impact-parameters, Appelsh*ä*user et al., (NA49 Collaboration) [194] experimentally calculated the directed flow of charged pions and protons at energy 158 GeV/nucleon. The rapidity and p_t dependence of the flow has also been calculated [194]. Directed flow for $^{197}_{79}Au +^{197}_{79} Au$, $^{131}_{54}Xe + CsI$ and $^{58}_{28}Ni +^{58}_{28} Ni$ at incident energy between 90 to 400 MeV/nucleon is measured experimentally by Andronic et al., (FOPI Collaboration) [195] and experimental data is compared with IQMD model calculations.

Under various assumptions on the nucleon-nucleon cross section, the investigation of centrality dependence of deuteron and proton in $^{101}_{44}Ru+^{101}_{44}Ru$ collisions at incident energy 400 MeV/nucleon has been carried out by Hong et al. [196] (FOPI Collaboration) and extracted data have been compared with IQMD calculations for different rapidity intervals. In isospin asymmetric collisions, the calculations of the ratio of baryon rapidity distributions displays incomplete mixing of the target and projectile nuclei. Partial transparency at the said beam energy has also been observed [196]. Directed flow has been studied at incident energies between 40 and 150 MeV/nucleon in the $^{197}_{79}Au+^{197}_{79}Au$ collisions by (ALADIN and INDRA Collaborations). The reactions have been calculated with the 4π multi-detector INDRA at the GSI facility [188].

At incident energies between 40 and 150 MeV/nucleon, directed flow for the $^{197}_{79}Au+^{197}_{79}$ Au system has been measured using the INDRA 4π multi-detector and claimed that directed flow changes its sign as bombarding energy increases from 50 to 60 MeV/nucleon [83]. Reisdorf et al.(FOPI collaboration) [60] calculated the experimental data on different aspects of directed flow for $^{40}Ca +^{40} Ca$, $^{58}Ni +^{58} Ni$, $^{96}Ru +^{96} Ru$, $^{96}Zr +^{96} Zr$, $^{129}Xe + CsI$ and $^{197}Au +^{197} Au$ for different energies and centralities. The data has also been compared to earlier data and with calculations of transport models [60].

Mass asymmetric systems have influenced the reaction dynamics of directed flow and

many experimental groups have studied these effects in the literature [80–82]. D. Krofcheck et al. have studied the collective flow of $^{40}_{18}Ar +^{51}_{23} V$ collisions for light fragments from the K1200 cyclotron of the National Superconducting Cyclotron Laboratory [197]. The first systematic study of the entrance-channel mass dependence of the E_{bal} is carried out by Westfall et al. [72] for the $^{12}_{6}C +^{12}_{6} C$, $^{20}_{10}Ne +^{27}_{13} Al$, $^{40}_{18}Ar +^{45}_{21} Sc$, and $^{84}_{36}Kr +^{93}_{41} Nb$ systems. It was showed that E_{bal} scales as $A^{1/3}$ where A is the mass of the combined system using Michigan State University 4π Array at the National Superconducting Cyclotron Laboratory (NSCL) with beams from the K1200 cyclotron. Huang et al. bombarded $^{78}_{36}Kr$ beams at $^{197}_{79}Au$ targets with energy 200 MeV/Nucleon at Laboratoire National SATURNE at Saclay to calculate sideward fragment flow [198]. $^{64}_{30}Zn +^{27}_{13} Al$ reactions were measured by Zhi. et al. for light charged particles at beam energies 49, 57, 69 and 79 MeV/Nucleon with a 4π multidetector array at GANIL [199]. At the BEVELAC, Plastic-Ball group in Berkeley have been the foremost group to quantify the squeeze-out in symmetric systems [98, 99]. E_t(transition energy) was first observed at GANIL by the NAUTILUS Collaboration using Zn+Ni reaction in 1994 [200]. The theoretical observations are in agreement with the experimental results of FOPI, INDRA and ALADIN Collaborations [57,83]. The MINIBALL/ALADIN Collaboration observed the outset of out-of plane expansion of the excited nuclear matter for $^{197}_{79}Au +^{197}_{79} Au$ reaction at the incident energy of 400 MeV/nucleon [57, 83].

Further, these observations have been being studied by the E895 Collaborations, with the measurement of proton elliptic flow in $^{197}Au +^{197} Au$ at the beam energies of 2-8 GeV/nucleon and seen the cross-over to in-plane at about 4 GeV/nucleon [101, 201]. The excitation function of $< v_2 >$ from low energies to relativistic energies for $^{197}_{79}Au +^{197}_{79} Au$ reaction has been also studied by E895 collaboration and very interestingly, a change in sign of $< v_2 >$ have been reported around energy 100 MeV/nucleon [202, 203]. Crochet found that $< v_2 >$ becomes less positive in value (over the entire rapidity region) or more negative (in the mid-rapidity region) with the enhancement in the beam energy, up to a some value of energy, and then again changes its sign [204].

Excitation function of $< v_2 >$ has been also verified experimentally by Bastid et

al. [205]. FOPI Collaboration also provided information regarding the relation of the global stopping with flow as well as with the cluster formation during expansion [25, 206–208]. Experimentally, transition energy is explored by NA49 [209] for pions and for E877, STAR [187], PHENIX [210], CERES [211–213], PHOBOS [214] and provided data for the charged particle flow. Many other experimental groups also explored different aspects of elliptic flow [215–221]. The FOPI collaboration gives a good number of experimental data on various dependents of elliptic flow [60].

The first measurement of the higher harmonics $< v_3 >$, $< v_4 >$, and $< v_5 >$ of charged particles at $\sqrt{S_{NN}} = 2.76$ TeV in ${}^{208}_{82}Pb + {}^{208}_{82}Pb$ collisions, with the ALICE detector [222–224] has been observed. The measurements by STAR collaboration for the v_4 as a function of particle-type, pseudo-rapidity, transverse momentum and centrality in ${}^{197}_{79}Au + {}^{197}_{79}Au$ collisions at RHIC is explored by Y. Bai and P. Soren [225,226]. Despite many efforts, the investigation on the influence of rapidity constraints on anisotropic flow, their scaling and rotational dynamics at intermediate energy has not been studied widely. Therefore, the main objective of this thesis is to explore the collective flow as a function of rapidity in intermediate energy regime. Moreover, the investigation on the effect of scaling and rotational dynamics study among the mass asymmetric nuclear reactions has also been included.

1.13 Organisation of thesis

The thesis has been organized below:

- In **Chapter 2**, a brief description of various isospin dependent primary and secondary models has been discussed. The primary model used to carried out present work i.e., Isospin-dependent Quantum Molecular Dynamics (IQMD) model has been discussed thoroughly. In addition, the various clusterization techniques has also been briefed.

- In **Chapter 3**, the elliptic flow of nucleons as a function of rapidity has been studied for the reactions of ${}^{197}_{79}Au+{}^{197}_{79}Au$, ${}^{150}_{60}Nd+{}^{150}_{60}Nd$, ${}^{124}_{50}Sn+{}^{124}_{50}Sn$, ${}^{96}_{44}Ru+{}^{96}_{44}Ru$, ${}^{78}_{36}Kr+{}^{78}_{36}Kr$, ${}^{48}_{20}Ca+{}^{48}_{20}Ca$ and ${}^{40}_{20}Ca+{}^{40}_{20}Ca$. Our findings reveal that the sigma (width) of yield obtained varies with mass of colliding system at a given energy. Transition energy as well as width of distribution of nucleons as a function of rapidity depends on the mass of fragment for a given centrality. The results of elliptic flow as a function of rapidity and transition energy are also compared with experimental data.

- In **Chapter 4**, the rotational dynamics has been studied for different mass asymmetric systems ${}^{122}_{49}In+{}^{126}_{50}Sn$, ${}^{114}_{48}Cs+{}^{134}_{54}In$, ${}^{100}_{40}Mo+{}^{148}_{64}Gd$, ${}^{86}_{36}Kr+{}^{162}_{67}Ho$, ${}^{71}_{31}Ga+{}^{177}_{71}Lu$, ${}^{60}_{28}Ni+{}^{188}_{76}Os$ and ${}^{50}_{24}Cr+{}^{198}_{78}Pt$ for incident energies between 40 MeV/nucleon and 400 MeV/nucleon for impact parameter range $0.25 < \hat{b} < 0.45$ using IQMD model. Our calculations reveal that the time evolutions of rotational quantities for participant and spectator nuclear matter are different in mass asymmetric heavy ion reactions. Theoretical data of BUU model's azimuthal distributions for free protons have been compared successfully with IQMD model calculations. The rotational flow of free protons with increasing incident energies and elliptic flow (calculated from the fits of azimuthal distributions of free protons) dependence with energy has also been investigated.

- In **Chapter 5**, scaling of anisotropic flow (directed and elliptic flow) of fragments have been studied in mass asymmetric nuclear reactions ${}^{122}_{49}In+{}^{126}_{50}Sn$, ${}^{114}_{48}Cs+{}^{134}_{54}$

In, $^{100}_{40}Mo +^{148}_{64} Gd$, $^{86}_{36}Kr +^{162}_{67} Ho$, $^{71}_{31}Ga +^{177}_{71} Lu$, $^{60}_{28}Ni +^{188}_{76} Os$, $^{50}_{24}Cr +^{198}_{78} Pt$ and $^{40}_{20}Ca+^{208}_{82}Pb$ for incident energies between 50 MeV/nucleon and 400 MeV/nucleon at the range of centrality $0.25 < \hat{b} < 0.45$ using IQMD model. Our findings reveal that strength of flow depends on the fragment mass, rapidity intervals and mass asymmetry content of the reaction. Rapidity constraints plays a dominant role in the calculation of scaling of fragments.

- In **Chapter 6**, the summary and outlook of the thesis have been discussed.

Chapter 2

Methodology

2.1 Introduction

The dynamics at intermediate energies needs a precise knowledge of nucleon-nucleon collisions as well as mean field. In addition to this, the collisions of neutron rich nuclei or nuclei away from the drip line also need correct information about their isospin degree of freedom. The isospin enters into the calculations via the real part of iso vector (symmetry) potential, Coulomb potential and through imaginary part as Pauli blocking and isospin dependent in-medium nucleon-nucleon cross sections. Several comprehensive isospin-dependent and mostly semi-classical transport model such as IBUU (isospin-dependent Boltzmann-Uehling-Uhlenbeck) [227, 228], FMD (Fermionic Molecular Dynamics) [229–232], AMD (Antisymmetric Molecular Dynamics) [233–235], ImQMD (Improved Quantum Molecular Dynamics) [236] and IQMD (Isospin dependent Quantum Molecular Dynamics) [19] have been well utilized in recent years to explain nuclear reactions influenced by neutron-rich nuclei in intermediate energy range [237].
Initially, author has given an overview of the models that explain the reaction mechanism taking isospin effects into account. These models are capable to explain the essential isospin physics which govern the complex interactions among the neutrons and protons (particles with different charge states interacting inside reaction zone).

2.2 Different theoretical models based on iso-spin effects:

2.2.1 Isospin-dependent Boltzmann-Uehling-Uhlenbeck (IBUU)

The isospin-dependent Boltzmann-Uehling-Uhlenbeck (IBUU) [227, 228] is a modified form of BUU (Boltzmann-Uehling-Uhlenbeck) [238] transport model. It has the capability to describe several isospin based phenomena successfully in heavy ion collisions at intermediate energies like nuclear flow and stopping. The BUU equation gives an accurate depiction of the time dependence of the one body distribution function. Precise explanation of the BUU equation average out the fluctuations in the density that might result in the formation of fragments in a single collision. This is commonly attained by resolving the BUU equation with a number of test particles per nucleon N_{test}.

In this model, isospin dependence was involved in the dynamics by using the elementary nucleon-nucleon cross sections, the nuclear mean field, the symmetry, and Coulomb potential. This model has been utilised to measure the fraction of yield of neutrons to protons in pre-equilibrium emission. In BUU equation, the density fluctuations that give rise to the fragment production are suppressed, this is the reason that, the calculation of fragment yield is not possible using, BUU model. To overcome these drawbacks, alternate model like, Isospin dependent Quantum Molecular Dynamics (IQMD) model has been developed to address the density fluctuations.

2.2.2 Fermionic Molecular Dynamics (FMD)

In the initialization of QMD type models, the initialized nuclei are not truly in their ground state with reference to the Hamiltonian that has been used for the propagation of nuclei. The parameters of the Hamiltonian are modified equivalently with the infinite nuclear matter equation of state, in accordance with the properties of finite nuclei i.e., its root mean square radius and binding energy. Nevertheless, the nucleus would fall to a single point in the momentum space, if the energy of the nucleons among the nucleus is minimized with respect to the Hamiltonian. The convenient an-

swer to this complication is the involvement of nucleons's Fermionic properties through the anti-symmetrization of the its wave function. This approach was refined by Feldmeier [229–231] and is termed as Fermionic Molecular Dynamics (FMD).

This model links from the very beginning Fermi-Dirac statistics with a semi-quantum trajectory illustration. It changes into classical molecular dynamics in the limit where the system's phase space is reduced i.e., low density and for high temperature(low mass systems). This model does not explain all wave mechanical interference effects, therefore is not termed as fully quantum mechanical. Though, the Fermi-Dirac statistics is admitted on the many-body level. The elementary objective of this model is to find a parametrization which include important degrees-of-freedom of the system.
It is a true quantum mechanical treatment that symbolize the many-body state as an anti-symmetrized Slater determinant, made from single particle wave packet of Gaussian form. FMD models includes very flexible basis with clusters and can be applied to lighter nuclei. However, it has several disadvantages too like numerical difficulties so, correct calculations are not possible. Moreover, the interactions have to be soft in operator form and also much more tough to involve boundary conditions for resonance or scattering states [232].

2.2.3 Antisymmetrized Molecular Dynamics (AMD)

The above FMD approach has been limited by omitting the change in time of the width parameters and spin wave functions [233–235]. By doing so, it becomes feasible to handle many-nucleon systems. In addition to this, it has been verified that the anti-symmetrized version of the molecular dynamics linked with the frictional cooling method [239] is capable for the investigation of nuclear structure because this method is free from model suppositions such as axial symmetry and clustering structure. Though, it is essential to involve the nucleon-nucleon collisions process to treat heavy-ion collisions. Ono et al. [240–243] have been succeeded in including the nucleon-nucleon collisions into the anti-symmetrized version of molecular dynamics termed as Anti-symmetrized Molecular Dynamics (AMD) model.
Another distinction of this approach from the FMD approach is the width parameter

which is constant in AMD, but dynamical variable in FMD. The main disadvantage of this approach is that, the total angular momentum conservation is violated in nucleon-nucleon collisions and thus the measured values of the AMD fragments's spins may not be so trustworthy. Furthermore, like FMD, the use of AMD model is also restricted due to critical numerical problems, to lighter nuclear systems only.

2.2.4 Improved Quantum Molecular Dynamics (ImQMD)

Further refinement in the QMD (by including isospin degree of freedom) is carried out at Chinese Institute of Atomic Energy (CIAE) by Wang et al. [236] in order to explore the fusion reactions (near barrier) and termed it as Improved Quantum Molecular Dynamics (ImQMD) model. In this model, neutrons and protons density distributions are achieved by means of Relativistic Mean Field (RMF) calculations. Later on, same group [244] modified this model, to attain the stability of individual nucleus to investigate the dynamical process of fusion reactions.

The major refinement is in the potential energy functional parameters. The conventional potential energy parameters are replaced by new parameters, which are developed by considering the SkM [245] and SLy parametrizations [246, 247] as reference (which are formulated to explain the surface tension and properties of nuclear systems away from β-stability line, respectively). Along with the improvement in potential parameters, the surface symmetry energy and a small correction term is also introduced in the mean field. This model has also been used in investigating isospin effects in reaction dynamics [248, 249]. The ImQMD model can successfully illustrate the yields of clusters in intermediate energy reactions. The introduction of the full Skyrme potential energy density functional excluding the spin-orbit term in the local interaction part permits to take the various Skyrme interactions that explain the ground states of nuclei [59].

Thus, we see that a lot of efforts have been carried out in enhancing theoretical approaches that can enable one to explore reaction dynamics of neutron-rich nuclei. In today's research scenario, isospin asymmetric nuclear matter's equation of state has attracted the nuclear physics community due to its the experimental advancement of

radioactive ion beams. Therefore, in theoretical research also, there is need of involving the isospin degree of freedom in various approaches that have been developed over the years to study heavy-ion reactions. A symmetry term has been involved to include the asymmetry between neutrons and protons, to get the fundamental concept of isospin in Bethe-Weizsäcker mass formula. Taking this fact, isospin degree of freedom has been involved in QMD model, and this in turn took to the development of Isospin-dependent Quantum Molecular Dynamics (IQMD) model discussed in next section.

2.3 Isospin-dependent Quantum Molecular Dynamics model (IQMD)

The Isospin-dependent Quantum Molecular Dynamics (IQMD) model has been developed by Hartnack et al. [19]. It is an improvement of the QMD model in which isospin degree of freedom is not included. The isospin degree of freedom enters into IQMD model through nucleon-nucleon scattering cross section, Coulomb potential as well as symmetry potential (similar to that in IBUU model). It considers the different charge states of nucleons, deltas and pions. The universal flowchart of this model is comprised of three necessary steps: Initialization is the first step where the nuclei are generated. Propagation is the second step, where the generated nucleons are propagated under the dominance of mean field's vicinity. Finally, the nucleons are forced to collide, when they approaches beyond a certain distance and this step is dubbed as binary nucleon-nucleon collisions. The elastic and in-elastic cross-sections for proton-neutron, neutron-neutron and proton-proton are assumed to be influenced by the iso-spin. All these parts are discussed as follows:

2.3.1 Initialisation

The nucleons in the reacting or colliding partners are initialized in their rest frame of reference and their position in the phase space is decided randomly within the radius of $r \leq 1.12A^{1/3}$ and momentum $p \leq p_F$ (here, A is the atomic mass of the nucleus considered and p_F is Fermi momentum) equivalent to normal nuclear matter density ($\rho_0 = 0.17fm^{-3}$). Each nucleon occupies a space with volume h^3, so that phase

space is evenly filled. The initial momenta are arbitrarily chosen between 0 and Fermi momentum (p_F), without any further local constraints. In IQMD model, each nucleon is represented by a Gaussian wave packet with a fixed width L, that depends on the system's size and this dependence of L is however introduced to attain the maximum stability of nucleus. The value of L lies between 4.33 fm^2 and 8.66 fm^2 for the lighter and heavier systems, respectively. These nucleons interact by mutual two and three body interactions. The baryons are presented by Gaussian-shaped density distributions in this model as:

$$f_i(\mathbf{r},\ \mathbf{p}, \mathbf{r}_i(t),\ \mathbf{p}_i(t)) \ = \ \frac{1}{(\pi\hbar)^2} e^{-(\mathbf{r}\ -\mathbf{r}_i(t))^2/2L}\ e^{-(\mathbf{p}\ -\mathbf{p}_i(t))^2 2L/\hbar^2}, \tag{2.1}$$

where $\mathbf{r}_i(t)$ and $\mathbf{p}_i(t)$ define the phase-space's Gaussian wave packet, whereas the Gaussian width L is presumed to be independent of the time.

The density of i^{th} particle in coordinate space and momentum space is calculated as:

$$\begin{aligned} \rho_i(\mathbf{r}, \mathbf{r_i(t)}) \ &= \ \int\ f_i(\mathbf{r}, \mathbf{p}, \mathbf{r}_i(t), \mathbf{p}_i(t))\ d^3p, \\ &= \ \frac{1}{(2\pi L)^{3/2}}\ e^{-[\mathbf{r}\ -\ \mathbf{r}_i(t)]^2/2L}. \end{aligned} \tag{2.2}$$

$$\begin{aligned} g_i(\mathbf{p}, \mathbf{p_i(t)}) \ &= \ \int\ f_i(\mathbf{r}, \mathbf{p}, \mathbf{r}_i(t), \mathbf{p}_i(t))\ d^3r, \\ &= \ \left(\frac{2L}{\pi\hbar}\right)^{3/2}\ e^{-[\mathbf{p}\ -\ \mathbf{p}_i(t)]^2 2L/\hbar^2}. \end{aligned} \tag{2.3}$$

To initialize a nucleus, one has to allot the coordinates and momenta to all the nucleons. In three dimensional space (inside a sphere of radius R) the center of Gaussian wave packet is evenly assigned polar coordinates by:

$$\begin{aligned} r \ &= \ R\ x_1^{1/3}, \\ cos\theta \ &= \ 1\ -\ 2x_2, \\ \phi \ &= \ 2\pi\ x_3, \end{aligned}$$

where $x_1,\ x_2,\ x_3$ are the random numbers. The coordinates of nucleons are denied if the distance among them is less than 1.5 fm. The local Fermi momentum is calculated using the relation

$$P_F(\mathbf{r}_i) \ = \ \sqrt{-2mU(\mathbf{r}_i)}, \tag{2.4}$$

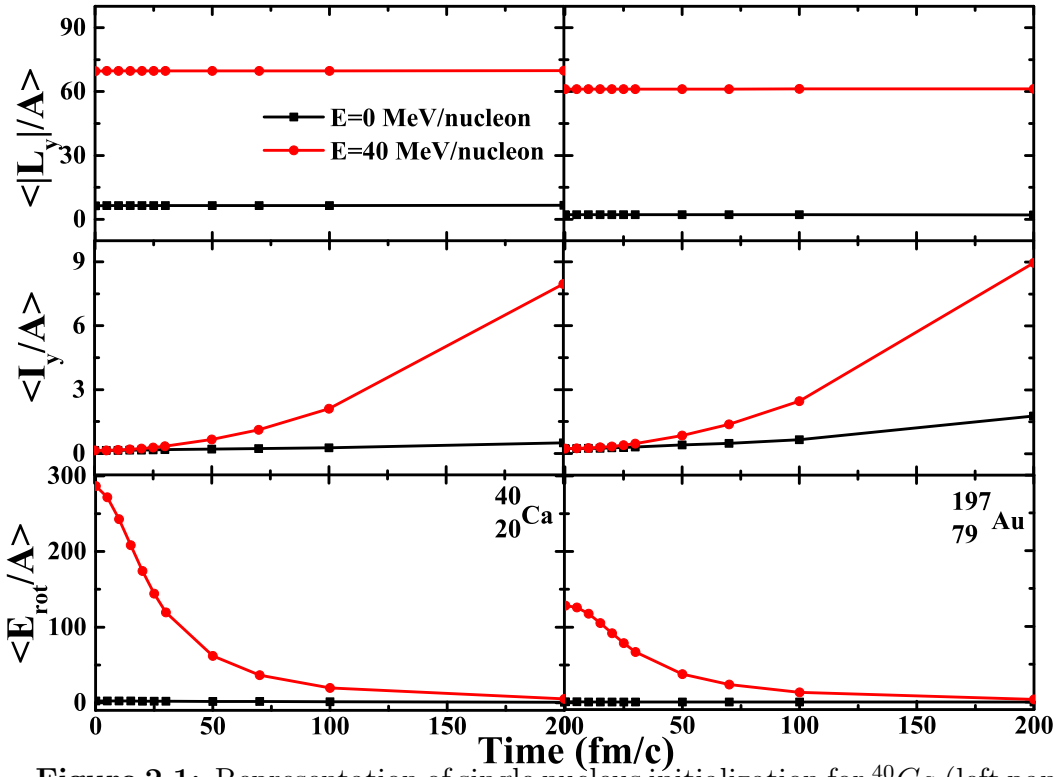

Figure 2.1: Representation of single nucleus initialization for $^{40}_{20}Ca$ (left panel) and $^{197}_{79}Au$ (right panel).

where $U(\mathbf{r}_i)$ is the local potential. The center of every Gaussian wave packet in momentum space is consistently distributed in polar coordinate by:

$$\begin{aligned} p_i &= P_F(\mathbf{r}_i)x_4^{1/3}, \\ cos\theta &= 1 - 2x_5, \\ \phi &= 2\pi x_6. \end{aligned}$$

Only those distributions are considered which satisfy the criteria of d_{min} i.e.,

$$(\mathbf{r}_i - \mathbf{r}_j)^2 \, (\mathbf{p}_i - \mathbf{p}_j)^2 \geq d_{min}. \tag{2.5}$$

Usually, only 1 out of 50,000 initializations is accepted under present test. Furthermore, the IQMD model also includes Lorentz contraction of nucleus coordinate distribution which plays a significant role at higher incident energies.

Fig. 2.1 shows that the single initialized nucleus irrespective of their mass shows rotational mechanism at incident energies, E = 0 MeV/nucleon and 40 MeV/nucleon.

These rotational features are responsible for various phenomenon in nuclear physics like calculations of magic numbers using rotational bands of deformed nucleus in shell model. Here in this Fig. 2.1, one can observe that the even at E = 0 MeV/nucleon incident energy, all the quantities like <angular momentum/nucleon> (L_y), <moment of inertia/nucleon> (I_y) and <rotational energy/nucleon> ($E_{rotational}$) have non-zero values.

2.3.2 Propagation

The initialized nuclei are boosted towards each other along the original beam-axis with suitable center-of-mass velocity using relativistic kinematics. The center of each and every distribution progresses along the Coulomb trajectories. This distribution remained fixed as far as the distance among the nuclei's surfaces is 2 fm. The nucleons of the target and projectile interact with the help of two and three body Skyrme interactions, a momentum dependent interactions and Yukawa interactions.

The isospin degree of freedom is considered clearly by operating explicit Coulomb forces and a symmetry potential between protons of colliding masses. The propagating nuclei moves in an averaged field generated by nucleons and undergo hard stochastic scattering, which changes the quantum state of considered nucleon. For each scattering, the momenta and energy are conserved, but angular momentum is not conserved. The accumulative effect of this non-conservation of angular-momentum has been found to be very negligible [250, 251]. The hadrons propagate using Hamilton's equations of motion:

$$\dot{\mathbf{p}}_i \;=\; -\frac{\partial\langle H\rangle}{\partial\mathbf{r}_i}\;;\;\dot{\mathbf{r}}_i \;=\; \frac{\partial\langle H\rangle}{\partial\mathbf{p}_i} \tag{2.6}$$

Assume, the Hamiltonian for the system is given by local Skyrme nucleon-nucleon interaction consisting of two-body and three-body interactions only, then

$$V_{loc} = t_1\delta(\mathbf{r_1}-\mathbf{r_2}) + t_2\delta(\mathbf{r_1}-\mathbf{r_2})\delta(\mathbf{r_1}-\mathbf{r_3}), \tag{2.7}$$

where t_1 and t_2 are (two-) and (three-) body coefficients, respectively. It is well acclaimed that the three-body part of above equation is similar to a density-dependent

two-body force. Nonetheless, since $IQMD$ model is an N-body theory, so it is accepted to use the three-body form moderately than the density-dependent form. The total energy H_i of i^{th} particle is the sum of potential and kinetic energies as:

$$H_i \;=\; T_i + V_i \;= T_i \;+ \frac{1}{2}\sum_{j;i\neq j} V_{ij}^{(2)} \;+ \frac{1}{3!}\sum_{j,k;i\neq j\neq k} V_{ijk}^{(3)}, \tag{2.8}$$

where T_i indicates to the kinetic energy of i^{th} particle and $V_{ij}^{(2)}$ and $V_{ijk}^{(3)}$ are the two- and three-body interactions. The two-body interactions $V_{ij}^{(2)}$ is acquired by folding the two-body interactions with the densities of both particles.

$$\begin{aligned}
\frac{1}{2}\sum_{j;i\neq j} V_{ij}^{(2)} \;&= \tfrac{1}{2}\;\sum_{j;i\neq j}\int f_i(\mathbf{r}_i,\mathbf{p}_i,t)\; f_j(\mathbf{r}_j,\mathbf{p}_j,t)\; V(\mathbf{r}_i,\mathbf{r}_j) \qquad (2.9)\\
&\quad \times d^3r_i\; d^3r_j\; d^3p_i\; d^3p_j,\\
&= \frac{1}{2}\sum_{j;i\neq j}\int f_i(\mathbf{r}_i,\mathbf{p}_i,t)\; f_j(\mathbf{r}_j,\mathbf{p}_j,t)\; t_1\\
&\quad \times\delta(\mathbf{r}_i-\mathbf{r}_j) d^3r_i\; d^3r_j\; d^3p_i\; d^3p_j,\\
&= \frac{1}{2}\sum_{j;i\neq j}\; t_1\int f_i(\mathbf{r}_i,\mathbf{p}_i,t)\; f_j(\mathbf{r}_j,\mathbf{p}_j,t)\\
&\quad \times\; d^3r_i\; d^3p_i\; d^3p_j,\\
&= \frac{1}{2}\sum_{j;i\neq j}\; t_1\int \frac{1}{(\pi\hbar)^3} e^{-(\mathbf{r}-\mathbf{r}_i(t))^2/2L} e^{-(\mathbf{p}-\mathbf{p}_i(t))^2 2L/\hbar^2}\\
&\quad \times\frac{1}{(\pi\hbar)^3} e^{-(\mathbf{r}-\mathbf{r}_j(t))^2/2L}\; e^{-(\mathbf{p}-\mathbf{p}_j(t))^2 2L/\hbar^2}\; d^3r_i\; d^3p_i\; d^3p_j,\\
&= \frac{1}{2}\sum_{j}\; t_1 \frac{1}{(4\pi L)^{3/2}} e^{-(\mathbf{r}_i-\mathbf{r}_j)^2/4L},\\
&= \frac{t_1}{2}\sum_{j;i\neq j}\rho_{ij}. \qquad (2.10)
\end{aligned}$$

Where,

$$\rho_{ij} = \int d^3\mathbf{r}\;\rho_i(\mathbf{r})\;\rho_j(\mathbf{r}) = \frac{1}{(4\pi L)^{3/4}} e^{-(\mathbf{r}_i-\mathbf{r}_j)^2/4L}. \tag{2.11}$$

The three-body interactions can be calculated as:

$$\begin{aligned}
\frac{1}{3!}\sum_{j,k;i\neq j\neq k} V_{ijk}^{(3)} &= \frac{1}{3!}\sum_{j,k;i\neq j\neq k}\int f_i(\mathbf{r}_i,\mathbf{p}_i,t)\ f_j(\mathbf{r}_j,\mathbf{p}_j,t)\ f_k(\mathbf{r}_k,\mathbf{p}_k,t)\ V(\mathbf{r}_i,\mathbf{r}_j,\mathbf{r}_k) \\
&\quad \times d^3r_i\ d^3r_j\ d^3r_k\ d^3p_i\ d^3p_j\ d^3p_k, \\
&= \frac{1}{3!}\sum_{j,k;i\neq j\neq k}\int f_i(\mathbf{r}_i,\mathbf{p}_i,t)\ f_j(\mathbf{r}_j,\mathbf{p}_j,t)\ f_k(\mathbf{r}_k,\mathbf{p}_k,t)\ t_2 \\
&\quad \times\delta(\mathbf{r}_i-\mathbf{r_j})\ \delta(\mathbf{r}_i-\mathbf{r}_k)d^3r_i\ d^3r_j\ d^3r_k\ d^3p_i\ d^3p_j\ d^3p_k, \\
&= \frac{1}{3!}\frac{t_2}{(2\pi L)^3\cdot 3^{3/2}}\sum_{j,k;i\neq j\neq k} e^{-\left[(\mathbf{r}_i-\mathbf{r}_j)^2+(\mathbf{r}_i-\mathbf{r}_k)^2+(\mathbf{r}_k-\mathbf{r}_j)^2\right]/6L}, \\
&= \frac{1}{3!}\frac{t_2}{(2\pi L)^3 3^{3/2}}\sum_{j,k;i\neq j\neq k} e^{-\left[(\mathbf{r}_i-\mathbf{r}_j)^2+(\mathbf{r}_i-\mathbf{r}_k)^2\right]/6L\times\frac{3}{2}}, \\
&= \frac{1}{3!}\frac{t_2\ (4\pi L)^{3/2\times 2}}{(2\pi L)^3\cdot 3^{3/2}}\left[\sum_{j\neq i}\frac{1}{(4\pi L)^{3/2}}e^{-(\mathbf{r}_i-\mathbf{r}_j)^2/4L}\right]^2, \\
&= \frac{1}{3!}\frac{t_2\ 2^3}{3^{3/2}}\left[\sum_{j\neq i}\rho_{ij}\right]^2. \qquad (2.12)
\end{aligned}$$

From above derivation, one can see that for three-body interactions, the mean field can be written as $[\sum_{j\neq i}\rho_{ij}]^2$. The total momentum in IQMD is maintained because the Hamiltonian is well described for the whole system. The total potential including the isospin effects reads as:

$$V^{ij} \ = \ V_{ij}^{loc} \ + \ V_{ij}^{Yuk} \ + \ V_{ij}^{Coul} \ + \ V_{ij}^{mdi} \ + \ V_{ij}^{sym}, \qquad (2.13)$$

Under normal conditions, the nuclear density is consistent, the interaction density adds up with the density of single particle, and $V_{loc}^{(2)}$ as well as $V_{Yuk}^{(2)}$ are directly proportional to $(\frac{\rho}{\rho_o})$. The three-body part $V_{loc}^{(3)}$ of the interaction is equivalent to $(\frac{\rho}{\rho_o})^2$. In nuclear matter, the local potential energy is given by:

$$V^{loc} \ = \ \frac{\alpha}{2}(\frac{\rho}{\rho_o}) \ + \ \frac{\beta}{\gamma+1}(\frac{\rho}{\rho_o})^2. \qquad (2.14)$$

The potential has two free (α and β) parameters, that can be fixed by the condition that at normal nuclear matter density, total energy should have a minimum at ρ_o and the average binding energy should be -15.75 MeV. For the sake of investigating the effect of different compressibilities, one can conclude the above potential energy to

$$V^{loc} \ = \ \frac{\alpha}{2}(\frac{\rho}{\rho_o}) \ + \ \frac{\beta}{\gamma+1}(\frac{\rho}{\rho_o})^\gamma. \qquad (2.15)$$

Table 2.1: Parameters of static potentials [252]

K(MeV)	$\alpha(MeV)$	$\beta(MeV)$	γ	EOS
200	-356	303	1.17	S
380	-124	70.5	2	H

Depending upon different values of α, β, γ, the above equation (2.15) leads to various type of equation of state. The set of parameters and compressibilities analogous to different equation of state is listed below in Table 2.1. The Skyrme parametrization of nuclear equation of state includes two sets of parameter giving the same correct saturation density and binding energy, but, with two different incompressibility K (one corresponds to soft EOS with $K = 200$ MeV (at smaller value of γ), another corresponds to hard EOS with $K = 380$ MeV (at larger value of γ)). The total Skyrme potential then can be written as

$$V^{Skyrme} = \sum_{j;i\neq j} t_1\delta(\mathbf{r_i} - \mathbf{r_j}) + t_2\delta(\mathbf{r_i} - \mathbf{r_j})\rho^{\acute{\gamma}-1}((\mathbf{r_i} + \mathbf{r_j})/2). \tag{2.16}$$

Other values of α, β and γ are also available in the literature, e.g. super-stiff and super-soft EOS [253, 254].

The finite-range Yukawa potential is included to stabilise the surface of finite nucleus [255, 256]. The attractive Yukawa potential increases the interaction range compared to the δ-like Skyrme potential. The addition of Yukawa potential also reduces the fluctuations produced due to lack of pressure build up by the Fermi momentum. The parameterized form of Yukawa potential is given by:

$$V_{ij}^{Yuk} \;=\; t_3\frac{exp\{-|\mathbf{r}_i - \mathbf{r}_j|\}/\mu}{|\mathbf{r}_i - \mathbf{r}_j|/\mu}, \tag{2.17}$$

Here, with $\mu = 0.4$ fm and $t_3 =$ -6.66 MeV.

In this model, real charge i.e., $Z_{proton} = 1$ and $Z_{neutron} = 0$ is included for the isospin dependence of Coulomb potential. The Coulomb interactions among the nucleons plays a significant role in the study of heavy-ion collisions. It is an important asymmetry term that can be used to understand the isospin effects at intermediate energies. The

Coulomb potential is represented as:

$$V_{ij}^{Coul} \;=\; \frac{Z_{eff}^2\; e^2}{|\mathbf{r}_i - \mathbf{r}_j|}. \tag{2.18}$$

An enough description of the heavy-ion collisions need thorough knowledge of momentum dependent interactions. The momentum dependent interactions adds additional repulsion among the nucleons of projectile and target. The momentum dependence of real part of optical potential is parameterized as follow:

$$V_{ij}^{mdi} \;=\; t_4 ln^2[t_5(\mathbf{p}_i - \mathbf{p}_j)^2 + 1]\delta(\mathbf{r}_i - \mathbf{r}_j). \tag{2.19}$$

Here t_4 = 1.57 MeV and $t_5 = 5{\times}10^{-4}\ MeV^{-2}$ are fitted to the experimental data [257, 258]. The momentum dependence of nucleon-nucleon interaction may optionally be used in IQMD. However, introducing the momentum dependence in IQMD, one has to rearrange the parameters of the Skyrme interactions to have exact saturation properties for normal nuclear matter and the same in-compressibilities as those of the soft and hard EOS. This give rise to new equations of state, i.e., Hard Momentum Dependent (HMD) and Soft Momentum Dependent (SMD).

The symmetry energy term has already been explained in the Chapter 1 in isospin section. The Coulomb and symmetry potentials are isospin dependent however, the momentum dependent Skyrme and Yukawa potentials are isospin independent. After comparing to the Bethe-Weizsäcker mass formula, the Skyrme interaction, the kinetic energy and the momentum-dependent interactions provide the volume energy, the Yukawa interaction corresponds to the volume and surface energy, and the symmetry interactions denotes the volume symmetry energy. The total baryon-baryon potential in IQMD model can be written as:

$$\begin{aligned} V_{ij} \;&=\; V_{ij}^{Skyrme} + V_{ij}^{Yukawa} + V_{ij}^{Coul} + V_{ij}^{MDI} + V_{ij}^{Sym} \\ &=\; \left(t_1\delta(\mathbf{r_i} - \mathbf{r_j}) + t_2\delta(\mathbf{r_i} - \mathbf{r_j})\rho^{\zeta-1}\left(\frac{\mathbf{r_i} + \mathbf{r_j}}{2}\right)\right) \\ &\quad + t_3\frac{exp(|\mathbf{r_i} - \mathbf{r_j}|/\mu)}{(|\mathbf{r_i} - \mathbf{r_j}|/\mu)} \;+\; \frac{Z_i Z_j e^2}{|\mathbf{r_i} - \mathbf{r_j}|} \\ &\quad + t_4\ln^2[t_5(\mathbf{p_i} - \mathbf{p_j})^2 + 1]\delta(\mathbf{r_i} - \mathbf{r_j}) \\ &\quad + t_6\frac{1}{\varrho_0}T_{3i}T_{3j}\delta(\mathbf{r_i} - \mathbf{r_j}). \end{aligned} \tag{2.20}$$

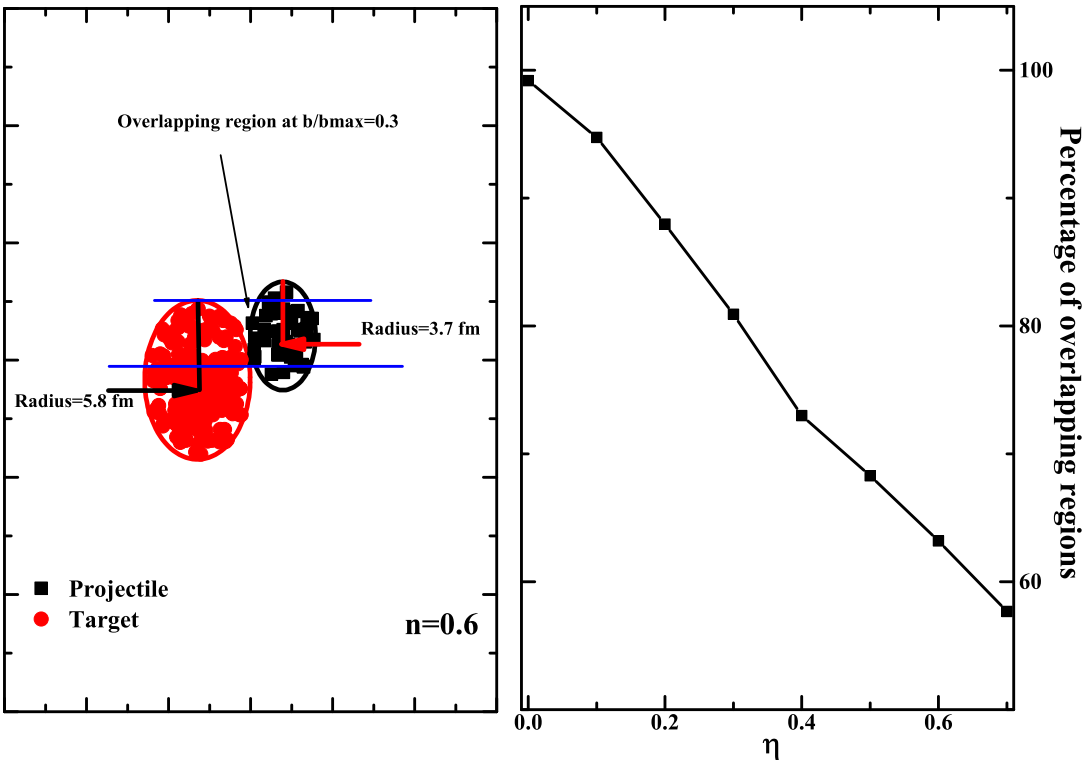

Figure 2.2: The ratio of overlapping regions of colliding nuclei as a function of mass asymmetry of the reaction.

It is worth mentioning that all these components of nuclear potential are influenced by each other, but order of adding these potentials do not influence the final calculations.

In Fig. 2.2, the percentage of the theoretically calculated overlapping regions of two colliding nuclei at fixed impact parameter, $b/b_{max} = 0.3$ has been calculated. Here, the case of $\eta = 0.6$ has been shown in the left panel of the figure. The right panel shows that the ratio of the overlapping regions is exhibiting a decreasing trend with increasing mass asymmetry of the reaction. This trend is justifying the Fig. 2.2, because the number of collisions are due to the overlapping regions of two colliding nuclei. Therefore, when the percentage of overlapping regions are decreasing with η, the number of collisions will automatically be decreased.

The final step is studied in the next section.

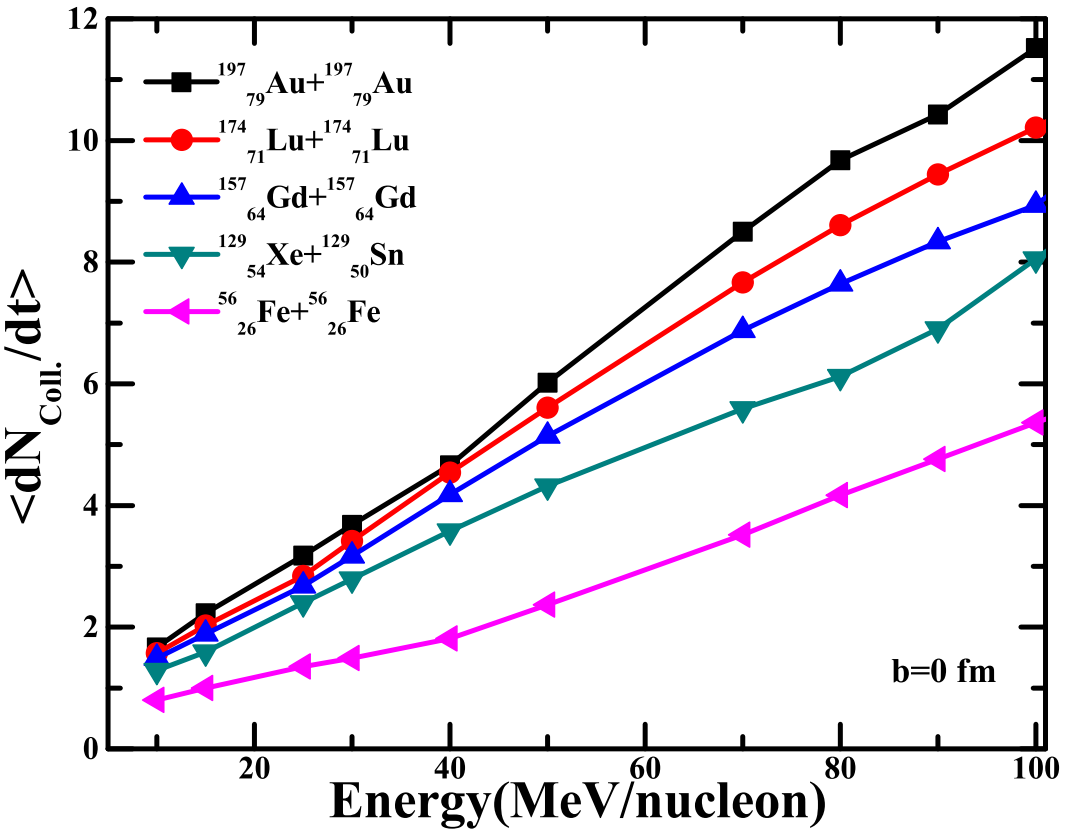

Figure 2.3: The total number of maximum allowed nucleon-nucleon collisions as a function incident energy for the different reactions.

2.3.3 Nucleon-Nucleon collisions

The nucleon-nucleon collisions are incorporated in IQMD model by implementing the collision terms of the common *VUU-BUU* equations [259–264]. A general explanation is used for describing the collision term that, two nucleons are made to collide with each other, if the minimum distance between their centres of Gaussian's distributions fulfills the requirement given below:

$$|\mathbf{r_i} - \mathbf{r_j}| \leq \sqrt{\frac{\sigma_{tot}}{\pi}}, \quad \sigma_{tot} = \sigma(\sqrt{s}, type), \tag{2.21}$$

where σ_{tot} is the total cross section and "type" indicates the ingoing collision partners (N-N, N-Δ, N-π,....). The total cross section is the sum of elastic and all inelastic cross sections.

$$\sigma_{tot} = \sigma_{el} + \sigma_{inel} = \sigma_{el} + \sum_{channels} \sigma_i. \tag{2.22}$$

Fig. 2.3 displays the collision dynamics for symmetric systems. The results displayed are the maximum number of allowed collisions at each energy. One can see a linear relationship between the nucleon-nucleon collisions and size of the interacting system as a function of energy considered for calculations. This dependence is more pronounced in case of heavier system compared to the lighter systems due to the increase in the number of nucleons.

Fig. 2.4 shows the maximum collision are suffered by the nucleons as a function of mass asymmetry of the reaction, η (where $\eta = \frac{A_T - A_P}{A_T + A_P}$, A_T and A_P are, respectively, the masses of the target and the projectile). Very clearly, the number of maximum collisions decrease with the enhancement in mass asymmetry. The reason behind this is that, by increasing mass asymmetry, the projectile mass is decreasing with the increment of mass of the target. Thus, the nuclei have very smaller region to collide in this way, consequently the both terms show falling trend with η.

In addition to nucleons, delta resonances are also produced in IQMD model simulations, which additionally decay into pions. The following inelastic channels are specifically

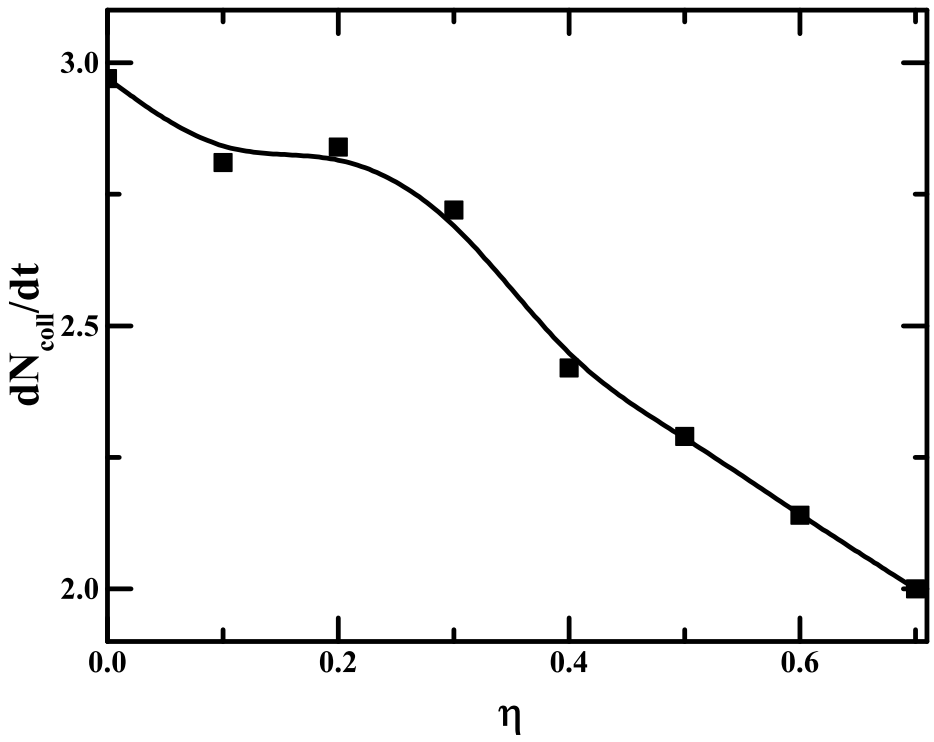

Figure 2.4: The total number of maximum allowed nucleon-nucleon collisions as a function of mass asymmetry of the reaction.

considered into account and comprised the imaginary part of the pion optical potential

$$
\begin{aligned}
N\ N &\rightarrow\ \Delta\ N \qquad (a),\\
\Delta &\rightarrow\ N\ \pi \qquad (b),\\
\Delta\ N &\rightarrow\ N\ N \qquad (c),\\
N\ \pi &\rightarrow\ \Delta \qquad (d).
\end{aligned}
$$

Elastic $\pi-\pi$, $\pi-N$, $\pi-\Delta$, $\Delta-\Delta$, $\Delta-N$ scattering are not considered. Experimental cross sections are used for the processes (a) and (d) [261–264], as well as for the elastic nucleon-nucleon cross sections. Experimentally, inaccessible channels like ΔN $\rightarrow$ NN are calculated from their reverse reactions (here NN $\rightarrow$ ΔN) using modified detailed balance formula [265]. The angular distribution for the elastically scattered nucleons is given by:

$$\frac{d\sigma_{el}}{d\Omega} \sim e^{A(s)\cdot t} \tag{2.23}$$

where,

$$t = -2p^2(1-cos\theta) \quad and \quad A(s) = 6\frac{[3.65(\sqrt{s}-1.8766)]^6}{1+[3.65(\sqrt{s}-1.8766)]^6}, \tag{2.24}$$

with $\sqrt{s}$ is the c.m. energy in GeV and A(s) is given in $(GeV/c)^{-2}$. The inelastic channels are evaluated in a similar manner. The parametrization proposed by Huber and Aichelin [266] is employed where fitted differential cross sections are obtained from one-boson-exchange (OBE) calculations:

$$\frac{d\sigma_{in}}{d\Omega} \ \approx\ a(s)exp\left[b(s)cos\theta\right]. \tag{2.25}$$

The $a(s)$ and $b(s)$ are functions of $\sqrt{s}$ and alter in their definition for different intervals

Table 2.2: a(s) and b(s) as a function of the c.m. energy.

$\acute{x}\ =\ \sqrt{s}\ (GeV)$	$a\ (fm)$	b
2.104 - 2.12	$294.6(\acute{x}-2.014)^{2.578}$	$19.71(\acute{x}-2.014)^{1.551}$
2.12 - 2.43	$\frac{0.01224}{(\acute{x}-2.225)^2\ +\ 0.004112}$	$19.71(\acute{x}-2.014)^{1.551}$
2.43 - 4.50	$\left(\frac{2.343}{\acute{x}}\right)^{43.17}$	$33.14\ arctan(0.5404(\acute{x}-2.146)^{0.9784})$

of $\sqrt{s}$ (see Table 2.2). θ is the polar angle. Scaled density as a function of time is another property to study the collision dynamics. This study has been carried out for different

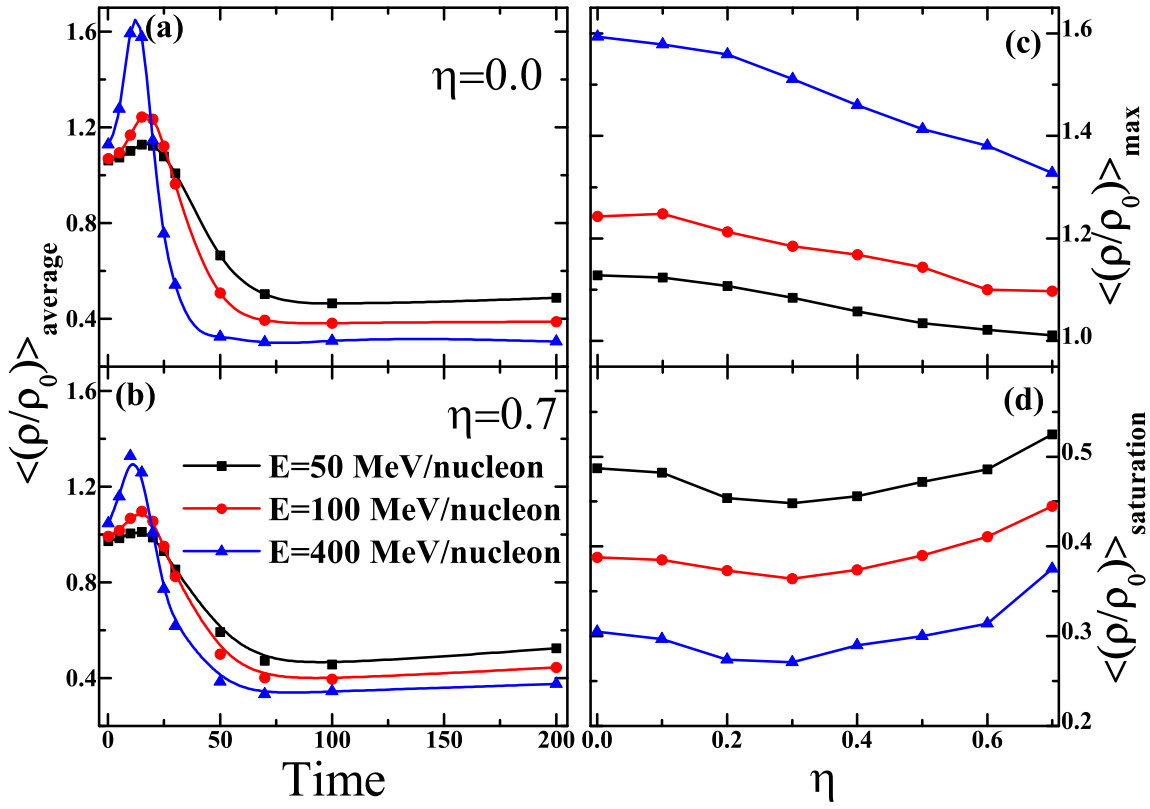

Figure 2.5: (a) and (b)Scaled density as a function of time for different mass asymmetric reactions at semi-central collision,(c) and (d)Maximum and saturated scaled density as a function of mass asymmetry.

mass asymmetric reactions at semi-central collision for different energies shown in Fig. 2.5. The scaled density as a function of time and incident energy for symmetric and highly mass-asymmetric reaction has been shown in Fig. 2.5(a and b). Peak value of scaled density (Fig. 2.5(c)) keeps on decreasing, but the saturation density (Fig. 2.5(d)) keeps on increasing with mass asymmetry content and incident energy. The reason behind this is the reduction of interacting matter as well as collisions as shown in Fig. 2.5. The maximum scaled density is achieved due to the maximum overlapped region of the colliding nuclei, which is consequently falling with η (as shown in Fig. 2.5) and thus the peak value is decreasing with η (Fig. 2.5(c)). Although on the other hand in Fig. 2.5(d), higher mass asymmetry yields the heavier fragments equivalent to the size of the target and in this way the system gets stabilised more frequently as in case of symmetric systems.

2.3.4 Pauli blocking

Pauli blocking is an essential property which is required to be employed within the semi classical theory (IQMD model) for the better understanding of reaction dynamics with large accuracy. There are mainly two methods that are mentioned in the literature to include the Pauli exclusion principle inside a transport model simulation. Souza et al. [267] proposed a method in which the Pauli principle will be implemented in two situations; first, to ensure a reasonable initial phase-space occupation which will be achieved by the generation of initial configuration of the nucleus and second, during nucleon-nucleon collisions by obstructing the collisions and hence blocking the nucleons from being in an overcrowded state of phase space.

To achieve Pauli blocking by restricting the collisions is highly favored method to be employed to study the heavy-ion reactions as the initial phase-space occupation (first method) includes the production of highly excited and large in size fragments. Moreover, an additional statistical break-up has to be applied with the first method, to achieve exact fragment multiplicities. To prevent such disturbances, collision blocking method is followed for the present study. The phase space around the emitted nucleons is examined during the evolution of reaction. The collisions among the nucleons are

restricted if the scattered nucleons are expected to enter an already occupied (fully or partially) state in the phase space volume. For sake of simplicity, one can assume that, each nucleon occupies a sphere in coordinate and momentum space whereas two spheres are not permitted to overlap in accordance with the Pauli exclusion principle. This method yields the same Pauli blocking ratio as achieved by an accurate measurement of the overlap of the Gaussian surfaces. We calculate the fractions P_1 and P_2 of final phase spaces for each of the scattering partners that is already being occupied by other nucleons. The collision is obstructed with a probability

$$P_{block} = 1 - [1 - min(P_1, 1)] [1 - min(P_2, 1)], \tag{2.26}$$

and, respectively, is granted with probability $1 - P_{block}$. For a nucleus in its ground state, one can obtain an average blocking probability $< P_{block} >$ of 0.96. For absolute blocking, this factor should be one. From above description, it is clear that the Pauli factor will be zero or one depending on whether the final phase-space is occupied or not.

The phase space generated by IQMD model is analysed using clusterization method. The secondary models are discussed in the last section.

2.4 Secondary Models:Methods of Clusterization

2.4.1 Minimum Spanning Tree (MST) method

Minimum Spanning Tree (MST) is the most broadly employed method to clusterize the nucleons [252]. In this method, if the distance between the centroids of two nucleons is less than d_{min}, then these two nucleons share the same fragment, where d_{min} is given as:

$$|\mathbf{r}_i - \mathbf{r}_j| \leq d_{min}, \tag{2.27}$$

where $\mathbf{r}_i$ and $\mathbf{r}_j$ are the spatial co-ordinates of both the nucleons. The minimum distance d_{min} has been used as a free-parameter and it varies over the range of 3-4 fm. This spatial distance based approach cannot identify the fragments that are nearly overlapping therefore, will provide a single big fragment during the initial phase of the reaction and hence density is extremely high and the interactions between the

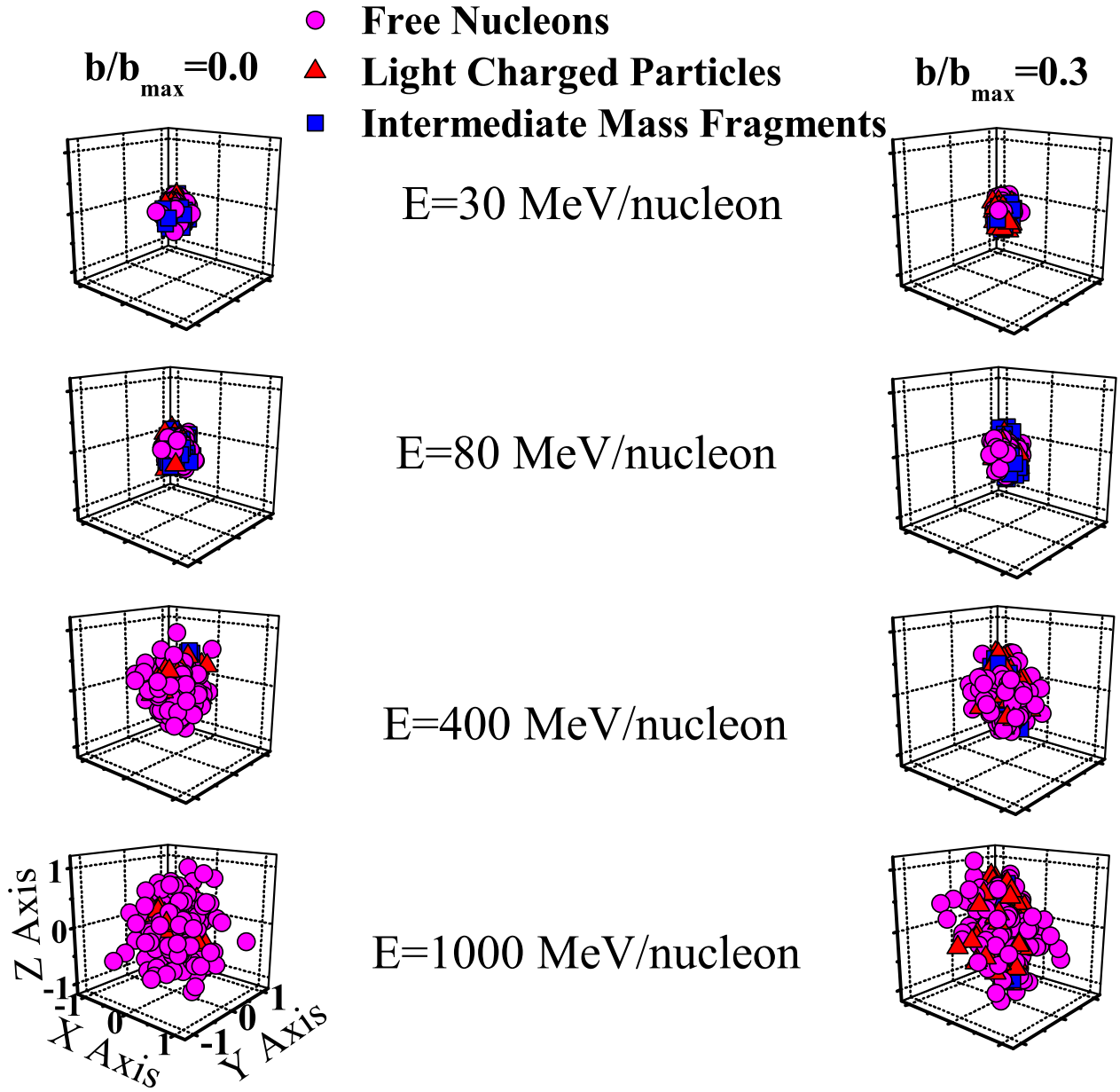

Figure 2.6: 3-dimensional phase-space analysis for $^{197}_{79}Au + ^{197}_{79}Au$ reaction at different energies and impact parameters.

nucleons are in participant zone. In other words, this approach cannot convey towards the problem of fragments's time scale. Improved methods have been deviced which are capable of detecting the overlapping fragments [268].

Fig. 2.6 shows the 3-dimensional phase-space snap-shot of different mass fragments for ${}^{197}_{79}Au + {}^{197}_{79}Au$ reaction at different energies and centralities calculated by the MST method.

2.4.2 Minimum Spanning Tree with Momentum cut (MSTP) method

In addition to spatial constraints, Kumar *et al.* [269] introduced a constraint on relative momenta of two nucleon:

$$|p_i - p_j| \leq p_F \tag{2.28}$$

Here, p_F is the average Fermi momentum of nucleons bounded in a nucleus in its ground state. It will help to get rid of fragments that are however close in spatial co-ordinate space, but are far in momentum space. This method checks the formation of artificial and unstable fragments by excluding those nucleons having relative momenta larger than p_F. Both MST as well as MSTP method give different results at the early reaction stage. MST gives one largest fragment of size ($= A_P + A_T$), while MSTP method gives two distinct clusters of masses A_P and A_T having very large relative momenta. This algorithm identifies the largest fragment A^{max} as early as 50-60 fm/c [269].

Chapter 3

To probe elliptic flow with rapidity constraints

3.1 Introduction

In last three decades, it is well-demonstrated that the occurrence of azimuthally asymmetric emission of nucleons (nuclear flow) appears over the broad spectrum of energy and colliding masses [121, 139, 140, 158, 165, 270–275]. The study of collective flow presents logical understanding regarding the nuclear matter which is emitted during de-compression stage of the hot (and highly dense) matter developed during the collision. Anisotropic flow is one among the influential observable associated with the participant zone. Anisotropic distributions in momentum space is due to initial asymmetries of the colliding partners.

Nuclear flow can be utilized as a probe to gather the knowledge regarding the nuclear equation of state (NEOS) and its associated isospin dependence. In non-central collisions, the overlap region of colliding nuclei is almond in shape. The reaction plane has short axis in the transverse direction, which is parallel to the vector connecting the center of two nuclei. Nucleons along minor axis undergo more pressure gradient as compared to nucleons in any other direction. This pressure dependent correlation amidst the nucleon position and momentum is known as collective flow. Collective flows are defined by Fourier expansion of particle invariant distribution as the n^{th} harmonic coefficients v_n [69] in equation 1.4.

The elliptic flow, the Fourier expansion's second harmonic has been proven to be one

of the most influential probe to provide deep insight of the dynamics of heavy-ion collisions and the equation of state (EOS). The term elliptic flow was put forward in 1997 by H. Sorge [28,276]. Mathematically, elliptic flow can be written as in equation 1.6. A positive value of $< v_2 >$ describes in-plane enhancement of the nucleons emission and illustrates the eccentricity of an ellipse-like distribution. Negative value characterises squeeze-out flow perpendicular to the reaction plane [57, 58].

The anisotropic flow of the nucleons is basically rapidity constraint dependant [22]. Similarly, elliptic flow and its transition from the in-plane flow to out-of-plane emission can also be extracted from the mid-rapidity zone [63]. The yield of the nucleons participating in the elliptic flow over the whole rapidity intervals gives us clue about the strength of the flow at target like and projectile like rapidity region in comparison to mid-rapidity zone. The nucleons emitted within the rapidity region near the beam rapidity show maximum collective flow.

The fragments/nucleons which are emitted from the mid-rapidity zone are suppose to encounter the maximum compression and thus are, expected to be most sensitive towards equation of state (EOS) [277, 278]. From highly compressed mid-rapidity zone, nucleons are emitted in direction perpendicular to the reaction plane (squeeze-out). Also, the average energy of these squeezed out nucleons is larger in comparison to in-plane nucleons. This is the reason that why elliptic flow is generally studied and extracted from the mid-rapidity region only [63].

In recent years, several groups have calculated many different aspects of elliptic flow. The PLASTIC BALL, INDRA and FOPI collaborations [57,58,83] are effectively associated in measuring the elliptic flow's excitation function specifically for the reaction of $^{197}_{79}Au+^{197}_{79}Au$. Many investigations on the transition energy (E_T) have been carried out theoretically and experimentally by several groups [58, 59, 83, 169, 279–281]. Recently, different aspects of elliptic flow for the reactions of $^{197}_{79}Au +^{197}_{79} Au$ and $^{40}_{20}Ca +^{40}_{20} Ca$ have been explored by Reisdorf et al. (at Schwerionen- Synchrotron (SIS) at GSI by using the large acceptance FOPI apparatus) [60], Russotto et al. [280, 281], Wang et al. [138, 170] and Ritter et al. [282].

The physics concerning the elliptic flow is much more complex and interesting. El-

liptic flow is highly sensitive to isospin content of the colliding nuclei [169]. Elliptic flow is also a powerful tool to probe the symmetry energy's density dependence [278]. As discussed above, there exists several attempts in the literature to study different aspects of elliptic flow. Still, the effect of rapidity constraints on elliptic flow has not been explored or carried out extensively for different colliding nuclei, different mass fragments and different impact parameters.

3.2 Results and discussion

Several thousands events have been simulated for the present analysis [88], for the reactions of ${}^{197}_{79}Au + {}^{197}_{79}Au$, ${}^{150}_{60}Nd + {}^{150}_{60}Nd$, ${}^{124}_{50}Sn + {}^{124}_{50}Sn$, ${}^{96}_{44}Ru + {}^{96}_{44}Ru$, ${}^{78}_{36}Kr + {}^{78}_{36}Kr$, ${}^{48}_{20}Ca + {}^{48}_{20}Ca$ and ${}^{40}_{20}Ca + {}^{40}_{20}Ca$ (neutron to proton ratio (N/Z) = 1.5, 1.5, 1.48, 1.5, 1.18, 1.16, 1.14 and 1.0 respectively) at incident energy 400 MeV/nucleon for the centrality $0.25 < \hat{b} < 0.45$ (with $\hat{b} = \frac{b}{b_{max}}$,here maximum impact parameter is defined as b_{max} = 1.12 $(A_P^{1/3} + A_T^{1/3})$ fm calculated as per experimental data [60]). Reduced value of energy and isospin dependent cross-section $\sigma_{reduced} = 0.8\sigma_{free}^{nn}$ [283] have been used. Another set of ${}^{197}_{79}Au + {}^{197}_{79}Au$ reaction was carried out at incident energies between 50 and 1000 MeV/nucleon for the centralities range $\hat{b} < 0.25$ and $0.45 < \hat{b} < 0.55$ using a soft EOS. The choice of colliding partners, incident energies and centrality ranges are selected on the basis of experimental data [60] available. Using the IQMD model, the generated phase-space has been analyzed with the help of MST [252, 268, 284–286]. The time evolution of reaction has been followed up to the typical saturation time of a heavy ion reaction (i.e., 200 fm/c). These similar calculations of input reaction parameters are considered in the next two chapters also.

Firstly, the role of mass dependance on elliptic flow is explored in the next section.

3.2.1 Mass dependance of elliptic flow

The aim of present study [88] is to interpret the influence of spectator-participant matter on the mass dependence of elliptic flow. In the literature, two approaches have been proposed to define participant-spectator matter. First, if one of any nucleon encounter at least one collision, is considered as participant otherwise as spectator [287]. In sec-

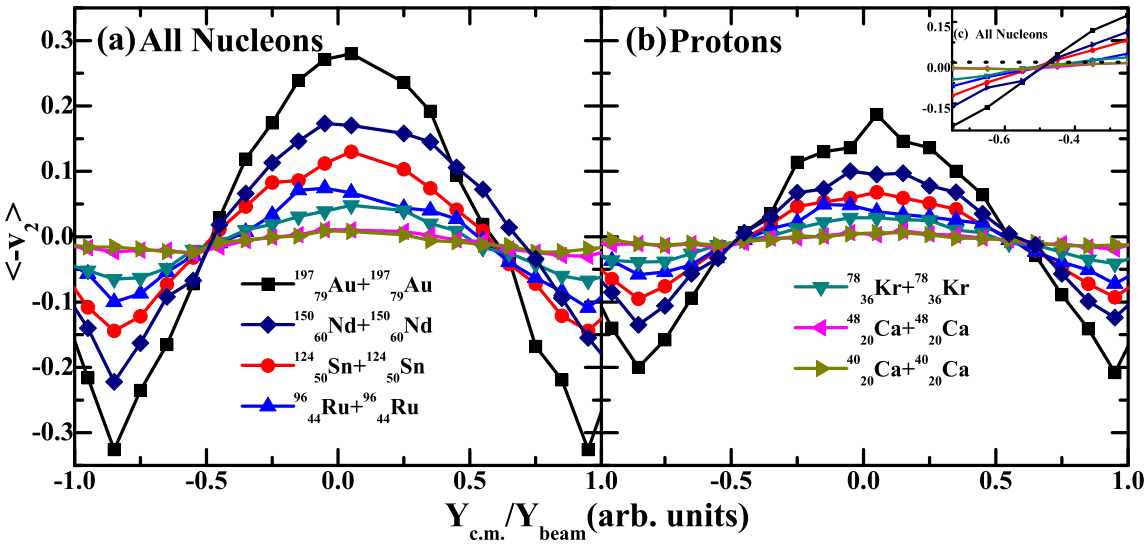

Figure 3.1: Elliptic flow as a function of rapidity for (a)All nucleons and (b)protons for different reactions at 400 MeV/nucleon for centrality $0.25 < \hat{b} < 0.45$.

ond approach, rapidity is employed as a tool to distinguish between participant and spectator. When two nuclei collides, they can be observed as producing cylindrical cut through each other. The participant nucleons from target and projectile encounter a violent collision process.

The residuals of projectile and target are less influenced by collision process and prefer to move with largely non-uniformly distributed velocities. During the violent progression stage of reaction, the behaviour of participant matter is effected by the spectators. In Fig. 3.1 (a and b), rapidity dependence of excitation function of elliptic flow $< -v_2 >$ has been exhibited for various reactions. During the initial phase of the reaction, there were two Gaussian peaks at projectile like and target like rapidity. As the nuclei begin to overlap, the density in the overlap zone increases. Number of nucleons in the overlap zone keeps on enhancing. As the energy increases furthermore, the nucleons are deflected close to the participant zone. One can observe from the Fig. 3.1 (a) that for both target like and projectile like rapidity, nucleons prefer to have in-plane emission. At both sides of target like and projectile like rapidity, the peaks corresponds to the spectator matter produced at the non-central collisions.

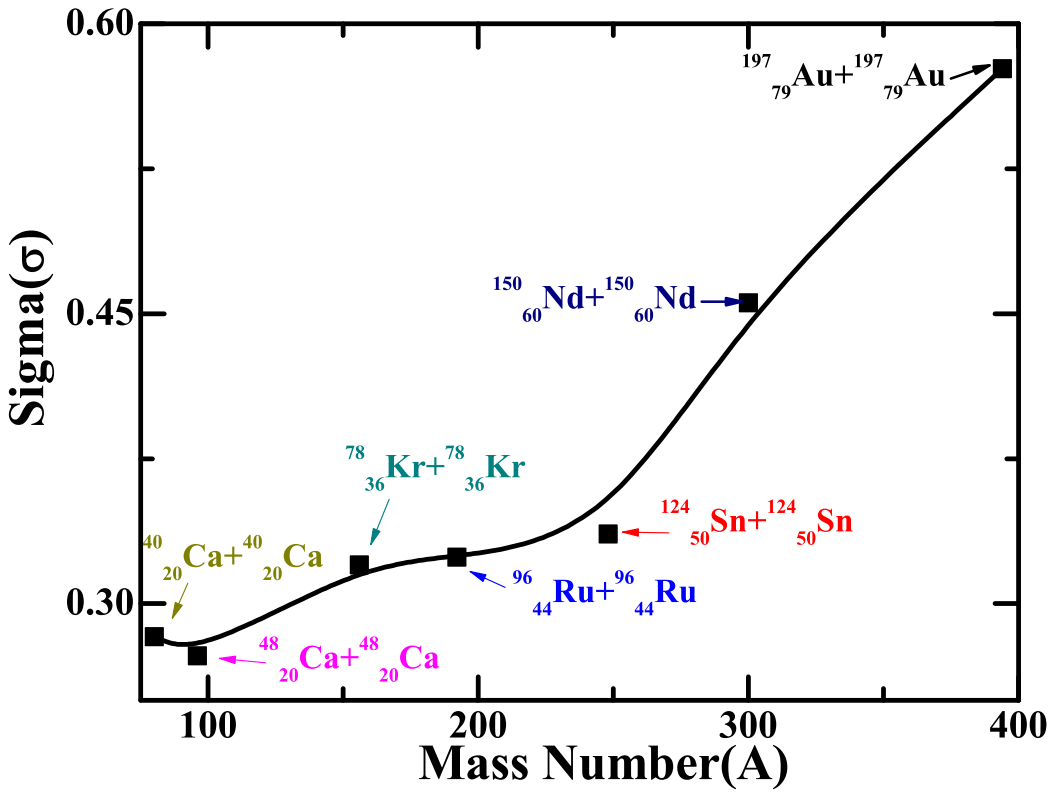

Figure 3.2: Variation of Sigma(σ) extracted from the rapidity dependence of nucleons of elliptic flow with Mass Number(A) for different reactions for centrality $0.25 < \hat{b} < 0.45$ at incident energy 400 MeV/nucleon.

It is originally the compressed matter that is produced in the process of the interplay between the expansion of participant matter and shadowing or passing of the spectator matter. The movement of these two zones is noticed over the whole rapidity range, where squeezed out participant matter is observed at mid-rapidity region. Un-interacted spectator matter is seen for peripheral target and projectile like rapidity. More energy transferred into the participant zone leads to squeeze out, whereas reverse in the spectator zone leads to in-plane flow. Therefore one can get $-$ve value of $< v_2 >$ around mid rapidity zone, while +ve value of $< v_2 >$ at target like and projectile like rapidity. [63].

Similar trends have been observed in recent studies [60]. The peak values of $< -v_2 >$ at zero value of rapidity in ${}^{197}_{79}Au + {}^{197}_{79}Au(0.28)$, ${}^{150}_{60}Nd + {}^{150}_{60}Nd(0.17)$, ${}^{124}_{50}Sn + {}^{124}_{50}Sn(0.13)$, ${}^{96}_{44}Ru + {}^{96}_{44}Ru(0.062)$, ${}^{78}_{36}Kr + {}^{78}_{36}Kr(0.048)$, ${}^{48}_{20}Ca + {}^{48}_{20}Ca(0.01)$ and ${}^{40}_{20}Ca + {}^{40}_{20}Ca(0.008)$ respectively are directly proportional or related to masses of colliding nuclei. More squeeze-out is detected for heaviest nuclei in comparison to the lighter one. Recent studies exhibits that the isospin dependent Coulomb and symmetry potential governs the reaction dynamics drastically [169]. The repulsive nature of symmetry energy and Coulomb potential results in more squeeze-out in the case of heavier nuclei.
The interesting thing to note here is the well ordered transition from +ve to -ve side. One can see in the inset Fig. 3.1 (c), a very clear systematics can be observed which depends on the colliding nuclei's mass. Similar trend of rapidity dependence are obtained if one concentrate on elliptic flow associated with protons only (shown in Fig. 3.1 (b)). The upward swing of nucleons/protons shows that nucleons close to mid-rapidity zone experience squeeze-out and nucleons prefer to have in-plane flow especially at target like/projectile like rapidity intervals. The nucleons of heavier nuclei at target like/projectile like rapidity display more flow compared to lighter nuclei. Due to presence of large number of nucleons, the effect of Coulomb interactions and symmetry energy is more in case of heavier nuclei.

Now the question arises, whether the width of yield of nucleons in elliptic flow as function of rapidity depends on mass of colliding partners or not? A very feeble impact of isospin content on elliptic flow has been reported in ref. [280]. Another characteristic

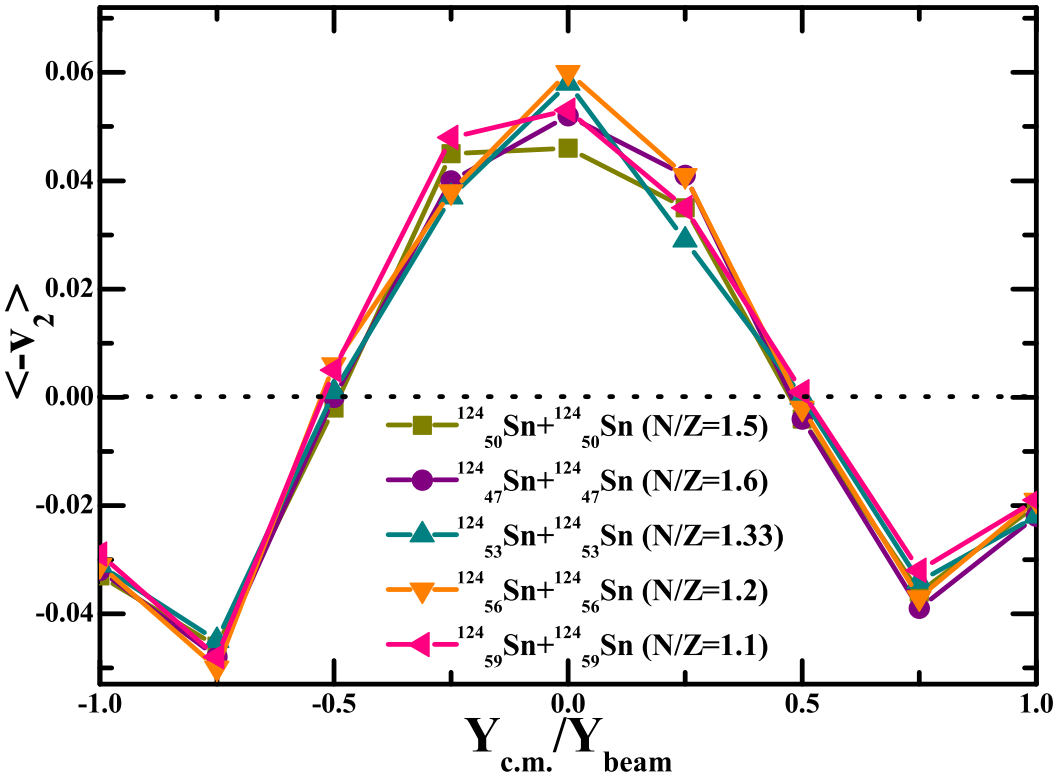

Figure 3.3: Elliptic flow as a function of rapidity for different isobars of ^{124}Sn at centrality $0.25 < \hat{b} < 0.45$ at incident energy 400 MeV/nucleon.

that can be studied here is the yield of colliding nucleons for different nuclei. One can notice that the yield of nucleons changes with mass of nuclei. The parameter which can give clue about the spread of yield of nucleons is sigma (width). The calculation of sigma(σ) of the curves of rapidity dependence of Fig. 3.1 (a) has been carried out using Gaussian distribution function:

$$y = y_o + \frac{A}{w\sqrt{\frac{\pi}{2}}} e^{-\frac{2(x-x_o)^2}{w^2}} \tag{3.1}$$

Here y_o is the base-line offset, A is the total area under the curve from the base-line, x_o is center of the peak represents the mean and w= 2 sigma, the width of the peak at half height, w/2 is the standard deviation. The range taken for fitting is $-1.0 \leq \frac{Y_{c.m.}}{Y_{beam}} \leq 1.0$. The variation of sigma with mass number have been displayed in Fig. 3.2.

The value of sigma is highest for the reaction of $^{197}_{79}Au +^{197}_{79} Au$ and then decreases towards the reaction of $^{40}_{20}Ca +^{40}_{20} Ca$. The drifting of nucleons in transverse direction is effected by Coulomb interactions and symmetry energy. Also the peak as well as saturation density depends on the mass of colliding nuclei at a certain energy. One can say that, the large number of nucleons are populated in the mid-rapidity zone for the reaction of $^{197}_{79}Au +^{197}_{79} Au$, so the height and width are maximum. The influence of Coulomb interactions and the symmetry energy increases proportionally with size of the system, both these interactions are repulsive in nature. As elliptic flow is extracted from high density zone, therefore contribution of density dependent symmetry energy is larger in comparison to Coulomb interactions at higher energies [279]. The repulsive interactions are feeble in $^{40}_{20}Ca +^{40}_{20} Ca$, give rise to the lesser width (σ) of yield of nucleons.

The role of iso-spin in isobars of $^{124}_{50}Sn +^{124}_{50} Sn$ (Fig. 3.3) has also been explored, where the isospin factor (N/Z=neutron to proton ratio) has been changed. It has been concluded that the width of the yield almost remained unchanged by doing so. If one consider only the mid-rapidity region, the influence of Coulomb interactions and symmetry energy [169] is seen. Although, the peak does not follow the same criteria around the mid-rapidity region. Recently, similar study has been carried out for the reaction of $^{197}_{79}Au +^{197}_{79} Au$ and $^{40}_{20}Ca +^{40}_{20} Ca$ by Reisdorf el al. [60] and analogous trend

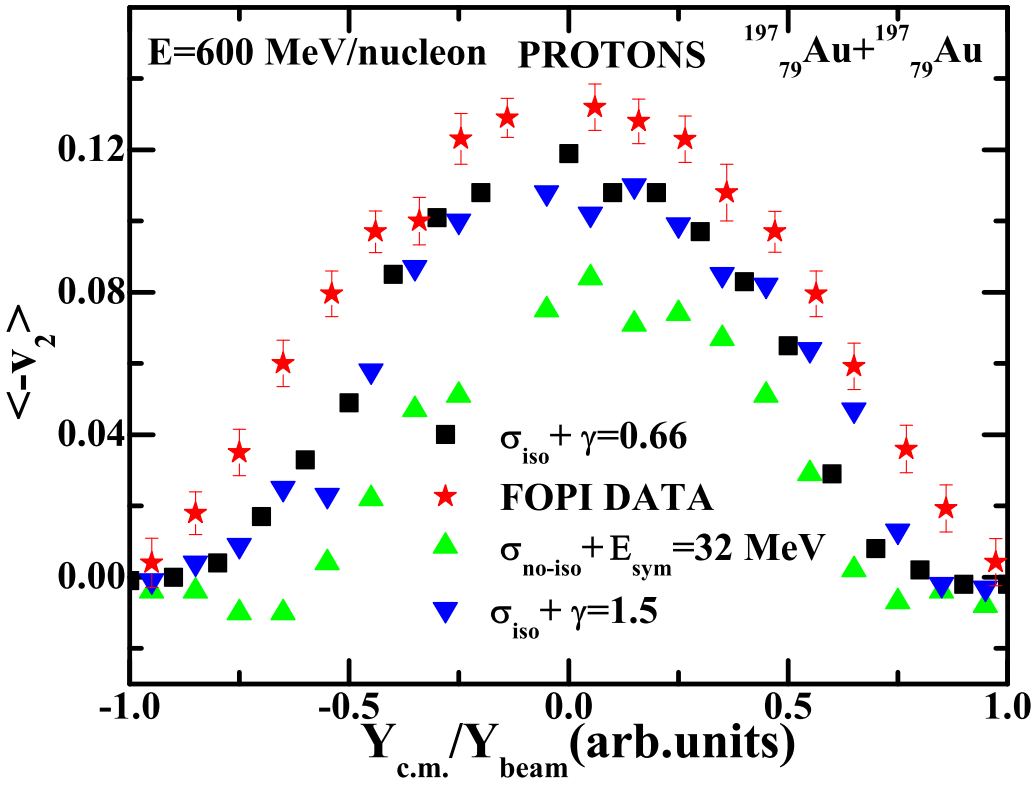

Figure 3.4: Comparison of Rapidity dependence of $-v_2$ between theoretical results and experimental data extracted by FOPI Collaboration for centrality $0.45 < \hat{b} < 0.55$.

was reported. If range for fitting of rapidity dependence of yield is decreased, then width increases. This is in agreement with the study carried out in ref. [60]. The effect of centrality and iso-spin dependance on elliptic flow has been explored in the next section.

3.2.2 Effect of cross-section and centrality on elliptic flow

It would be of great interest to study the influence of isospin dependent symmetry energy and nucleon-nucleon cross-section at higher energies, because the effect of Coulomb interactions diminishes with increasing energy. Fig. 3.4 shows the comparison of rapidity dependence of $< -v_2 >$ between theoretical calculations and experimental observations extracted for the reaction of $^{197}_{79}Au+^{197}_{79}Au$ at an incident energy 600 MeV/nucleon

by the FOPI collaboration at centrality $0.45 < \hat{b} < 0.55$. It is worth mentioning here that the results follow the similar trend as reported in the measurement [60]. Recently, analogous type of studies has also been carried out by Russotto et al. [280, 281], Wang et al. [138] and Ritter et al. [282]. We specifically want to check the effect of isospin on elliptic flow as a function of rapidity.

The influence of different equations of state has been checked by Wang et al. [170] and almost identical rapidity dependence of elliptic flow have been reported for different equations of state. So, in the present study, soft equation of state has been used. Secondly, the role of isospin dependent (σ_{iso}) and isospin independent (σ_{no-iso}) cross-sections have been presented. As in σ_{iso}, the neutron-proton cross-section is about three times the neutron-neutron and proton-proton cross-sections i.e., $[\sigma_{np} = 3\sigma_{nn} = 3\sigma_{pp}]$ and in σ_{no-iso} , $\sigma_{np} = [\sigma_{nn} = \sigma_{pp}]$ which consequences in weaker squeeze-out flow.

Iso-spin independent cross-section along with constant symmetry energy is not sufficient to explain the experimental data. Here, one can easily demonstrates that the data lies close to the σ_{iso} points revealing the impact of isospin dependence. Finally, in order to explore the role of density dependance of symmetry energy $E_{sym}(\rho) = E_{sym}(\rho_o)\left(\frac{\rho}{\rho_o}\right)^{\gamma}$, the term gamma ($\gamma$) is altered for values : 0.66 and 1.5. The influence of symmetry energy for these two values is clearly visible in the figure. The elliptic flow appears to be sensitive towards the different forms of density dependent symmetry energy. One can observe that isospin dependent cross-section and symmetry energy with $\gamma = 0.66$ is able to explain the experimental data over the entire rapidity intervals.

The influence of centrality on rapidity dependence of elliptic flow of nucleons has been investigated (shown in Fig. 3.5) for centralities $\hat{b} < 0.25$, $0.25 < \hat{b} < 0.45$ and $0.45 < \hat{b} < 0.55$. The strong centrality dependence recommends an increasing shadowing due to the existence of spectator matter in the reaction plane as compared to central collisions. The width and the peak of the yield of nucleons is more in the case of semi-peripheral ($0.45 < \hat{b} < 0.55$) impact parameter range. Here one can observe that elliptic flow is more enhanced as lesser number of nucleons participate for this centrality due to increase of spectator zone. Also the azimuthal anisotropy becomes

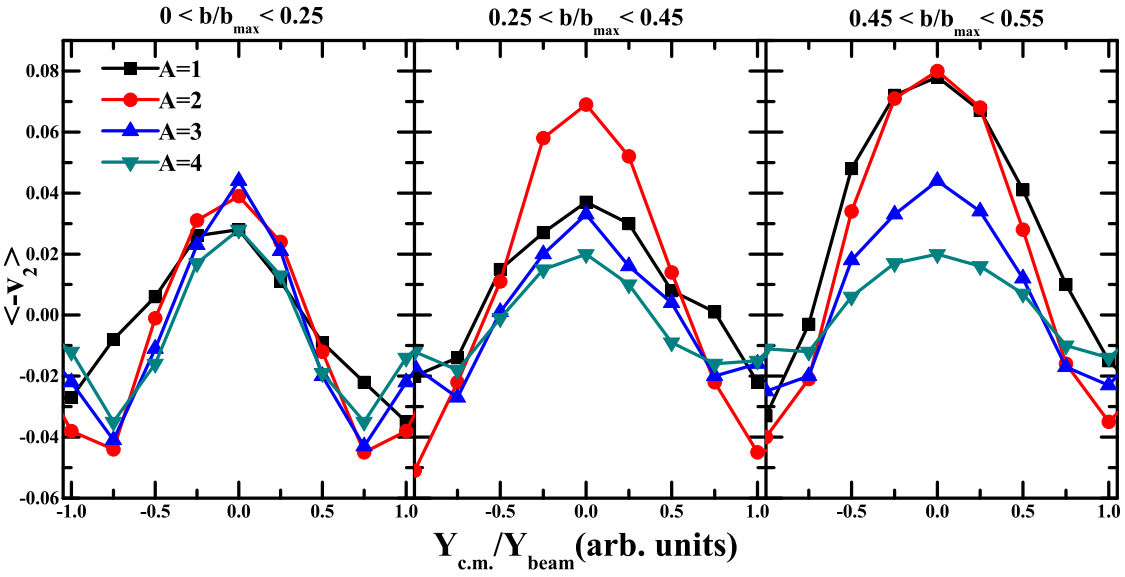

Figure 3.5: Comparison of $-v_2$ as a function of rapidity for the $^{197}_{79}Au+^{197}_{79}Au$ reaction at different centralities at 400 MeV/nucleon.

larger with increase in centrality. But for the other centrality $\hat{b} < 0.25$ (which is almost central collision) the spreading of yield of nucleons is hardly changed or remain unaltered. Because for nearly central collisions, large number of nucleons participate resulting in an enhancement in the participant zone. Therefore, the yield of nucleons is isotropic or the shape is nearly spherical.

The squeeze-out is maximum at $0.45 < \hat{b} < 0.55$ impact parameter range for A = 1 and A = 2 or light mass fragments, because the light mass fragments have lesser value of momentum and high value of velocity as compared to the heavy masses. Due to this reason, the lighter masses experiences more squeeze out or are emitted more in number in the mid-rapidity region. Similar behaviour has also been seen at other incident energies (50, 150, 600 and 1000 MeV/nucleon).

3.2.3 Influence of incident energy on elliptic flow

After cross-section and centrality dependance, another parameter influence the elliptic flow related to fragments produced from mid-rapidity zone, is the energy dependence. We further expand our study to elliptic flow of different mass fragments for centrality

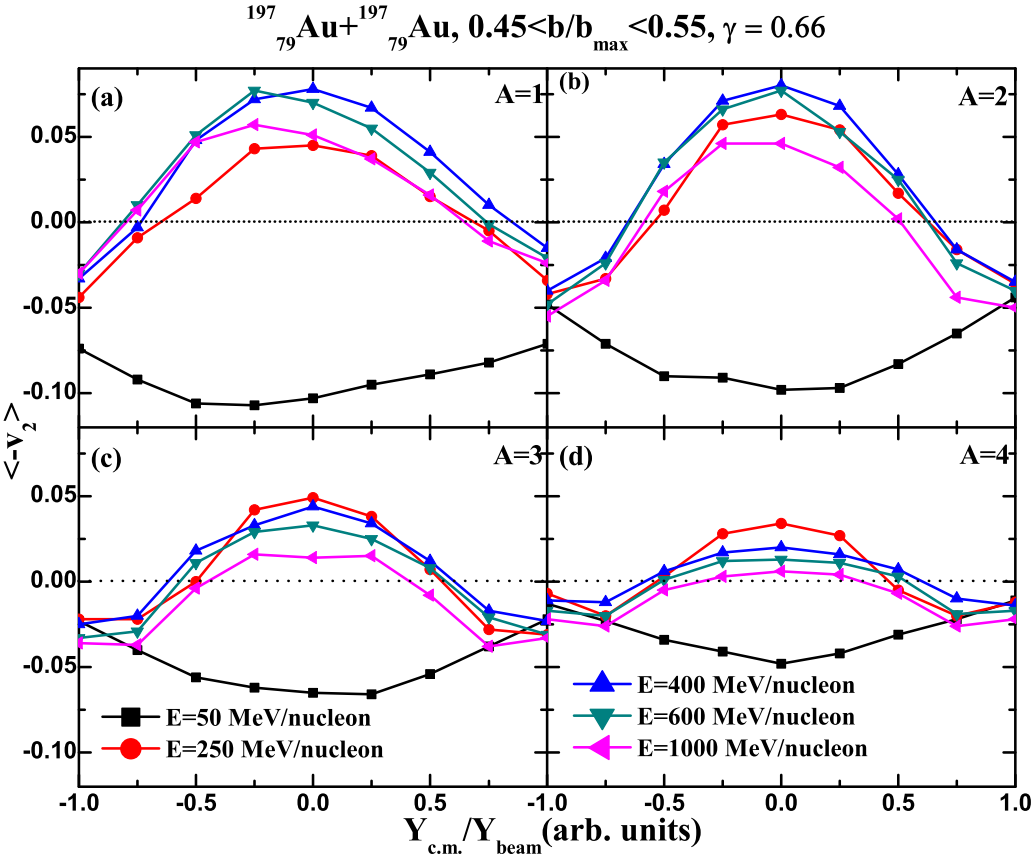

Figure 3.6: Elliptic flow of $^{197}_{79}Au + ^{197}_{79}Au$ reaction as a function of rapidity for different mass fragments at centrality $0.45 < \hat{b} < 0.55$ at different energies.

$0.45 < \hat{b} < 0.55$ at various beam energies (shown in Fig. 3.6). Symmetry energy with $\gamma = 0.66$ and isospin dependent cross-section has been used in further analysis. The investigation has been carried out at semi-peripheral centrality and the same analysis has been examined at $\hat{b} < 0.25$ centrality (not shown here). Here, one can see that width of yield of fragments decreases with the increment in the mass of fragment. Fig. 3.6 (a) unveils that free nucleons spread over the entire rapidity intervals, but light mass fragments are emitted around the region near to mid-rapidity as shown in Fig. 3.6 (b,c and d). At lower incident energy i.e., at 50 MeV/nucleon, the $< -v_2 >$ is -ve, while at higher energies it becomes +ve. The fragments follow an in-plane flow at energy E = 50 MeV/nucleon, but at higher increases, the fragments shows out-of-plane/squeeze-out flow around the mid-rapidity zone.

Another salient feature that can be extracted from the mid-rapidity zone($-0.1 \leq \frac{Y_{c.m.}}{Y_{beam}} \leq 0.1$) is the transition energy [58]. The energy at which this phenomenon of transition has been observed is termed as transition energy (E_T), which gives information about participant zone. Transition energy varies inversely with fragment mass, because it has been observed that A = 4 fragments show transition at lower incident energy in comparison to other lighter fragments. Analogous findings have been reported in literature also [288]. In the mid-rapidity zone, the occurrence of transition from in-plane to out-of-plane has been observed [59].

Figs. 3.7 (a) and (b) portrays elliptic flow at centralities $\hat{b} < 0.25$ and $0.45 < \hat{b} < 0.55$ as a function of incident energies. It has been observed that the common behaviour of $< v_2 >$ calculated for different mass fragments and centralities is same, i.e., elliptic flow evolves from a preferential in-plane (rotation like) emission to out-of-plane (squeeze out) emission with an increase in the bombarding energy. This comprehensive behaviour of the results for different mass fragments alters for different centralities. One can easily observe the difference in the results outlined in Figs 3.7 (a) and (b) that the transition energy depends on centrality and fragment mass which is also validated by the observations of Andronic et. al. [57, 58]. It has been demonstrated that $< v_2 >$ for A = 1, 2, 3 and 4 is positive at the lower incident energies i.e., around (50 MeV/nucleon) and presents rotational-like emission (in-plane flow). As the energy in-

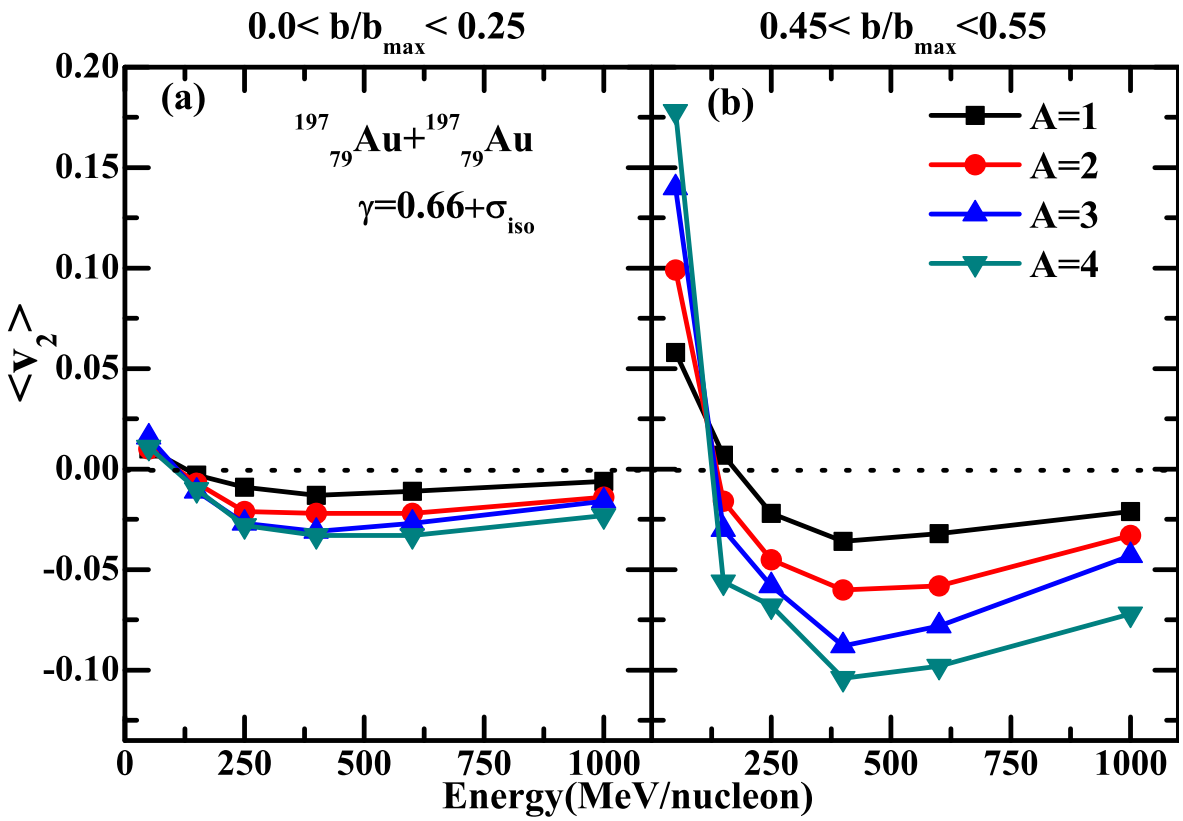

Figure 3.7: Elliptic flow at mid-rapidity for $^{197}_{79}Au +^{197}_{79} Au$ reaction for centrality (a)$0 < \hat{b} < 0.25$ and (b)$0.45 < \hat{b} < 0.55$ as a function of incident energy for different mass fragments.

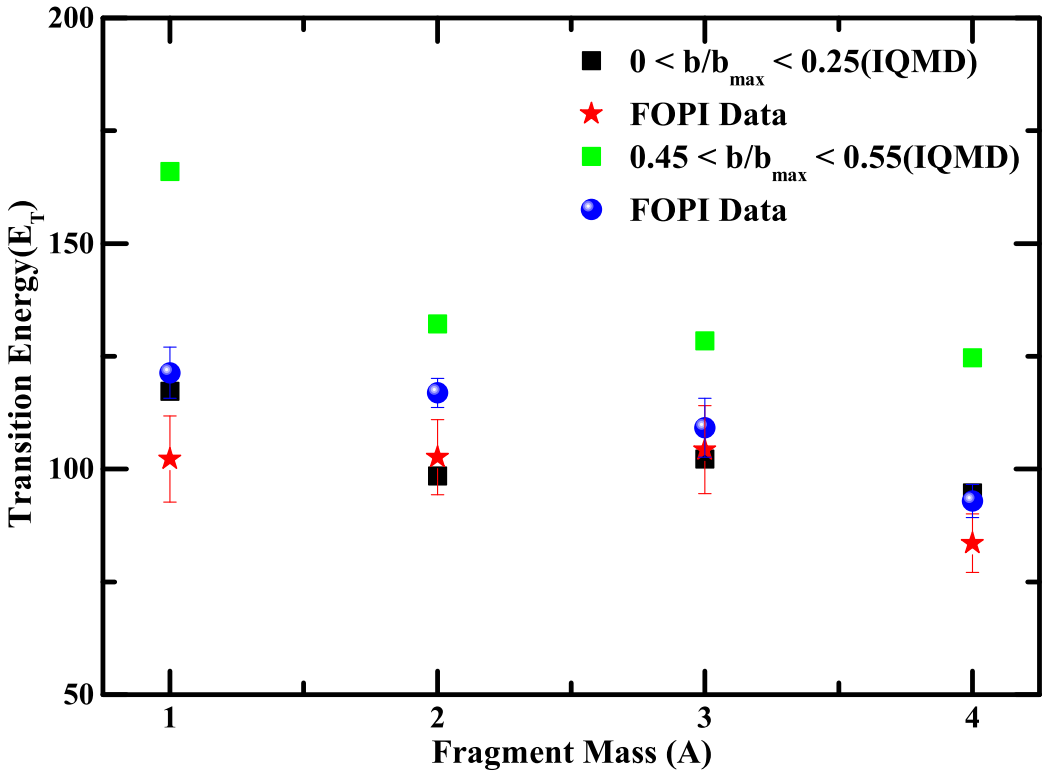

Figure 3.8: Transition energy of different mass fragments for centrality $0 < \hat{b} < 0.25$ and $0.45 < \hat{b} < 0.55$ for $^{197}_{79}Au +^{197}_{79} Au$ reaction.

creases (150 MeV/nucleon), the transition from in-plane to out-of-plane leads to overall enhancement in the out-of-plane emission with maxima around 400 MeV/nucleon with a negative magnitude (squeeze-out). Beyond this energy, $< v_2 >$ decreases and finally turns out to be in-plane rotational-like emission [289].

The magnitude of elliptic flow for heavier fragments is larger in comparison with lighter fragments [57, 290]. Here one can clearly observe that the magnitude of $< v_2 >$ is more positive (in-plane) at low incident energies and more negative (out-of-plane) at higher incident energies for A = 4 fragment than for lighter mass fragments. Also, the elliptic flow related with the fragments increases with impact-parameter [58]. The strength of squeeze-out (more negative) flow is more at $0.45 < \hat{b} < 0.55$ than $\hat{b} < 0.25$, because elliptic flow is basically the counter balancing of the expansion of highly com-

pressed interacting participant matter and spectator matter passing time. Moreover, semi-peripheral impact-parameter strengthens the spectator matter than at nearly central impact-parameter.

Consequently, in case of Fig. 3.7 (b), there is more spectator matter than the interacting participant matter, therefore the participant matter having less volume and high pressure gradient, expel out or squeeze-out with very high velocity after the passage of spectator and the nucleons experience the jet-like squeeze-out which is obviously more than that at central impact parameter. It is seen that the magnitude of elliptic flow for A = 4 fragment is highest for both in-plane at low energies and out-of-plane at higher energies for preceding centralities. It is due to the fact that as the mass of fragment is increased, the corresponding net momentum of fragment has also been enhanced. So, the heavier fragment encounters more in-plane flow at low energies and more squeeze out at high energies than the lighter fragments.

Although the trends obtained are analogous for in-plane to out-of-plane emission for incident energies between 50 MeV/nucleon and 400 MeV/nucleon, but the transition energies are somehow different for A = 1, 2, 3 and 4 as obtained in Fig. 3.7 (a) at centrality $0.0 < \hat{b} < 0.25$ (shown in Fig. 3.8). Large variation is noted in the E_T at the higher values of centralities. For the centrality range $0.45 < \hat{b} < 0.55$ (semi-peripheral collision) sufficient amount of energy is needed to counter-balance the in-plane flow with out-of-plane flow, due to the presence of larger spectator zone. Also the value of transition energy is dissimilar for different mass fragments [57, 290]. It has been observed that A = 1 fragment shows transition from in-plane to out-of-plane at incident energy 165.9 MeV/nucleon and A = 4 fragment undergoes this transition at incident energy 124.7 MeV/nucleon. Therefore, A = 4 fragment shows transition at lower incident energy as compared to lighter mass fragments, because the A = 4 fragment already has more value of net momentum associated with them.

At centrality $0.0 < \hat{b} < 0.25$ (central collision), the fragments are distributed nearly spherically, here the values of E_T is almost equivalent for different mass fragments (for A = 1 (117.2 MeV/nucleon) and for A = 4 (94.71 MeV/nucleon)). The reason behind this is the smaller spectator zone and larger participant zone. Therefore, it utilizes less

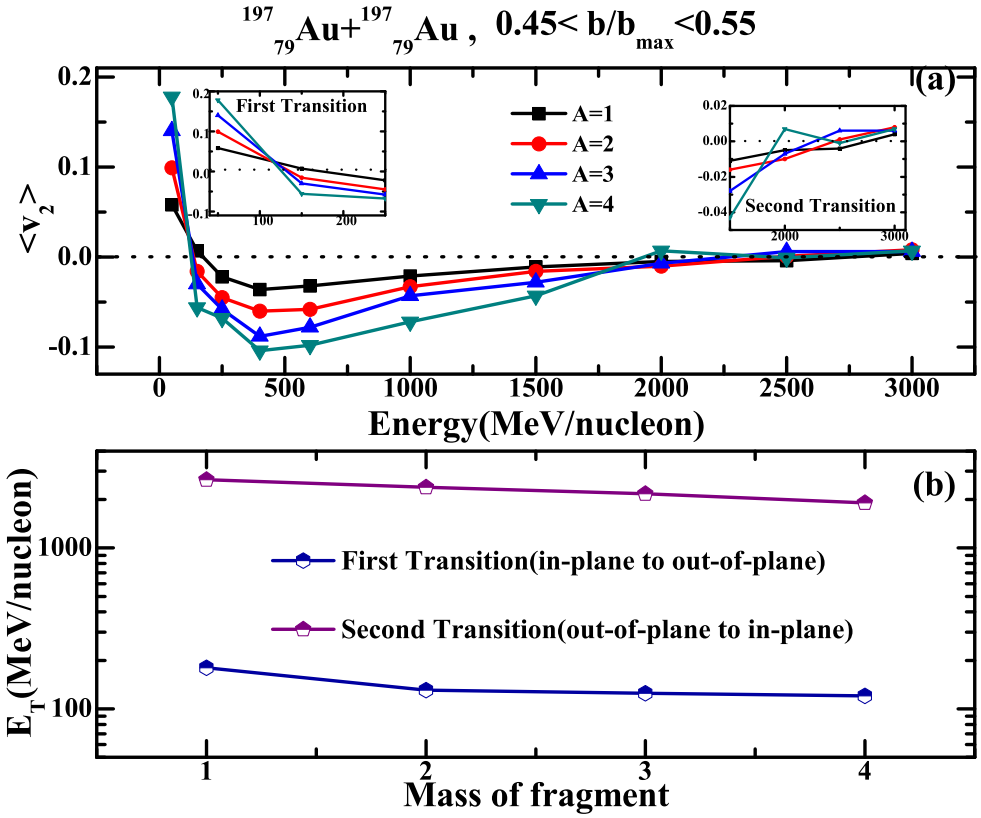

Figure 3.9: (a)Excitation function of elliptic flow for higher energy range at mid-rapidity for $^{197}_{79}Au +^{197}_{79} Au$ reaction for centrality $0.45 < \hat{b} < 0.55$ for different mass fragments (b)Energy as a function of mass of fragment for first and second transitions from in-plane to out-of-plane and vice versa.

energy to counter-balance the in-plane and out-of-plane flow at nearly central collisions. It can be seen clearly in the Fig. 3.8, that the transition energy is a function of centrality and mass dependence in accordance with the experimental findings [57,58,290]. Experimental data of Andronic et al.(FOPI) [58] are compared with our theoretical results at geometry that lies close to used geometry range for calculations and the trend is in agreement with the FOPI data points.

In recent studies, the IQMD model has been used for calculations upto incident energy 2 GeV/nucleon [291]. To inspect second transition of the elliptic flow, simulations have been performed upto incident energy 3 GeV/nucleon for $^{197}_{79}Au+^{197}_{79}Au$ reaction at $0.45 < \hat{b} < 0.55$. The results have been displayed in Fig. 3.9 (a) for the different mass fragments. Here, the second transition from out-of-plane to in-plane has been noticed

clearly. At high energies, the longitudinal shapes of the contracted nuclei or fragments becomes smaller in comparison to the transverse shapes and as a consequence, the passing time becomes too minimal as compared to the essential time required for the development of elliptic flow.

The cross over regions corresponding to first and second transitions have been displayed in the insets. The shadowing disappears and the elliptic flow fully establishes in-plane flow. It has been reported in [60] that second transition energy is independent of particle type. But one can notice that A = 4 fragments undergoes transition from out-of-plane to in-plane very early (nearly around incident energy 2 GeV/nucleon) than the other mass fragments. Lighter fragments take more energy to undergo this transition. This is because, the heavier fragments having more mass and therefore suffers more squeeze out than rest of the lighter fragments at the same energy for a given centrality.

Furthermore, deviation in energy for both transitions of elliptic flow i.e., from in-plane to out-of-plane or vice-versa with energy has been displayed in Fig. 3.9 (b) as a function of fragment mass. Here it is clearly observed that the first transition for all the fragments observed around incident energy 100 MeV/nucleon and second transition take place between the incident energy range 2-3 GeV/nucleon. The first as well as second transition depends on the mass of fragments.

Rotation of elliptic flow with energy is another interesting thing to explore. Next section will put lime-light on this feature.

3.2.4 Rotation of elliptic flow with energy

It would be interesting to view the orientation of nucleons that participates in elliptic flow in the mid-rapidity zone. In Fig. 3.10, the momentum-space distribution of nucleons involved in elliptic flow at different energies has been displayed. In this Fig., the rotation of the ellipse is clearly noticed as a function of incident energy. It is obvious that at lower energies, the flow is in plane and with enhancement in energy, the flow shifts to out-of-plane. The shape and angle of ellipse with respect to the reaction-plane differs. Another feature about the strength of elliptic flow as a function of energy is

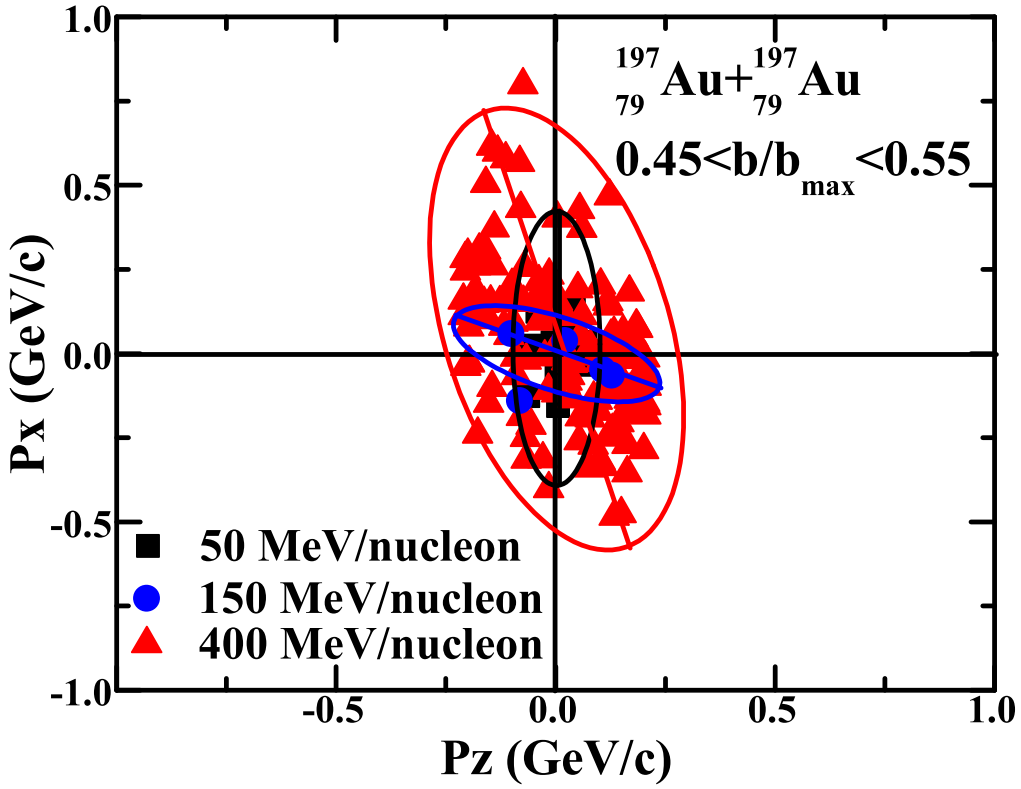

Figure 3.10: Momentum-space distribution of elliptic flow in x-z plane at different energies.

also seen. At lower incident energies, lesser number of nucleons participating in elliptic flow due to Fermionic nature of nucleons (Pauli blocking), the flow is positive and in-plane. As the incident energy increases up to 150 MeV/nucleon, the yield of nucleons is spherical around the transition energy point for $^{197}_{79}Au +^{197}_{79} Au$.
Finally, a squeeze-out is observed at 400 MeV/nucleon and the maximum spread of nucleons is seen at this energy. As it has been reported in literature that, the elliptic flow reaches its maximum negative value (maximum squeeze-out flow) at incident energy 400 MeV/nucleon and this similar observation has been confirmed in the Fig. 3.10. The rotation of ellipse with respect to the reaction plane is clearly viewed as the incident energy is increased. At incident energy 50 MeV/nucleon, the rotation of ellipse about the z-axis is 90^o, rotated to 112.87^o at incident energy 150 MeV/nucleon, finally squeeze-out and rotates to 165.58^o at incident energy 400 MeV/nucleon. The analogous observations are also checked(not shown here) for centrality $\hat{b} < 0.25$. This strength of elliptic flow depends on the impact parameter of colliding nuclei. It is maximum at peripheral or nearly peripheral impact parameter ($0.45 < \hat{b} < 0.55$) and minimum at nearly central or central collision ($\hat{b} < 0.25$).

3.3 Summary

In conclusion, we have explored elliptic flow for different mass symmetric colliding systems, centralities and incident energies using IQMD model for different rapidity intervals.

- It is found that the width of distribution of nucleons of $< -v_2 >$ as a function of rapidity enhances with mass of the colliding nuclei. Impact of symmetry energy and isospin dependent cross-section on elliptic flow has been noticed.

- Squeeze-out flow of different fragments masses for $^{197}_{79}Au +^{197}_{79} Au$ reaction has also been investigated and shown that more squeeze-out is observed for heavier fragments.

- Moreover, the transition energy is calculated for different mass fragments extracted in $^{197}_{79}Au +^{197}_{79} Au$ reaction at two centralities $\hat{b} < 0.25$ and $0.45 < \hat{b} < 0.55$

and calculated that the transition energy is dependent on centrality as well as on the mass of the fragment.

- The first transition of v_2 (from +ve to -ve) as well as and second transition of v_2 (-ve to +ve) too depends upon the mass of fragment.
- The distribution of nucleons participating(momentum-space of nucleons)in the elliptic flow and the rotation of ellipse as a function of incident energy has been shown.

Chapter 4

Rotational dynamics in mass-asymmetric nuclear reactions

4.1 Introduction

During the initial phase of nuclear reactions, the aligned movement of participating nucleons of target and projectile is disturbed, thus energy released during this process leads to rotational motion of the nucleons at low/intermediate energies [113]. Rotational motion of nucleons depend on the incident energy, impact parameter and the mass asymmetry of the nuclear reaction. These rotational effects are related to many phenomena in the heavy ion collisions at intermediate energies like nuclear stopping [47], side-splash, bounce-off and squeeze-out [114], which provide a deep insight of the azimuthal distributions of the emitted nucleons within or out of the reaction plane.

The rotational effects in the nuclear heavy ion collisions are calculated using various quantities like angular velocity, angular momentum, rotational energy and moment of inertia etc. These quantities show well defined behavior of nucleons at different incident energies, centralities and mass asymmetry of the reactions. For mass symmetric nuclear reaction at low incident energies, angular momentum plays a significant role in the reaction dynamics e.g. if the value of angular momentum is less than the critical angular momentum value then the complete fusion takes place and a hot rotating compound nucleus is formed. The formed compound nucleus further decays mainly by fission or by emission of other particles. Moreover, if the value of angular momentum is greater than that of the critical angular momentum value of the colliding nuclei

Figure 4.1: Representation of collision of two rotating galaxies [292].

(especially for highly mass asymmetric nuclear reaction), the incomplete fusion takes place and deep inelastic and direct reactions are observed [293]. However, at intermediate energies, the energy is sufficient for collision of target and projectile which results in multi-fragmentation [23] and collective flow [27, 28, 161]. The emitted nucleons or fragments exhibit the rotational properties. It has been reported in the literature that emission of fragments in a nuclear reaction plane is not uniform even around the beam axis or in other words, the emission of fragments/nucleons is anisotropic [294].

Deformations of the colliding nuclei are also accountable for the rotation of the compound nucleus at low incident energies, but at the intermediate energies the deformations are neglected due to the higher values of energy and momentum. Rotational behaviour of emitted nucleons and other particles at intermediate energies for mass asymmetric colliding nuclei has been investigated by many theoreticians [112–116]. The study of rotational quantities have been carried out by Chen et al. [116] for mass symmetric nuclear reactions for semi-peripheral collisions at 40 MeV/nucleon.

This rotational phenomenon of nuclei can be co-related with the rotational dynamical features of the galactic matter in the universe. Fig. 4.1 shows the collision of two rotating galaxies in the universe. The formation and evolution of the galaxies depend on the collision process of two rotating galaxies as shown in Fig. 4.1. It has been discussed in literature [6] that the elliptical galaxies were formed from collisions of rotating spiral galaxies. The collision of spiral galaxies would have heated up much of the gas, turning them into stars which can be seen today in the collisions of galaxies too. The rotation of galaxies decide the shape of the final galaxies after the collision process. In the present chapter, author has studied the rotational dynamics in mass symmetric and mass asymmetric nuclear reactions [8].

4.2 Results and discussion

Several thousands of events have been simulated using IQMD model for the mass asymmetric reactions of $^{122}_{49}In +^{124}_{50} Sn$, $^{114}_{48}Cs +^{134}_{54} In$, $^{100}_{40}Mo +^{148}_{64} Gd$, $^{86}_{36}Kr +^{162}_{67} Ho$, $^{71}_{31}Ga +^{177}_{71} Lu$, $^{60}_{28}Ni +^{188}_{76} Os$ and $^{50}_{24}Cr +^{198}_{78} Pt$ (η = 0.0, 0.1, 0.2, 0.3, 0.4, 0.5 and 0.6 respectively). The analysis has been performed at incident energies from 40 MeV/nucleon to 100 MeV/nucleon for impact parameter range $0.25 < \hat{b} < 0.45$ ($\hat{b} = \frac{b}{b_{max}}$).

The rapidity intervals used in the calculations is defined as in equation 1.3 [252]: The region around zero value $-0.5 \leq \frac{Y_{c.m.}}{Y_{beam}} \leq 0.5$ is labelled as mid rapidity region, which plays a crucial role in extracting the collective flow, nuclear stopping and isospin mixing etc. [61,169,275]. The region from $\frac{Y_{c.m.}}{Y_{beam}} < -0.5$ is termed as target like (T.L.) rapidity, which include the nucleons of spectators from target, while $\frac{Y_{c.m.}}{Y_{beam}} > 0.5$ side is known as projectile like (P.L.) rapidity comprised of spectator nucleons from projectile and these regions also provide crucial information of flow individually [62, 84]. This criterion of selecting the target-projectile like nucleons and mid-rapidity range nucleons is however applicable only for the symmetric nuclear reactions ($\eta = 0.0$). Since the reaction dynamics are significantly influenced by mass asymmetry of a reaction, therefore one has to choose asymmetric mid-rapidity range for different mass asymmetric reactions as shown in table 4.1.

Equations 1.9, 1.10, 1.11 and 1.12 have been used for the calculation of <moment of

Table 4.1: Rapidity ranges for different mass asymmetric reactions

η	Mid-rapidity range	T.L. like rapidity	P.L. like rapidity
0.0	$-0.48 \leq \frac{Y_{c.m.}}{Y_{beam}} \leq 0.50$	$\frac{Y_{c.m.}}{Y_{beam}} < -0.48$	$\frac{Y_{c.m.}}{Y_{beam}} > 0.50$
0.1	$-0.43 \leq \frac{Y_{c.m.}}{Y_{beam}} \leq 0.50$	$\frac{Y_{c.m.}}{Y_{beam}} < -0.43$	$\frac{Y_{c.m.}}{Y_{beam}} > 0.50$
0.2	$-0.34 \leq \frac{Y_{c.m.}}{Y_{beam}} \leq 0.50$	$\frac{Y_{c.m.}}{Y_{beam}} < -0.34$	$\frac{Y_{c.m.}}{Y_{beam}} > 0.50$
0.3	$-0.27 \leq \frac{Y_{c.m.}}{Y_{beam}} \leq 0.50$	$\frac{Y_{c.m.}}{Y_{beam}} < -0.27$	$\frac{Y_{c.m.}}{Y_{beam}} > 0.50$
0.4	$-0.20 \leq \frac{Y_{c.m.}}{Y_{beam}} \leq 0.50$	$\frac{Y_{c.m.}}{Y_{beam}} < -0.20$	$\frac{Y_{c.m.}}{Y_{beam}} > 0.50$
0.5	$-0.16 \leq \frac{Y_{c.m.}}{Y_{beam}} \leq 0.50$	$\frac{Y_{c.m.}}{Y_{beam}} < -0.16$	$\frac{Y_{c.m.}}{Y_{beam}} > 0.50$
0.6	$-0.13 \leq \frac{Y_{c.m.}}{Y_{beam}} \leq 0.50$	$\frac{Y_{c.m.}}{Y_{beam}} < -0.13$	$\frac{Y_{c.m.}}{Y_{beam}} > 0.50$

inertia/nucleon>, <angular momentum/nucleon>, <rotational energy/nucleon> and <angular velocity> respectively.

4.2.1 Angular Momentum

Fig. 4.2, shows the <angular momentum/nucleon> at incident energy, E = 50 MeV/nucleon. In general, angular momentum is the measure of rotation of the system comprising of nucleons after the collision. $<L_y/\mathrm{A}>$ is plotted for different η values and rapidity intervals. Table 4.1 shows the different rapidity ranges for mid-rapidity, T.L. and P.L. for each η value. These ranges have been estimated by calculating the equal contributions of nucleons from both sides of rapidity interval about zero value. These ranges for each η value have been utilised in the present calculations. In left panel of Fig. 4.2, the simulation results of $<L_y/\mathrm{A}>$ have been displayed for the mid-rapidity or participant region. The rotation of the participating nucleons is clearly influenced by the mass asymmetry of the reaction as well as the ranges of rapidity region. It has been checked (in Fig. 2.1) that the initialized nuclei have non-zero values of average angular momentum $<L_y/\mathrm{A}>$, indicating that the nuclei were themselves rotating around their own axis before the collision.

The participating nucleons experience a strong rotational motion initially at the time of collision but later on, this rotation slows down. This is because the nucleons start colliding with each other and therefore the value of their momentum decreases which leads to gradually decrease in the value of (angular momentum)/nucleon for all the

cases (except for η = 0.5-0.6). This trend is then followed by the regular increase in the values of $<L_y/\mathrm{A}>$ at freeze-out stage. At this stage, the participating nucleons start mixing with spectator nucleons and lead to enhance the rotational motion among the nucleons hence results in higher value of angular momentum.

Very interesting results were observed for the higher mass asymmetry content, η = 0.5 - 0.6. Here the size of projectile is very small as compared to the size of target. When the collision takes place around time 20 - 30 fm/c, the projectile needs a higher value of $<L_y/\mathrm{A}>$ to rotate the target nuclei, but this rotation slows down moderately with time. However, the impact of collision in these mass asymmetric reactions provides relatively higher value of $<L_y/\mathrm{A}>$ than the other η values. To verify this behaviour of η = 0.5 and 0.6, the simulations have also been performed for η = 0.7 ($^{40}_{20}Ca +^{208}_{82} Pb$) (not shown here), which give the analogous trend and higher values than all other mass asymmetric reactions at the collision time 20 - 30 fm/c. This trend is followed by the lower values of angular momentum at the freeze-out stage due to decay of spectator part into free nucleons/fragments.

In Fig. 4.2 (b), the angular momentum variation for different mass asymmetric reactions have been displayed. One can observe from this figure that till time 100 fm/c, both the participant as well as spectator show change in angular momentum value. After 100 fm/c, both spectator and participant nuclear matter tend to achieve equilibrium stage. The value of angular momentum is higher for spectator region as compared to participant zone and hence one can conclude that nucleons of spectators are moving with higher values of angular velocity. The presence of Coulomb interactions also strengthens the destruction of correlations among the nucleons of the colliding nuclei. Moreover, this phenomenon too depends on the mass asymmetry of the nuclear reaction because the sizes of the emitted fragments depend on the participant zone, which keeps on diminishing with increasing η. The value of $<L_y/\mathrm{A}>$ for mid-rapidity zone then increases steadily up to time 200 fm/c. The participating nucleons enter into the diluted phase up to the saturation time and hence suffers more rotation than the earlier phase leading to higher values of $<L_y/\mathrm{A}>$.

One can clearly observe the difference in the behavior of nuclear matter in the different

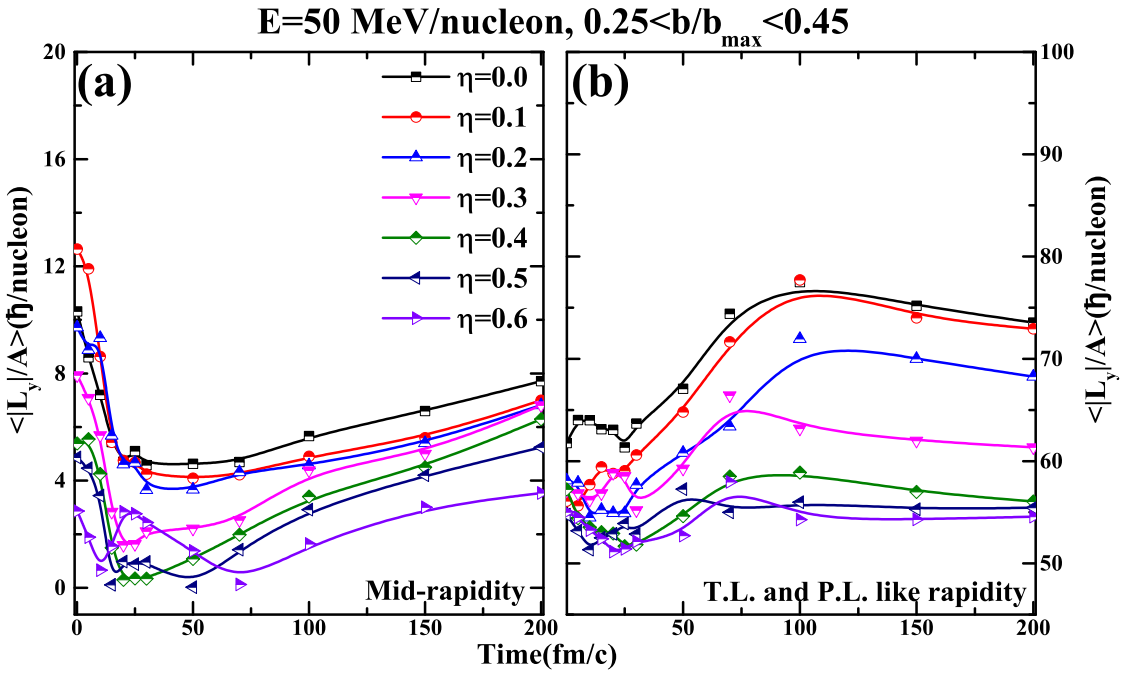

Figure 4.2: Angular momentum/nucleon for different mass asymmetric reactions and rapidity regions as a function of time.

rapidity regions, which are due to different mass asymmetry of the reaction as shown in Fig. 4.3. It is obvious that in the participant region, peak or saturated value of scaled density keeps on decreasing with the increase in mass asymmetry of the reaction (can be seen in Fig. 2.5). Here, the role of symmetry energy comes into play, which depends on the isospin asymmetry of nuclear matter and their instant density values too [50]. However the symmetry energy effects the rotational dynamics mainly for the participant or at mid-rapidity region. Therefore, the rotation at the given energy too behaves differently with the change in η values around the mid-rapidity and spectator rapidity region as shown in Fig. 4.3 (a) and (b) respectively. The variation of $<L_y/\mathrm{A}>$ with increasing η has been shown at time 30 fm/c (during collision stage) and time 200 fm/c (saturation stage) for mid-rapidity (upper panel) and away from mid-rapidity region (lower panel), which includes 80 % of rapidity region.

In the upper panel of Fig. 4.3, the lower values of angular momentum around time 30 fm/c indicate the compressional stage i.e., participant zone which slows down and then rotate very fast once compressed phase is over as one can see clearly in Fig. 4.2 (a)

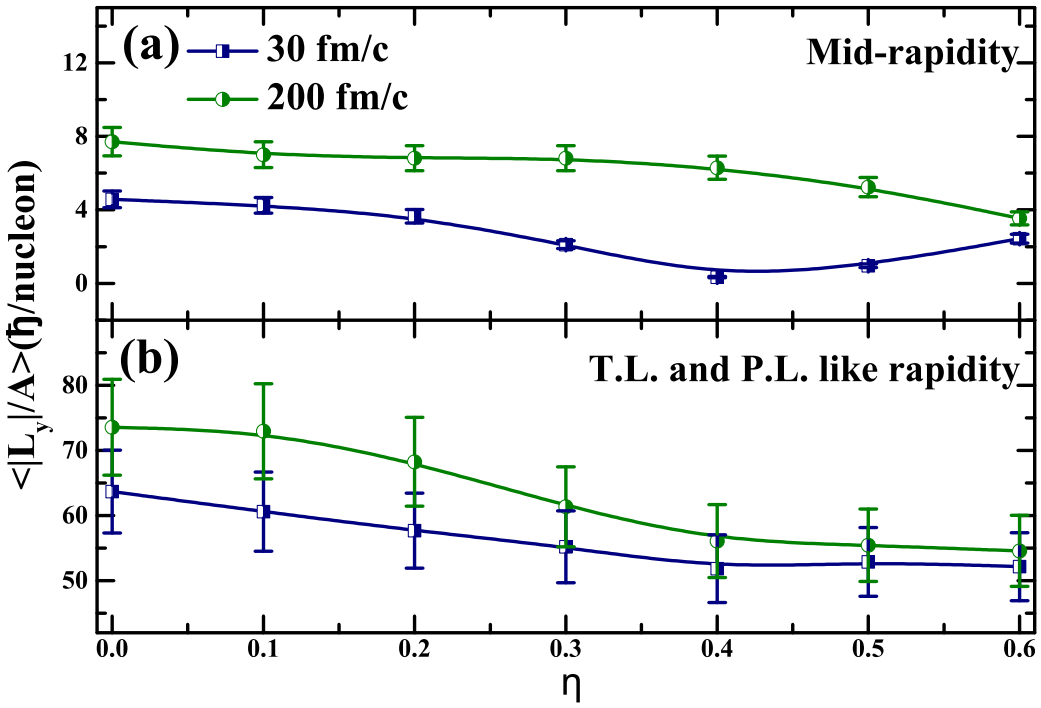

Figure 4.3: Angular momentum/nucleon as a function of mass asymmetry parameter at different time-steps and rapidity regions.

(at time 200 fm/c). In addition to this, the value of $<L_y/\mathrm{A}>$ increases at $\eta = 0.6$ as discussed earlier. In contrast to Fig. 4.3 (a), the higher values of angular momentum at time 200 fm/c is obviously due to the transition of the participant matter nucleons into the diluted phase. Moreover, the another feature that appears from the collisions verses η graph (Fig. 2.4) is that the number of collisions are decreasing with the increasing mass asymmetry of the reaction. This justify our results in Fig. 4.2 which shows that the angular momentum/nucleon decreases with the higher mass asymmetry of the reaction.

Fig. 4.3 (b) demonstrates the dynamics of spectator zone's nucleons on both sides of mid-rapidity region for different η on time scale. The rotation of the spectator nucleons attains higher values of $<L_y/\mathrm{A}>$ at the freeze-out stage than the compressional stage because the spectator matter further decays into the different mass fragments after the compressional stage around time 50 - 60 fm/c. That is why the value of angular momentum is lower at time 30 fm/c. The trend of $<L_y/\mathrm{A}>$ is somehow analogous for both the panels of Fig. 4.3, showing decreasing pattern constantly with η. Energy transfer to spectator nucleons is very small in highly mass asymmetric nuclear reactions. The spectator's part keeps on enhancing with the increasing mass asymmetry, but the rotation decreases because the spectator matter decay into more number of heavy fragments in order to reach the stability. It can therefore be concluded from Fig. 4.3, that the rotational dynamics varies inversely to the mass asymmetry content of the reaction. Theoretical error bars have been added to the calculated values of $<L_y/\mathrm{A}>$ using the statistical methods.

Theoretical results of both the panels of Fig. 4.3 have been fitted linearly (not shown here). This fitted values also justify the above statement that the change in slope value is very minimal for participant or mid-rapidity zone, but for spectator rapidity, an appreciable variation has been observed. These results indicate that the spectator matter rotates more rapidly with the mass asymmetry of the nuclear reaction. Hence, the value of angular momentum/nucleon is more for spectator nucleons as compared to participant nucleons. One can correlate the variation in angular momentum of nuclear matter with rotational behavior of galactic matter in universe when two galaxies collide

with each other.

4.2.2 Moment of inertia

Next quantity to be investigated, is the <moment of inertia/nucleon> shown in Fig. 4.4 (a and b). Very clearly, in both cases i.e., mid-rapidity and spectator rapidity regions show almost similar trends with time. The initial time steps have provided very interesting information. It is well known fact that any object having higher value of moment of inertia is harder to undergo rotation. Similarly when two already rotating nuclei collides with each other, their value of <moment of inertia/nucleon> increases very rapidly. This indicates that after the collision process, the rotation of the two colliding nuclei ceases for some duration and it becomes difficult to observe the rotational phenomenon. However after some time, this value of $<I_y/\mathrm{A}>$ increases with time, but differently for all the η values.

The rotational features are clearly visible around time interval 40-50 fm/c at the overlapping stage of both the colliding masses. After this time interval, rotation increases abruptly till saturation stage. The points of minima are seen clearly in both Fig. 4.4 (a and b) but the range is somehow different for both the rapidity regions. Value of minima lies between time interval 30 fm/c to 60 fm/c for mid-rapidity (Fig. 4.4 (a)) because in this participant region, the maximum exchange of interactions take place and leads to more rotation. However, the minima lies around time interval 25 fm/c for the other case of spectator rapidity region (Fig. 4.4 (b)), the reason is very clear. Here the heavier mass fragments are emitted from the spectator rapidity zone which further decays continuously to other fragments [24] and therefore exhibit more rotation.

Moment of inertia is rotational analogue of mass which refers to the body's resistance to undergo rotational motion. Larger the value of moment of inertia, greater is the force required to bring any rotation of the body. Therefore a heavy mass fragment having higher value of moment of inertia will rotate slower than a free nucleon with a low value of moment of inertia. Thus, the lower value of $<I_y/\mathrm{A}>$ means that the emitted nucleons have more rotational degrees of freedom. At time 200 fm/c, the centre of mass of the scattered nucleons is far from the axis of rotation and leads to the

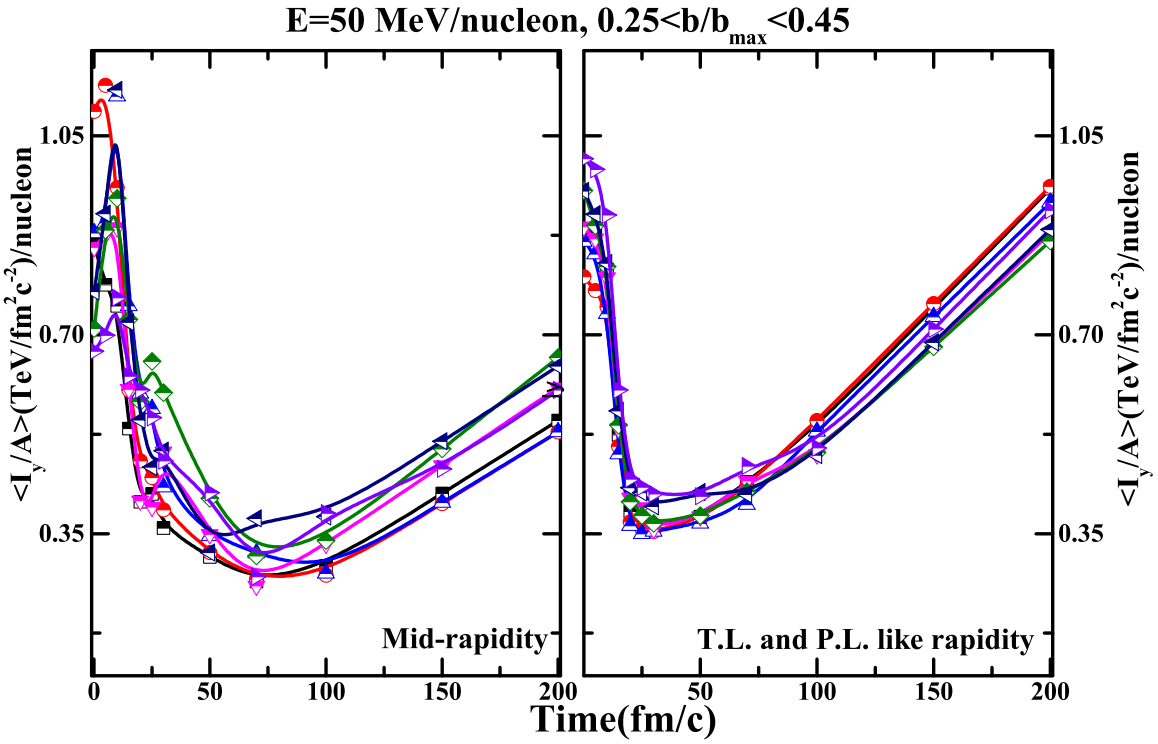

Figure 4.4: Moment of inertia/nucleon for different mass asymmetric reactions for different rapidity regions as a function of time.

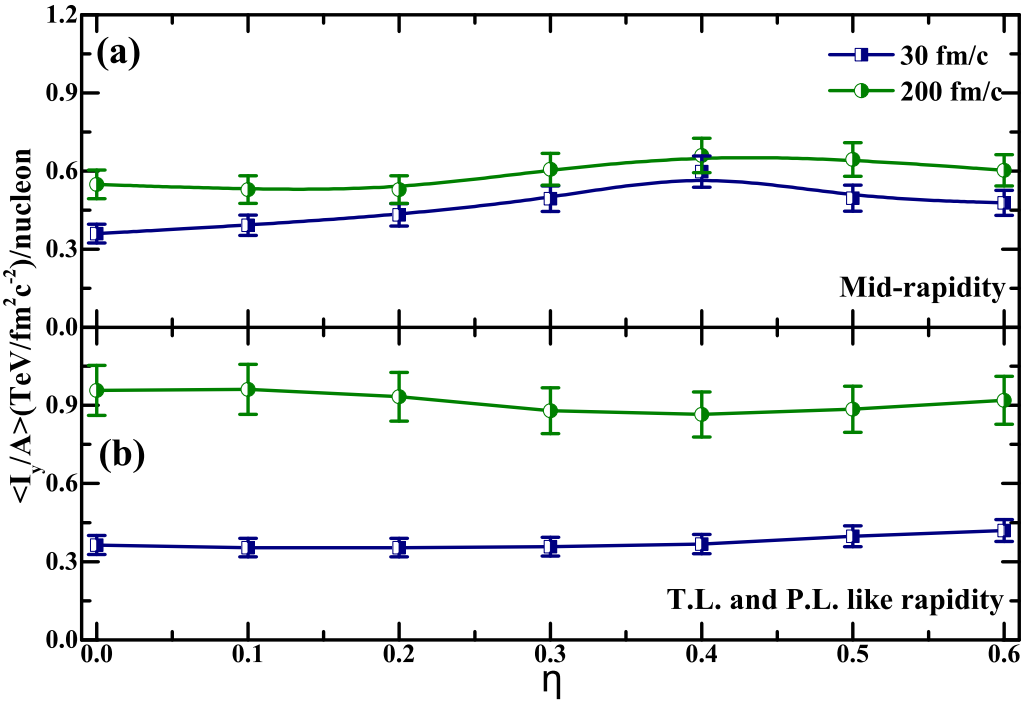

Figure 4.5: Moment of inertia/nucleon as a function of mass asymmetry parameter at different time-steps and rapidity regions.

enhancement in the magnitude of moment of inertia. The amount of torque needed to rotate nuclei depends on participant's mass distribution about the axis of rotation and this distribution is obviously changing with time.

Fig. 4.5 (a and b) displays the $<I_y/\mathrm{A}>$ variation with mass asymmetry of the reaction. It is obvious that in mass asymmetric nuclear reactions, the nucleons are distributed non-uniformly thus emitted nucleons will have different values of moment of inertia for each case of η. Both the Fig. 4.5 (a and b) shows slightly increasing pattern with η for both the time scales. As η increases, the size of target is enhanced as compared to projectile mass, which leads to emission of heavier mass fragments. These fragments are quite difficult to rotate therefore achieve higher values of moment of inertia.

In Fig. 4.5 (a), at time interval 30 fm/c, the highly dense participant region formed due to the exchange of nucleons from both sides of target and projectile and responsible for the rotation of nuclear matter and have a lower value of $<I_y/\mathrm{A}>$. However in Fig. 4.5

(b), the change is significant for the spectator rapidity and there is a large difference between the magnitudes at time 30 and 200 fm/c. Here, the spectator matter has been separated from this denser region and the remaining part, which includes the heavy mass fragments have higher values of $<I_y/\mathrm{A}>$ because of their size and thus are more difficult to rotate.

Theoretical results of Fig. 4.5 have also been fitted linearly (not shown here) and the value of slope indicates that variation in moment of inertia/nucleon versus η curve has been observed for the mid-rapidity region (upper panel). At time 30 fm/c, the nucleons are excited for small duration of time and their rotation is enhanced in this participant region. This process becomes more prominent with the increasing η. However in the lower panel at time 200 fm/c, there is slight change in values because the spectator nuclear matter is more in this rapidity region for all the values of η. This is responsible for more value of $<I_y/\mathrm{A}>$ in comparison with time 30 fm/c.

4.2.3 Rotational Energy and angular velocity

Fig. 4.6 illustrates the variation of rotational energy with time. It is obvious that the nuclei rotating around their axis of rotation will also have some rotational kinetic energy associated with them. This is the average of the kinetic energy of each individual participating nucleon of the nucleus. The independent contributions of all the participating nucleons is combined as total rotational kinetic energy ($<E_{rot}/A>$) of the rotating participating nucleons. Here, one can clearly observe that $<E_{rot}/A>$ becomes maximum around time 100 fm/c in mid-rapidity region and at time 50-70 fm/c for spectator rapidity region as shown in Fig. 4.6 (a and b).

In Fig. 4.6 (a), the higher value of rotational energy at the initial time steps is a validation that the participant nucleons are rotating at very high speed, thus the rotational kinetic energy is also maximum. After that the minima dip takes place around time interval 25 - 30 fm/c, because at that point the nuclear matter is compressed, thus the value of rotational energy is decreased. The overlapping stage during which the participant matter experiences high compression/density and hence leads to less rotational energies [295, 296]. In order to attain stability, compressed zone emits more free

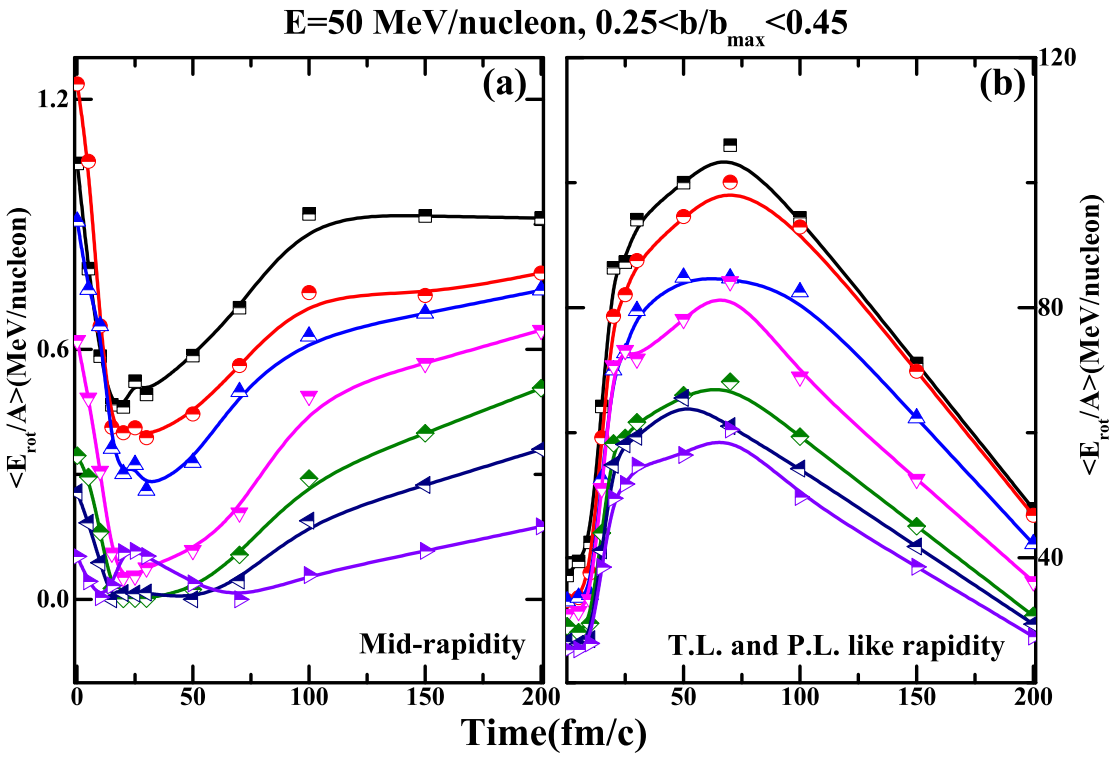

Figure 4.6: Rotational energy for different mass asymmetric reactions as a function of time for different rapidity regions.

nucleons/light mass fragments depending on their η values and they all move with different momentum values/kinetic energies. Thus rotational energy increases constantly during this process till freeze out stage. However, the values shows a decreasing pattern on y-axis because the intermediate/heaviest mass fragments are produced as the mass asymmetry of the nuclear reaction is increased [24]. These heavy fragments have low rotational energies in comparison to the free nucleons which are produced in majority for lower mass asymmetric reactions.

The exceptional behaviour of $\eta = 0.6$ at time interval 25 - 30 fm/c confirms the results of Fig. 4.2 (a) that during the collision time, the very high rotational process not only increases the angular momentum at this time but also enhances the angular velocity and thus rotational energy too. The results have been checked also for $\eta = 0.7$ value. This case gives much higher values of the angular velocity and rotational energy than $\eta = 0.6$ (not shown here). In the Fig. 4.6 (b), the rise and fall trend of rotational energy has been observed. The spectator part after being departed from the participant region have lesser rotational features in their early stage. After that, this departed spectator matter becomes unstable around time interval 50 - 70 fm/c and decays to more free nucleons/light mass fragments to attain maximum values of rotational energies. Finally, the process of rotation slows down or in other words saturates with time, that's why $<E_{rot}/A>$ is also decreasing but again systematically with η values.

Another important feature to be seen here, is the systematic behaviour of rotational energy with the mass asymmetry. To validate these results, angular velocity ($<w_y>$) has also been calculated with time, which reveals almost the similar trends for each rapidity range as for $<E_{rot}/A>$ in Fig. 4.7. These results indicate that the nuclear matter moves very fast with time and attains higher values of $<w_y>$ in the mid-rapidity zone. This value of angular velocity remains high till the thermalization then falls in the freeze-out zone as the rotating system slows down. The variation of $<w_y>$ too follows the systematic decreasing trend with η, which illustrates that the nucleons of highly mass asymmetric nuclei rotates slowly as compared to the symmetric mass nuclei for non-central impact parameters.

The nucleons from mid-rapidity zone experience high compression during the overlap-

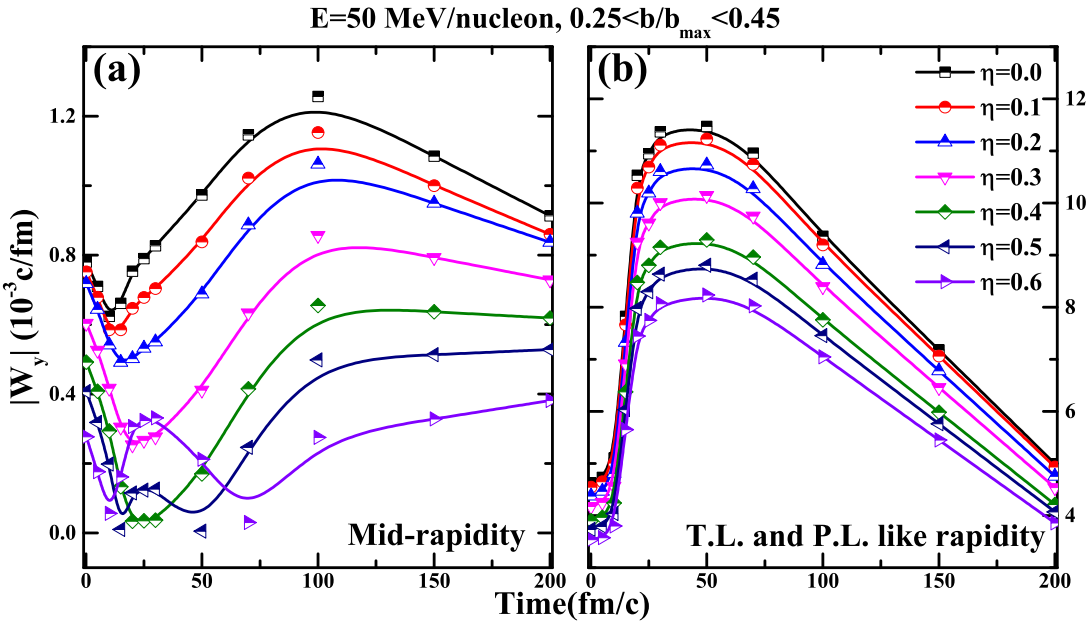

Figure 4.7: Angular velocity for different mass asymmetric nuclear reactions as a function of time.

ping of projectile and target nuclei, therefore the participant nucleons exhibit lesser rotational effects and lower values of $<w_y>$ as compared to the spectator matter. The symmetry energy and repulsive Coulomb interactions causes the expansion of highly dense matter during the overlapping process and thus fragmentation phenomenon takes place, which too depends on η. This phenomenon enhances the rotational motion of the participant nucleons and the values of $<w_y>$ are increased as shown in Fig. 4.7 (a). In the Fig. 4.7 (b), the spectator matter exhibit rise and fall pattern with increasing time. This might be due to the destruction of spectator matter in order to attain the stability. Initially the matter after being departed from the participant matter is at rest, but around time 50 fm/c, the unstable spectator part decays into fragments of different masses. The spectator matter is rotating very fast during this interval, but slows down at the freeze-out stage.

4.2.4 Rotational flow

Fig. 4.8 displays the azimuthal distribution of free protons for the reaction of $^{20}_{18}Ar+^{27}_{13}Al$ at incident energy 45 MeV/nucleon and impact parameter 4.5 fm. Here, the simulations

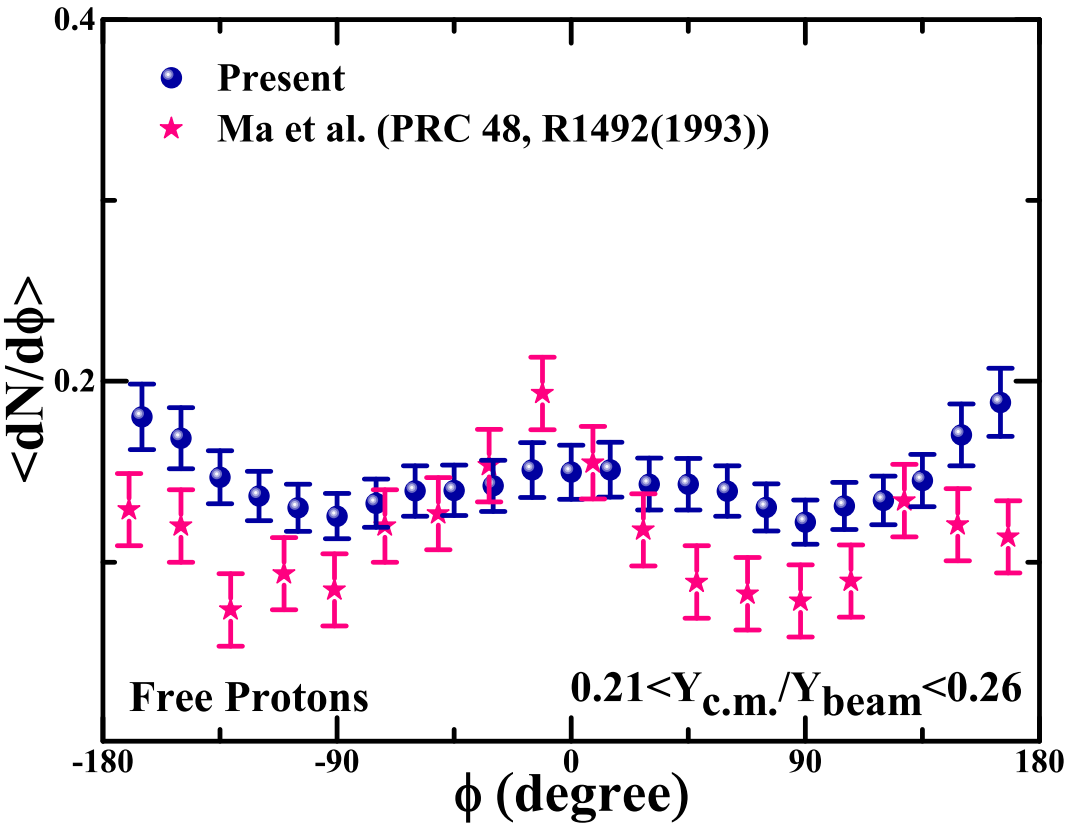

Figure 4.8: Comparison of IQMD model calculated results of azimuthal distribution of protons for the reaction ${}^{20}_{18}Ar + {}^{27}_{13}Al$ with BUU model.

have been carried out for rapidity region from $0.21 \leq \frac{Y_{c.m.}}{Y_{beam}} \leq 0.26$ (same rapidity as in ref. [112]). The azimuthal angle (ϕ) is taken between $-180^0 < \phi < 180^0$ and the azimuthal angle is calculated as [117]:

$$\phi = \arctan 2(P_y, P_x), \tag{4.1}$$

where P_x and P_y are the momentum coordinates. The distribution of free protons shows rotational flow and within this rapidity range, the contribution of positive in-plane component of transverse momentum results in the maximum values at 0^0, $\pm 180^0$ and minima at $\pm 90^0$. To validate our calculated results, a comparison has been carried out with the BUU model [112] calculations and our results are following the similar trend.

Now, it would be interesting to investigate whether the mass asymmetry influences the rotational flow of free protons with increasing incident energy or not? Expanding our calculations of azimuthal distribution, we have attempted to explore the distribution of rotational flow with the enhancement in bombarding energies for different η values for the range of $-180^0 < \phi < 180^0$ as shown in Fig. 4.9. However, the results have been shown for two extreme cases of $\eta = 0.0$ and $\eta = 0.6$ value only, but the calculations have been performed for all the mass asymmetric reactions values. The mid-rapidity regions for the calculations of both the cases have been taken from table 4.1.

In the left panel of Fig. 4.9, the results have been shown for mass symmetric nuclear reactions having ($\eta = 0.0$), here one can see very clearly that at low incident energies, the flow of free protons is following an in-plane flow as maxima points are observed at $0^0, \pm 180^0$ and minima at $\pm 90^0$ for the incident energies between 40 MeV/nucleon and 150 MeV/nucleon. Above incident energy 150 MeV/nucleon, the transition from in-plane to out-of-plane take place, which can also be seen from Fig. 4.10 (where the elliptic flow is plotted against the incident energy). The out-of-plane or squeeze-out flow can be seen at higher energies, where one can observe maxima at $\pm 90^0$ and minima at $0^0, \pm 180^0$.

One can observe clearly from right panel of Fig. 4.9 an in-plane or rotational flow for the case of $\eta = 0.6$. Small number of collisions at low incident energy, E = 50 MeV/nucleon result in the emission of few protons following in-plane flow around the

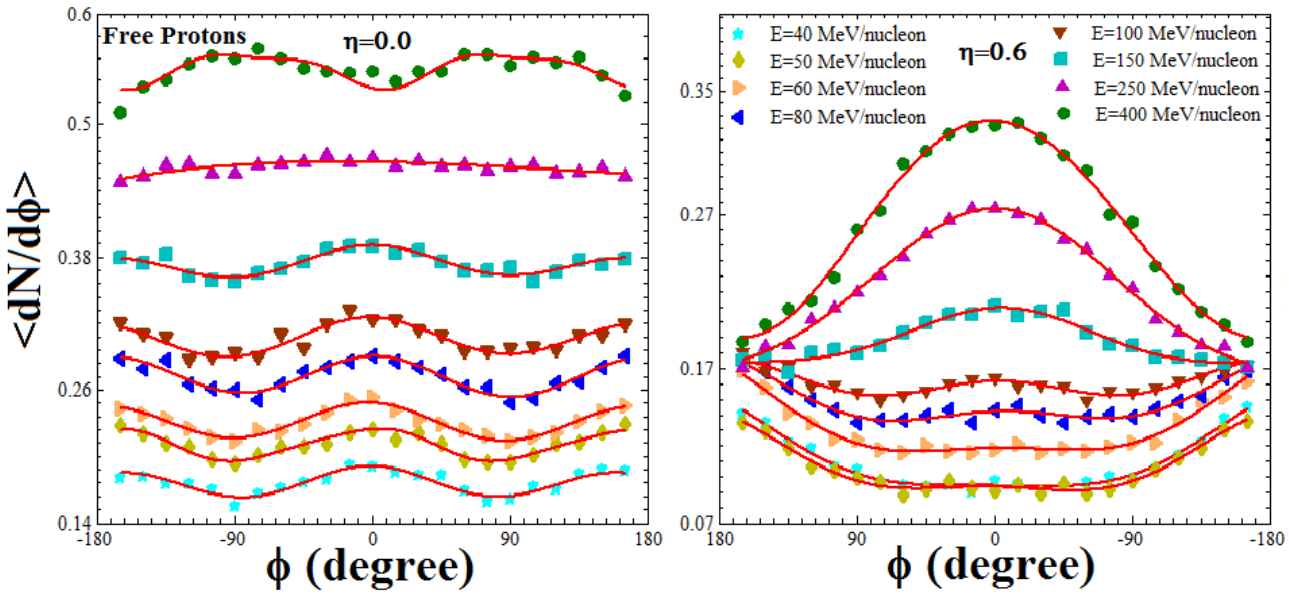

Figure 4.9: Azimuthal distribution of free protons for mid-rapidity region for ${}^{122}_{49}In + {}^{126}_{50}Sn$ ($\eta = 0.0$, left panel) and ${}^{50}_{24}Cr + {}^{198}_{78}Pt$ ($\eta = 0.6$, right panel), red lines are the fitting lines of the Fourier expansion.

0^0. With the enhancement in incident energy, the in-plane flow pattern keeps on spreading more and more due to more frequent nucleon-nucleon collisions. This observation indicates that the azimuthal distributions of free protons is showing peak at 0^0, which implies that there is rotational behavior and the protons are preferentially emitted with-in the reaction plane.

However, if the emission of protons would have followed the peak value at $\pm 90^0$, then it might have a squeezed-out flow with increasing incident energy but in right panel of Fig. 4.9, the calculations have been performed for a mass asymmetric nuclear reactions. There is requirement of sufficiently high incident energies for the transition from in-plane to out-plane to take place, therefore in-plane emission has been observed in this case, which have been verified from the results shown in Fig. 4.10 for $\eta = 0.6$. Azimuthal distributions of nucleons of Fig. 4.9 has been fitted with the Fourier expansion series up to second order for the calculation of v_2. The values of fitting parameter has been displayed in Fig. 4.10.

In general, anisotropic flows are defined as the nth harmonic coefficients of Fourier ex-

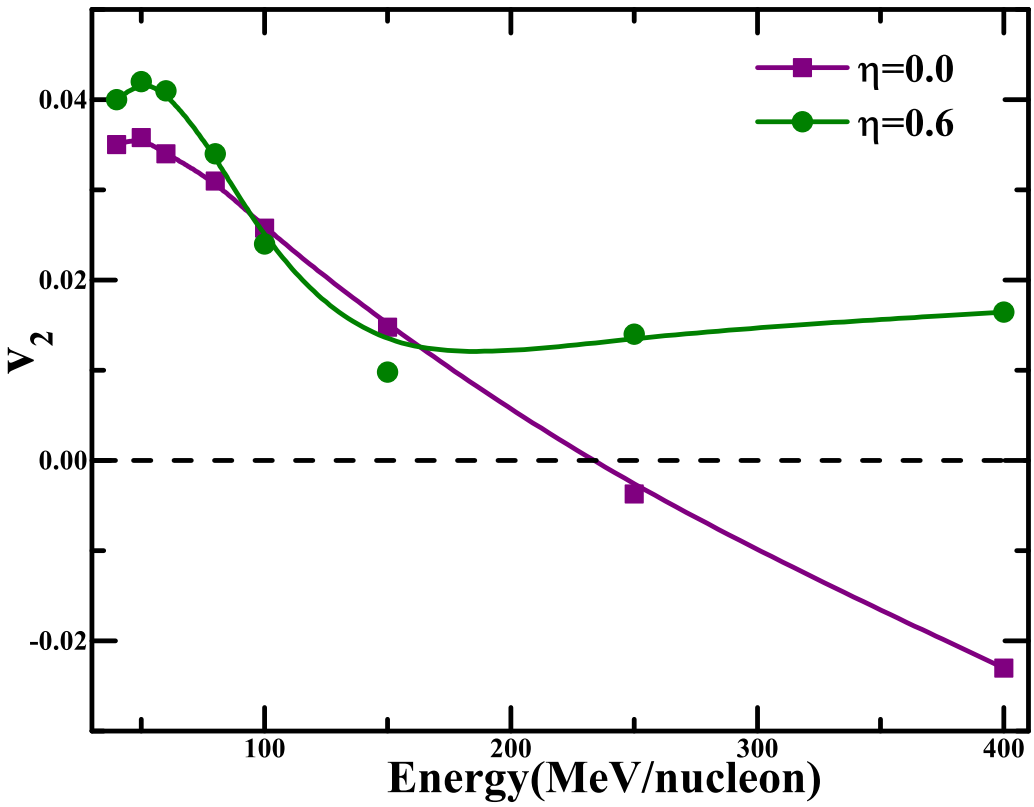

Figure 4.10: Elliptic flow calculated for free protons from the fits of Fig. 4.9 at different incident energies.

pansion of v_n as in equation 1.4 [69]. The elliptic flow, second harmonic of Fourier expansion plays a dominant role in the intermediate energy regime as the phase-transitions of nuclear matter and extraction of the equation of state (EOS) have been probed using this parameter [59]. This observable has been extracted from the mid-rapidity zone, where the transition energy (E_t) or transition of elliptic flow from in-plane (rotational flow) to out-of-plane (squeeze-out flow) has been calculated [88]. Mathematically, elliptic flow can be written as in equation 1.6 [69]. From this Fig. 4.10, it has been observed very clearly that, mass asymmetry of the reaction influence the reaction dynamics very strongly. The transition of nuclear flow from in-plane to out-of-plane takes place for the symmetric case ($\eta = 0.0$) around incident energy 250 MeV/nucleon, but for the mass asymmetric case of $\eta = 0.6$, the rise and fall behaviour in the v_2 with incident energies is present, but no transition has been observed. Here, for all incident energies, the elliptic flow remains in-plane or positive. However, there is a dip in the value around 150 MeV/nucleon, because at $\eta = 0.6$, the size of spectator zone is more in comparison to participant zone.

In addition, the rapidity region selection also affects the transition of flow from in-plane to squeeze-out flow. Our previous study show that E_t is weakly dependent on the rapidity interval, while it is highly sensitive to the size of the rapidity bin [63]. To verify this figure, we have calculated the $< v_2 >$ from equation 1.6 at freeze-out time (200 fm/c) for Z = 1 and Z = 2 fragments. This analysis has been carried out for energies between 40 MeV/nucleon and 600 MeV/nucleon to calculate the transition energies for all the mass asymmetric reaction shown in Fig. 4.11. The results of energy dependance of $< v_2 >$ have provided the similar values and trends as for Fig. 4.10.

4.3 Summary

In conclusion, by using the IQMD model, we have studied the influence of different mass asymmetry of nuclear reactions on <(angular momentum)/nucleon>, <(moment of inertia)/nucleon> and <(rotational energy)/nucleon> by keeping impact parameter range fixed but varying the incident energy and rapidity intervals.

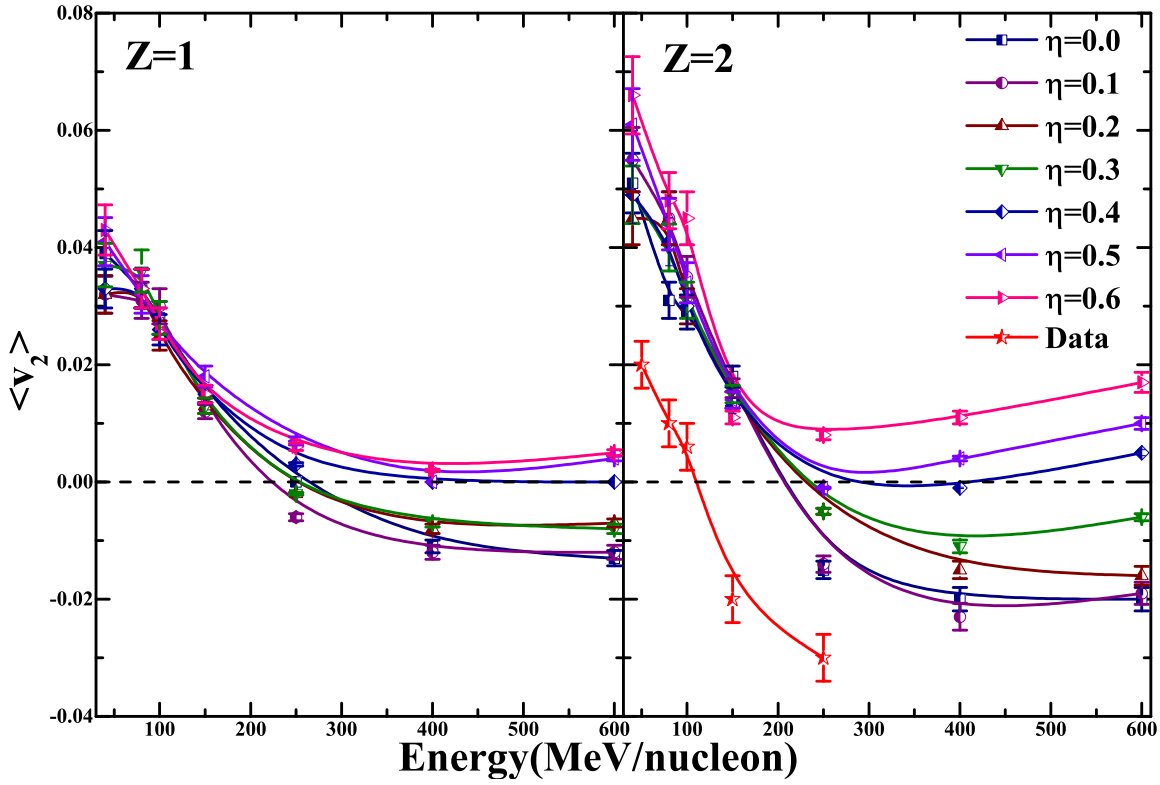

Figure 4.11: Dependence of elliptic flow for Z = 1 and Z = 2 fragments for different mass asymmetric nuclear reactions.

- The angular momentum/nucleon of nuclear matter is influenced by the mass asymmetry of nuclear reaction. However, Coulomb repulsive interactions effects the rotational dynamics at spectator rapidities with increasing η at a particular energy. Moment of inertia/nucleon variation with mass asymmetry also verify the former statement by showing converse trend in comparison to angular momentum/nucleon. Whereas the rotational energy/nucleon depends strongly on the fragmentation and expansion time of the participant matter.

- The mid-rapidity (participant zone) and T. L. like or P. L. like rapidity (away from mid-rapidity zone) influences the dynamics of all the rotational parameters differently.

- Comparison of the present simulations with the BUU model has been achieved successfully.

- Enhancement in the distribution of rotational flow of free protons and dependence of Fourier fitting parameter v_2 has also been reported. Transition energy of $\eta = 0.0$ has been calculated by using the fits of azimuthal distributions.

Chapter 5

Scaling of nuclear flow in mass asymmetric heavy ion reactions

5.1 Introduction

Collective flow is the azimuthally asymmetric emission of nucleons which provide a deep insight into nuclear equation of state (EOS), compressed and dense nuclear matter [227, 297–299]. Among different harmonics of flow, the first harmonic directed flow (v_1) arises due to the pressure gradient in hot nuclear matter which results into the preferential sideward deflection of fragments/nucleons. In the past, both hydrodynamics and theoretical transport models [300, 301] have revealed that directed flow is a promising observable for exploring possible phase transition of the nuclear matter. Whereas, the second harmonic i.e., elliptic flow comes into play due to the combined effects of rotation as well as expansion of highly compressed participant matter and shadowing of spectator matter. Thus elliptic flow can serve as a probe to investigate the dynamics of heavy ion reaction [276, 302].

At Relativistic Heavy ion Collider (RHIC), the number of constituent quark (NCQ) scaling is an important observation in the formation of hadrons through the parton coalescence mechanism [124, 125]. Similarly, nucleon coalescence/number-of-nucleon scaling can also be co-related with NCQ for anisotropic flow of light mass fragments (LMF) in nuclear collisions at low and intermediate incident energies [118]. Coalescence or recombination mechanism can be calculated at low transverse momentum values because LMFs ($1 \leq A \leq 4$) have the same anisotropies and momentum spectra

when studied as a function of (transverse momentum)/mass and rapidity dependence of fragment (p_t/A) [119].

The scaling phenomenon takes place in the light mass fragments/free nucleons due to similar velocities/momentum and originated from the regions where the emitted nuclear matter velocity equals the velocity of emitted fragments. However, the recombination mechanism is expected to be poor for heavier mass fragments like intermediate mass fragments (IMFs) ($A_{total}/6$) because of the instability which lead to further decay through emission of its constituents (free nucleons/LMFs) in different directions. The velocities of these emitted constituents exceeds the maximum value of the nuclear matter's velocity.

The strength of anisotropic flow is usually calculated with the help of Fourier expansion i.e., azimuthal distribution of emitted fragments w.r.t the reaction plane. Anisotropic flows are defined as in equation 1.4. In mass asymmetric nuclear reactions, the yield of nucleons cannot be symmetric w.r.t. azimuthal angle. Therefore, we have also included the sine term in our calculations for $< v_1 >$, $< v_2 >$, $< v_3 >$ and $< v_4 >$ as:

$$< v_1 > \;=\; \langle \cos\phi \rangle + \langle \sin\phi \rangle \;=\; \langle \frac{p_x}{p_t} \rangle + \langle \frac{p_y}{p_t} \rangle \tag{5.1}$$

$$< v_2 > \;=\; \langle \cos 2\phi \rangle + \langle \sin 2\phi \rangle \;=\; \langle \frac{p_x^2 - p_y^2}{p_t^2} \rangle + \langle \frac{2p_x p_y}{p_t^2} \rangle \tag{5.2}$$

$$< v_3 > \;=\; \langle \cos 3\phi \rangle + \langle \sin 3\phi \rangle \;=\; \langle \frac{p_x^3 - 3p_x p_y^2}{p_t^3} \rangle \;+\; \langle \frac{3p_x^2 p_y - p_y^3}{p_t^3} \rangle \tag{5.3}$$

$$< v_4 > \;=\; \langle \cos 4\phi \rangle + \langle \sin 4\phi \rangle \;=\; \langle \frac{p_x^4 - 6p_x^2 p_y^2 + p_y^4}{p_t^4} \rangle + \langle \frac{4p_y p_x^3 - 4p_y^3 p_x}{p_t^4} \rangle \tag{5.4}$$

where, the projection of transverse momentum is defined by p_x parallel and p_y perpendicular to the reaction plane and total transverse momentum is defined by $p_t = \sqrt{p_x^2 + p_y^2}$.

Several experimental and theoretical groups have explored the scaling or recombination mechanism [60,119–122]. This number-of-nucleon scaling originates from the nucleonic coalescence. At low incident energies, the scaling for light mass fragments has been observed for $< v_1 >$, $< v_2 >$, $< v_3 >$ and $< v_4 >$ with transverse momentum at various rapidity zones at peripheral collisions. The role of symmetry energy, isospin

dependent/independent nucleon-nucleon cross-section and equation of state have been investigated for the scaling analysis by Y. G. Ma et al. [119–122]. Scaling of deuterons and tritons in elliptic flow as well as in directed flow have been carried out by FOPI collaboration [60]. Motivated by the above attempts made in literature on scaling, the investigations have been carried out at intermediate energies by fixing the centrality and altering the mass asymmetry content of the reaction in the present chapter.

5.2 Results and discussion

For the present study, several thousands events have been simulated by fixing the total mass ($A_{TOTAL} = 248$) for reactions of ${}^{122}_{49}In + {}^{126}_{50}Sn$, ${}^{114}_{48}Cs + {}^{134}_{54}In$, ${}^{100}_{40}Mo + {}^{148}_{64}Gd$, ${}^{86}_{36}Kr + {}^{162}_{67}Ho$, ${}^{71}_{31}Ga + {}^{177}_{71}Lu$, ${}^{60}_{28}Ni + {}^{188}_{76}Os$, ${}^{50}_{24}Cr + {}^{198}_{78}Pt$ and ${}^{40}_{20}Ca + {}^{208}_{82}Pb$. The values of η for these reactions varies from 0.0 to 0.7. Analysis have been carried out at incident energies between 50 MeV/nucleon and 400 MeV/ nucleon over centrality range $0.25 < \hat{b} < 0.45$ (with $\hat{b} = \frac{b}{b_{max}}$) using a soft EOS. For the central collisions or symmetric colliding systems ($\eta = 0.0$), the maximum number of nucleons have interactions among themselves. The lighter projectile and at non-central collision or peripheral collision results into slightly non-equilibrated system [22].

To explore the scaling phenomenon in mass-asymmetric nuclear reactions, the study on scaled density has been carried out at different incident energies (shown in Fig. 2.5). Important information can be extracted when nuclear matter achieve higher densities i.e., two-three times the normal nuclear matter density. When two nearly mass symmetric nuclei collides, the nuclear matter compresses and hence temperature increases. Further compressed zone thus formed starts decaying. The time of compression or high density achieved (peak value of density) decreases with increment in energies and mass asymmetry. At high incident energies, due to large number of nucleon-nucleon collisions, both the temperature and density will increase. For the reactions having higher mass asymmetry, the participation of projectile part is very less and it just pass after hitting the heavy target at high incident energy.

The projectile and target totally merge into each other in mass symmetric collisions at

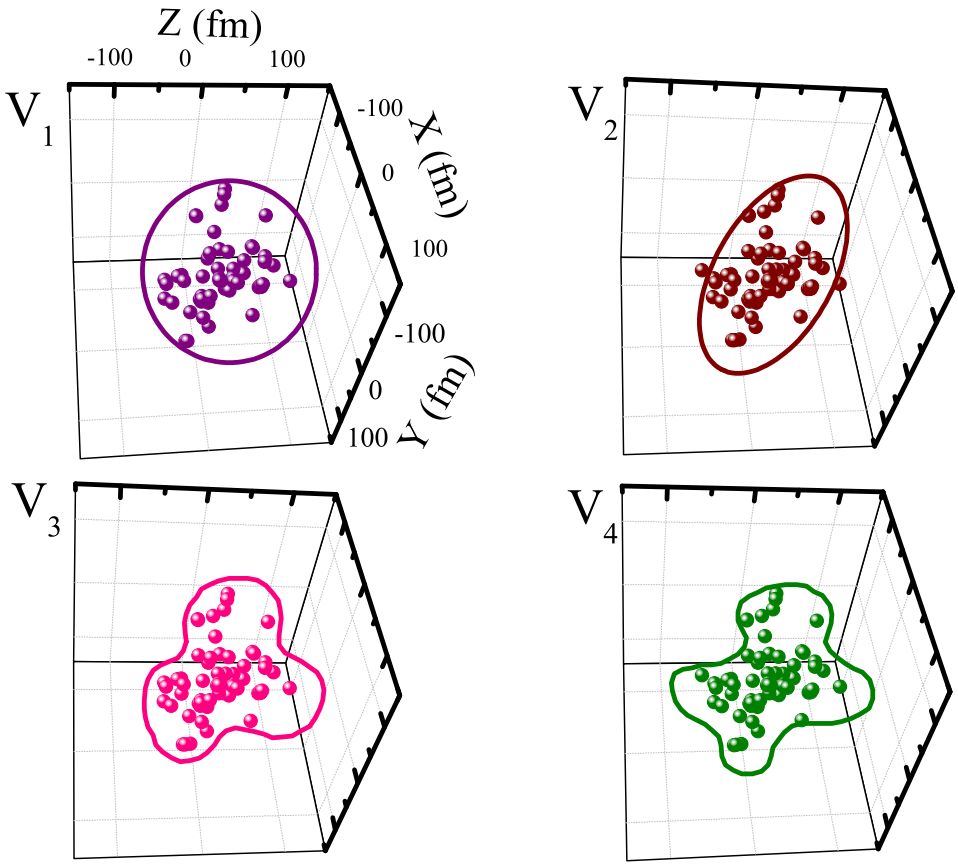

Figure 5.1: Phase space of different harmonic coefficients at centrality $0.25 < \hat{b} < 0.45$ at incident energy 400 MeV/nucleon.

low energies, resulting into high compression of nuclear matter. Hence, more time is taken by the nucleons and fragments to settle down. Moreover, the attractive mean-field plays a dominant role at lower incident energies, thus keeps the nucleons together for a significantly longer time and therefore it becomes tough for the system to equilibrate. However, for highly mass asymmetric reactions, the saturation density remains quite high. The main reason of this effect is that, major part of the heavy target remains un-interacted and thus least destruction of the nuclear matter takes place.

5.2.1 Phase-space evolution of nucleons participating in flow

Collision of two nuclei at non-central geometry lead to anisotropic distribution of nucleons. Phase space distribution of nucleons involved in different harmonics can be seen clearly. The 3-dimensional phase space of directed, elliptic, triangular and quadrangular flow have been shown in Fig. 5.1. Analysis have been carried out for the different cases of mass asymmetric reactions but, the only case of $\eta = 0.6$ have been shown here. One can clearly see that different number of nucleons participate in different harmonics of anisotropic flow.

5.2.2 Directed flow for different mass asymmetric reactions

In Fig 5.2, directed flow has been displayed for mass asymmetric nuclear reactions (heavy target and light projectile). The rapidity in center-of-mass frame is defined in equation 1.5 [22]. Both the projectile and target part covers equal region on both sides of rapidity intervals for the mass symmetric reaction ($\eta = 0.0$). But, as the η increases, the mass on heavier side (target side in our case) covers the major region on the rapidity intervals.

The projectile and target region are separated by a vertical line starting from the x-axis scale. Clearly, it has been seen that for $\eta = 0.7$, the whole rapidity region is covered by the heavier participant mass (target) on the projectile side rapidity region plus target side rapidity region. The vise-versa or reverse observation have been seen (not shown here), when the mass of target and projectile are interchanged (heavy projectile and light target). In that case, the participant part cover more area on the target side

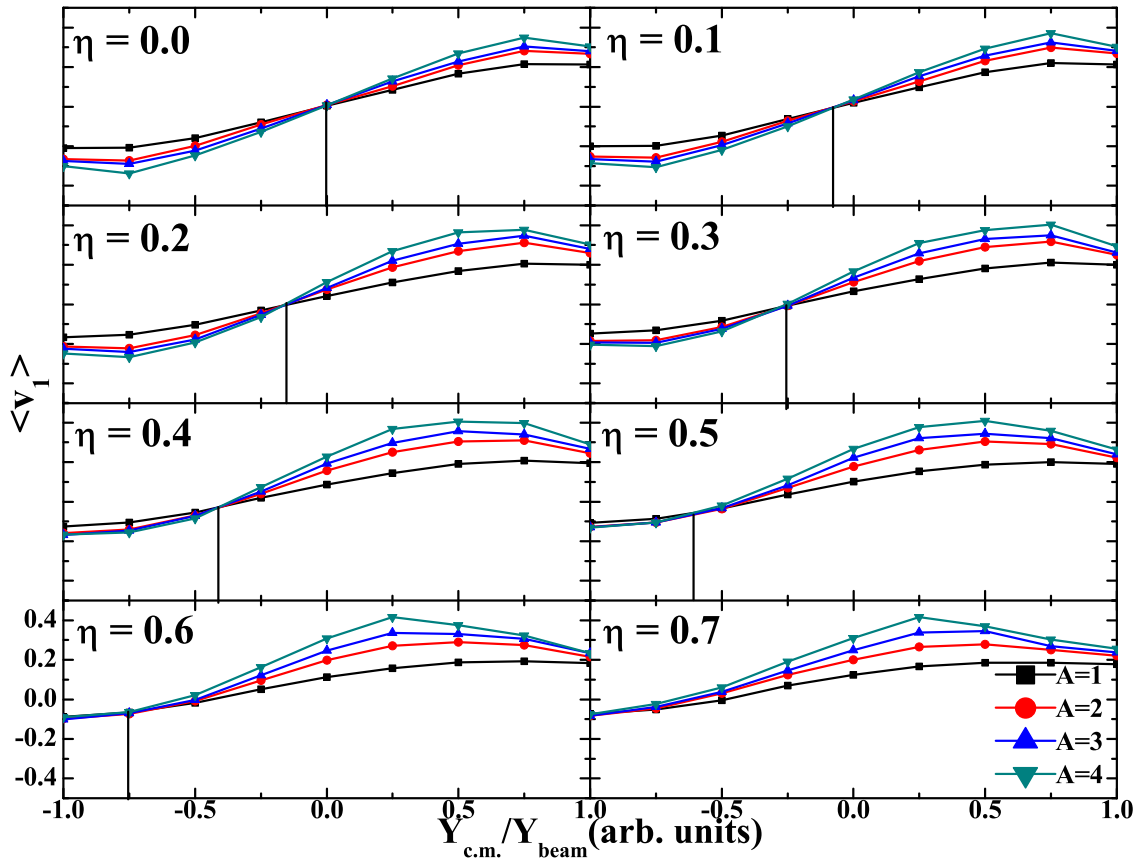

Figure 5.2: Directed flow for different mass asymmetric reactions at incident energy 400 MeV/nucleon.

rapidity region.

In highly mass asymmetric nuclear reactions and at peripheral impact parameters, the lighter projectile remains un-interacted with the heavy target. So, the directed flow value after the collision of target and projectile is entirely due to the heavier part. Therefore, it covers the major region on the rapidity bins. Second observation which have been observed here is that directed flow is maximum on both sides of the target and projectile region for A = 4 fragment. The directed flow increases with the mass of fragments [198].

5.2.3 Dependance of directed flow on mass asymmetry of the reaction

In Fig. 5.3 (a), directed flow as a function of mass asymmetry has been displayed at different energies. For different energies, the measurements have been performed at different values of transverse momentum to get the value of p_t, at which scaling is possible. Earlier studies reveal that scaling can be observed upto $p_t \leq 0.25$ GeV/c [119–122] for mass symmetric reactions, but no research has been performed for mass asymmetric nuclei. Therefore, we have explored scaling for mass asymmetric nuclear reactions. The analysis have been carried out at incident energies, E = 50, 100 and 400 MeV/nucleon respectively. The range of rapidity bins has already been discussed in chapter 4 for various mass asymmetric nuclear reactions.

The variation of transverse momentum shows that the overlapping of different curves of p_t decreases with increase in energy. To display clearly the variation of $< v_1 >$, curves have been multiplied by constant factors of 32, 16 and 64 respectively at three different incident energies i.e., E = 50, 100 and 400 MeV/nucleon to avoid overlapping. One can see clearly that slope of different p_t values is also changing with incident energies (Fig. 5.3 (b)), due to attractive interactions at lower incident energies and repulsive interactions at higher incident energies. The slope at different transverse momentum value infers that one should carry out the scaling at intermediate energies by varying transverse momentum of nucleons/fragments (p_t) from 0.05 to 0.25 GeV/c, because at higher values of p_t, the fluctuations among the values of directed flow have been

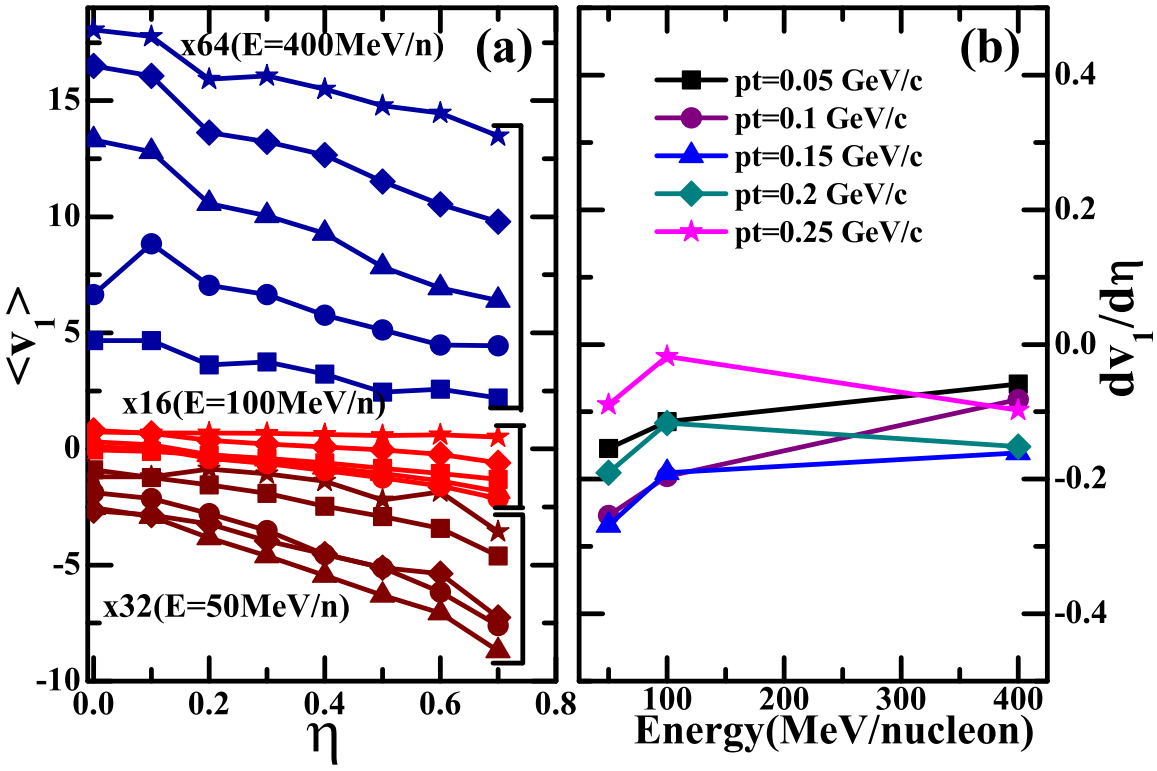

Figure 5.3: (a) Directed Flow as a function of asymmetry parameter (η) at three different energies (50, 100 and 400 MeV/nucleon). Analysis have been carried out for different transverse momentum (p_t) values at centrality $0.25 < \hat{b} < 0.45$ for free nucleons and (b) Slopes of transverse flow for each transverse momentum value at three different energies and mass asymmetries.

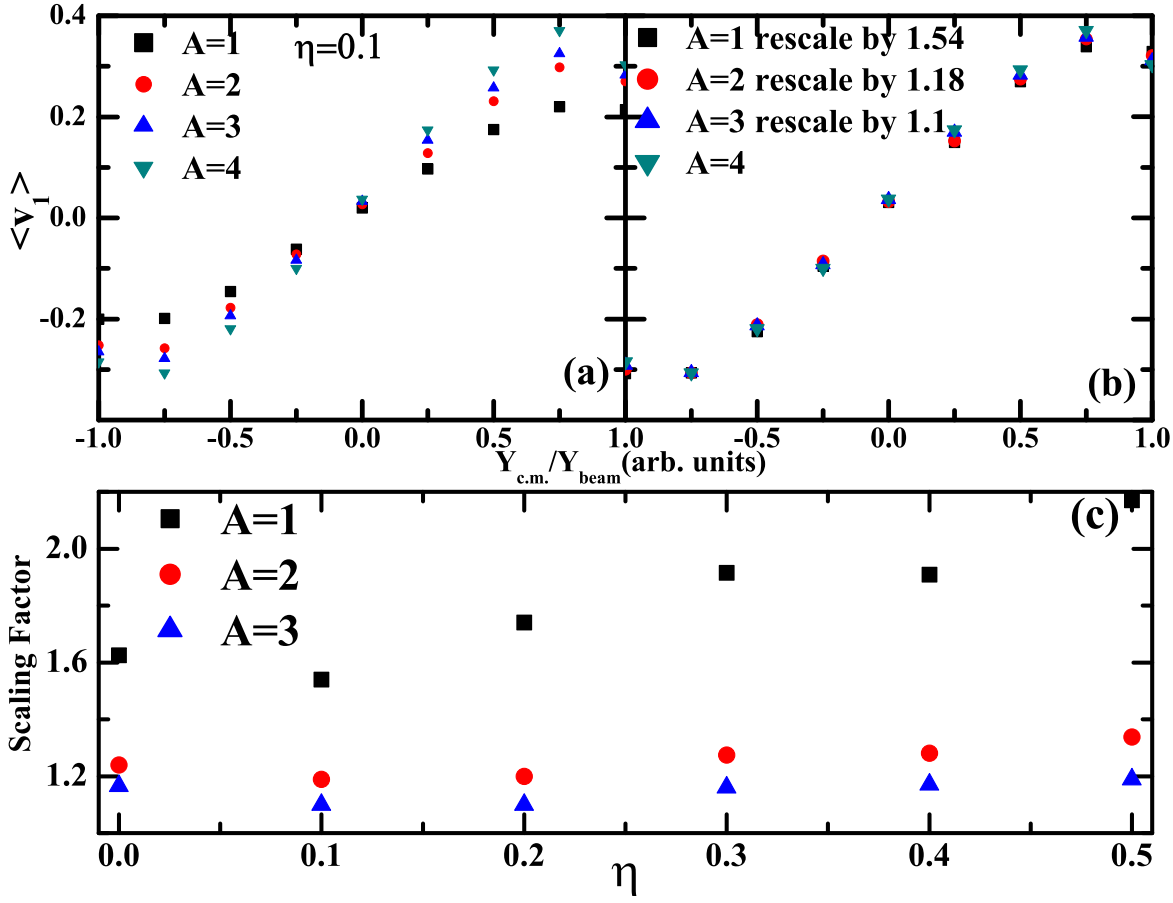

Figure 5.4: (a) shows the directed flow as a function of rapidity for different mass fragments (b) displays the re-scaled flow fragments at incident energy 400 MeV/nucleon for centrality $0.25 < \hat{b} < 0.45$ (c) shows the re-scaled factor as a function of mass asymmetry of the reaction.

observed (not shown here). The corresponding symbols in the Fig. 5.3 (b) have been used for slope at each momentum value.

5.2.4 Dependance of scaling of directed flow

In the Fig. 5.4 (a) and (b), $< v_1 >$ and re-scaled $< v_1 >$ as a function of rapidity for different fragment masses have been shown. Motive behind this study is to investigate the scaling behaviour over the full momentum range for different fragments masses produced in mass asymmetric nuclear reactions. The analysis have been carried out for all the values of η but, here we display only one case i.e., $\eta = 0.1$. In Fig. 5.4 (a), it is found that the slope of directed flow is positive pointing towards repulsive

nucleon-nucleon collisions. Before re-scaling in Fig. 5.4 (a), the value of directed flow is different for different fragment masses. Heavier the fragment, more will be the value of directed flow and this confirms the fact that $< v_1 >$ is proportional to the mass of fragment [198]. Fig. 5.4 (b) displays the re-scaling of flow of different mass fragments over the whole rapidity range. The motivation of this study has been taken from the Reisdorf et. al. [60], here the re-scaling of elliptic flow has been investigated for proton, deuterons and tritons. We have used the same analogy for A = 1, 2, 3 and 4 fragments and re-scaled the flow of lighter fragments to A = 4 fragment for different mass asymmetric reactions over the whole rapidity range. A = 4 fragment has more value of momentum in transverse direction and thus yield maximum value of $< v_1 >$.

The different reactions yields different values of re-scaling factors for A = 1, 2 and 3 fragments. The increment in mass asymmetry of nuclear reaction results into decrease in the relative fragments. The repulsive Coulomb forces and isospin asymmetric nuclear matter's symmetry energy destructs the nuclear matter into heavier un-interacted spectator part or heavier fragments and lesser participant part or lighter fragments [24, 50]. As η increases, the lesser interactions between the nucleons causes smaller participant region of target and projectile. The production of light fragments decreases and the heavy fragments increases with increase in the mass asymmetry of reaction [24].

Ultimately, to re-scale the free nucleons which originates from the participant zone to A = 4 fragments, a constant factor larger than the A = 2 and 3 fragments have to be applied (Fig. 5.4 (b)). The clear variation of these re-scaling factors with η value for A = 1, 2 and 3 fragments is presented in the lower panel (Fig. 5.4 (c)). As, the mass asymmetry increases, more value of momentum is needed to re-scale the free nucleon with A = 4 fragment. The A = 2 and 3 fragments are easy to re-scale with the A = 4 fragment, because they are of the similar size as that of the A = 4 fragment shown in the lower panel of Fig. 5.4. The value of slopes of re-scaling factors with η in the lower panel obeys a linear fitting relation with slope angles 57^o, 31^o and 9.6^o for A = 1, 2 and 3 fragments respectively. Small number of free nucleons are produced and higher value of re-scale factor have to be multiplied to scale it to A = 4 fragment.

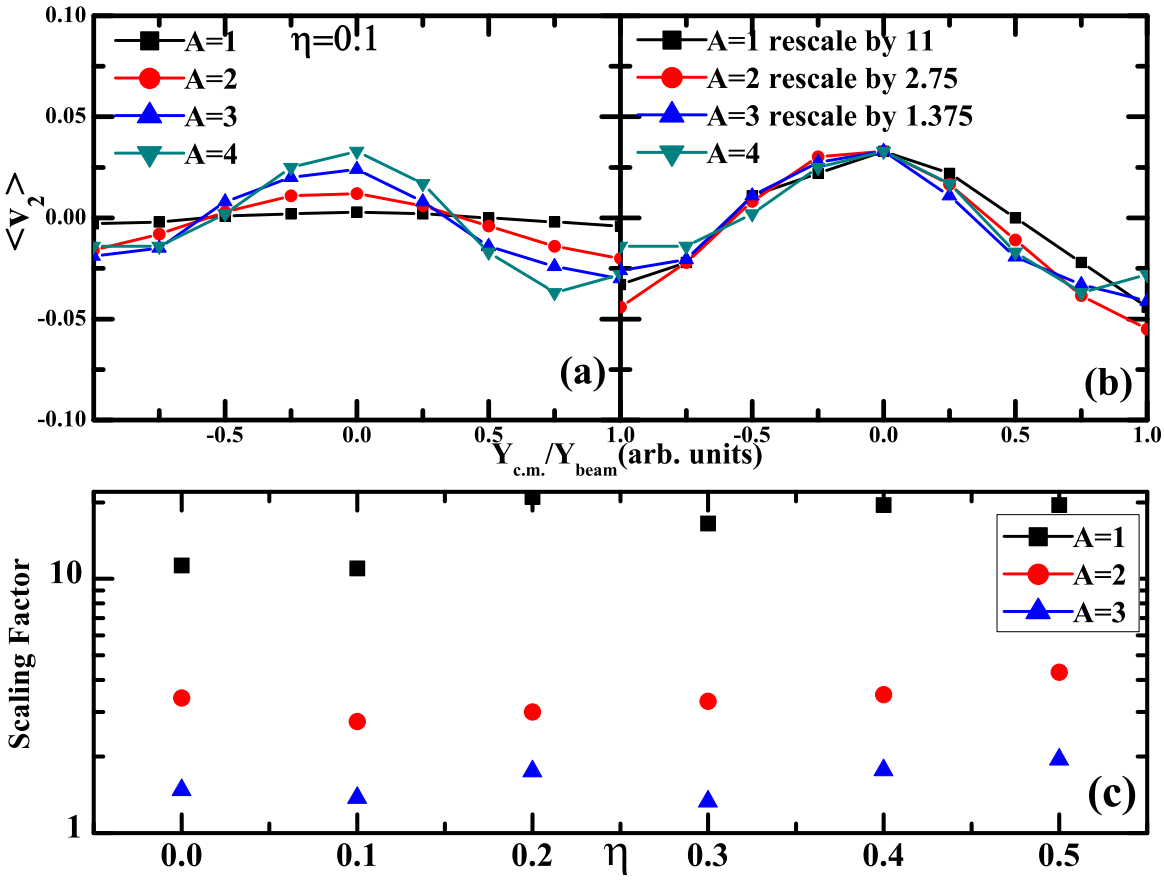

Figure 5.5: (a) shows the rapidity dependence of elliptic flow of different mass fragments (b) re-scaled flow of fragments for incident energy 400 MeV/nucleon at centrality $0.25 < \hat{b} < 0.45$ for η=0.1 and (c) shows the re-scaling factors as a function of mass asymmetry of nuclear reaction.

5.2.5 Scaling of elliptic flow as a function of rapidity

Fig. 5.5 (a) illustrates $< v_2 >$ of different mass fragments for $\eta = 0.1$ (other values of η are not shown here), Fig. 5.5 (b) shows the re-scaled $< v_2 >$ of fragments as a function of rapidity. Gaussian shapes have been observed for A = 1, 2, 3 and 4 fragments in the whole rapidity region. Heavier mass fragments have the higher peak value and wider Gaussian distribution [60]. A large number of fragments are released around the mid-rapidity zone from the highly compressed hot matter. The squeeze-out flow or out-of-plane flow occurred for energy range considered. As the mass asymmetry increases, one has to re-scale both of momentum components p_x and p_y. Whereas in case of $< v_1 >$, one has to re-scale only the p_x component. This consequences into

higher value of re-scaling factor in comparison for $< v_1 >$. Also with increasing η, decreasing of the participant part and enhancing of the spectator region result into lesser squeeze-out flow and lower $< v_2 >$ value.

Re-scaling of momentum of free nucleons with heavy mass fragments require a large constant value as one can see in the Fig. 5.5 (b). The variation of these re-scaling factors with η is shown in Fig. 5.5 (c). The clear difference is seen between all these fragments, which points towards the production rate of these fragments. By increasing the η, the phenomenology of the elliptic flow is altered. Therefore, the density and pressure gradient is not enough to produce the lighter fragments from the participant region. The values of slopes of the lower panel yield the angles 86^o, 62^o and 43^o for A = 1, 2 and 3 fragment masses respectively, which are much larger than the directed flow values. Reason behind is the flow of particles occurs in transverse direction only. In contrast in elliptic flow, the flow of particles in a direction perpendicular to the reaction-plane.

Extensive study have been carried by various groups in both experimental and theoretical areas using low and ultra-relativistic energy span for different mass fragments, quarks, strange particles for using different impact parameters and symmetric masses [65, 106, 119–121]. One clear observation which comes out during the analysis of Fig. 5.4 and 5.5, the scaling of different mass fragments is best suited to attain the directed flow than elliptic flow. The main reason is that to re-scale the momentum or velocity of fragments/nucleons emitted in one (transverse) direction is somehow easy. But scaling of momentum of fragments/ nucleons scattered in the perpendicular directions to each other is not that much appreciably attainable. Moreover the combined effects of repulsive Coulomb forces and asymmetric nuclear matter's symmetry energy have also affected the reaction dynamics. Re-scaling of fragments participating in directed and elliptic flow in higher mass asymmetric nuclear reactions shows significant results.

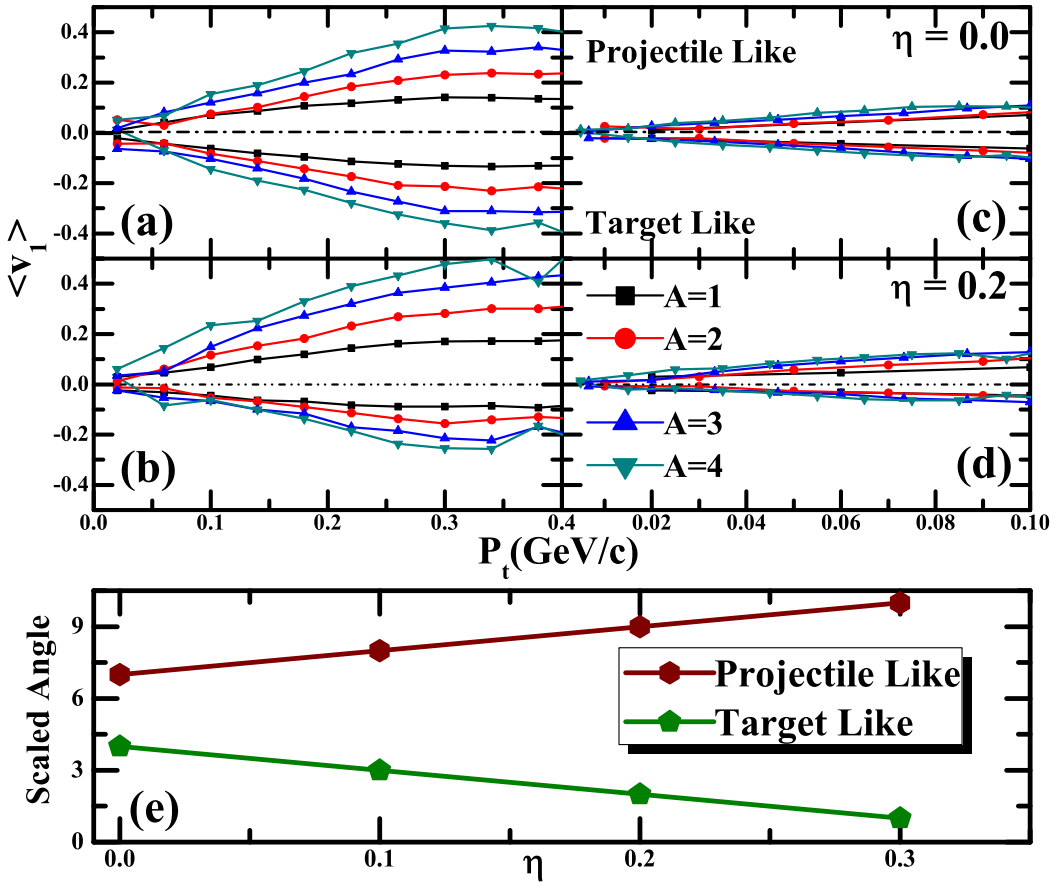

Figure 5.6: (a) and (b) shows $< v_1 >$ as a function of p_t for $\eta = 0.0$ and 0.2 and selected rapidity region for projectile-side and target-side rapidity (c) and (d) shows the scaling of fragments and (e) shows the scaled angle w.r.t. zero line for both cases as a function of η for incident energy 400 MeV/nucleon at centrality $0.25 < \hat{b} < 0.45$.

5.2.6 Transverse-momentum dependance of scaling of directed flow

Fig. 5.6 presents the directed flow as a function of transverse momentum by choosing a particular rapidity range $|0.3 \leq \frac{Y_{c.m.}}{Y_{beam}} \leq 0.5|$. This rapidity region has been calculated by taking the equal contribution of the participating nucleons from target and projectile nuclei. This mid-rapidity range changes with the mass asymmetry of the nuclear reaction [8]. The aim of this study is to explore the scaling of momentum of fragments in the different rapidity regions and it is expected that the P.L. and T.L. regions will behave reverse to each other or form a mirror image. Only the certain values of rapidity range for $\eta = 0.0$, 0.1, 0.2 and 0.3 shows this kind of opposite trend for P.L. and T.L. regions. Since, the value of participant zone keeps on changing with mass asymmetry of the reaction, due to this reason scaling of momentum of fragments over a fixed rapidity zone is not possible. Therefore, the spreading of fragments with transverse momentum is shown only for $\eta = 0.0$ (Fig. 5.6 (a)) and 0.2 (Fig. 5.6 (b)) for both P.L. and T.L. regions. At this energy, the positive flow due to nucleon-nucleon collisions dominate and flow of fragments occurs in the forward direction.

Rapidity intervals selections for P.L. and T.L. regions are greatly influenced by the mass asymmetry content of the reaction and effect the reaction dynamics [8]. Fig. 5.6 (a and b) shows that the heavier fragment results into maximum value of the directed flow than the lighter fragments on both sides of the rapidity interval for both the η cases. The other side of Fig. 5.6 (c and d) displays the scaling, when transverse momentum of fragments are divided by their masses. Although, Fig. 5.6 (a and c) appears to be mirror image to each other for symmetric nuclear reactions, but the trend is not symmetric for mass asymmetric reactions (Fig. 5.6 (b and d)). The method used is best suited for the target like rapidity region than for the projectile like rapidity region. With increment in mass asymmetry of the reaction, the majority of heavy target's fragments tend to occupy wider range for the projectile like rapidity region and cover some region of the target like rapidity interval too (as shown in Fig. 5.2). Clearly, to scale the flow of fragments is somehow easy than the more energetic fragments that are released in the projectile-side rapidity region.

Fig. 5.6 (e) displays the variation of angle calculated for scaled flow of fragments from zero value of $< v_1 >$ with η for P.L. and T.L. regions. The P.L. region shows an increasing trend than the later one. Both sides of distributions appears to be the mirror image of each other. The increase in projectile side of rapidity region with η justify the inclining trend of the spectator mass with mass asymmetry, whereas the decreasing trend of target side rapidity region is referring towards the decreasing mass of projectile. Other observation is that, there is very less difference between the angles of P.L. and T.L. for $\eta = 0.0$ and difference goes on increasing with η.

5.2.7 Transverse momentum dependance of even harmonics of flow

Now, it would be interesting to investigate scaling between the different harmonics of flow. Fig. 5.7 shows the $< v_4/v_2^2 >$ variation with p_t for distinct values of η (only selected values are shown here) for different mass fragments. Here, Fig. 5.7 ((a), (b) and (c)) displays $< v_4/v_2^2 >$ verses p_t for $\eta = 0.2$, 0.3 and 0.7. The dashed line represents the 0.5 value as in literature [119]. The similar analysis has been carried out for low and relativistic energy ranges by other theoretical groups [119–121,170,303–308] and the values comes out to be a constant factor 0.5. We try to reproduce the similar result for low energy and intermediate energies by varying mass asymmetries of the reactions and somehow approximately successful in reproducing the same results at incident energy E = 50 MeV/nucleon. As the η changes, the projectile part of heavier target starts occupying more region on the whole rapidity region as compared to target side. Therefore, we have selected the projectile side rapidity region for calculating this ratio ($< v_4/v_2^2 >$) verses p_t. It has been concluded that the scaling laws are not valid for A = 1, 2, 3 and 4 fragments respectively in mass asymmetric reactions as compared to value of 0.5 for mass symmetric reactions [119–121].

5.3 Summary

In conclusion, we have investigated the scaling among the different harmonics of the flow of nucleons/fragments for mass asymmetric nuclear reactions.

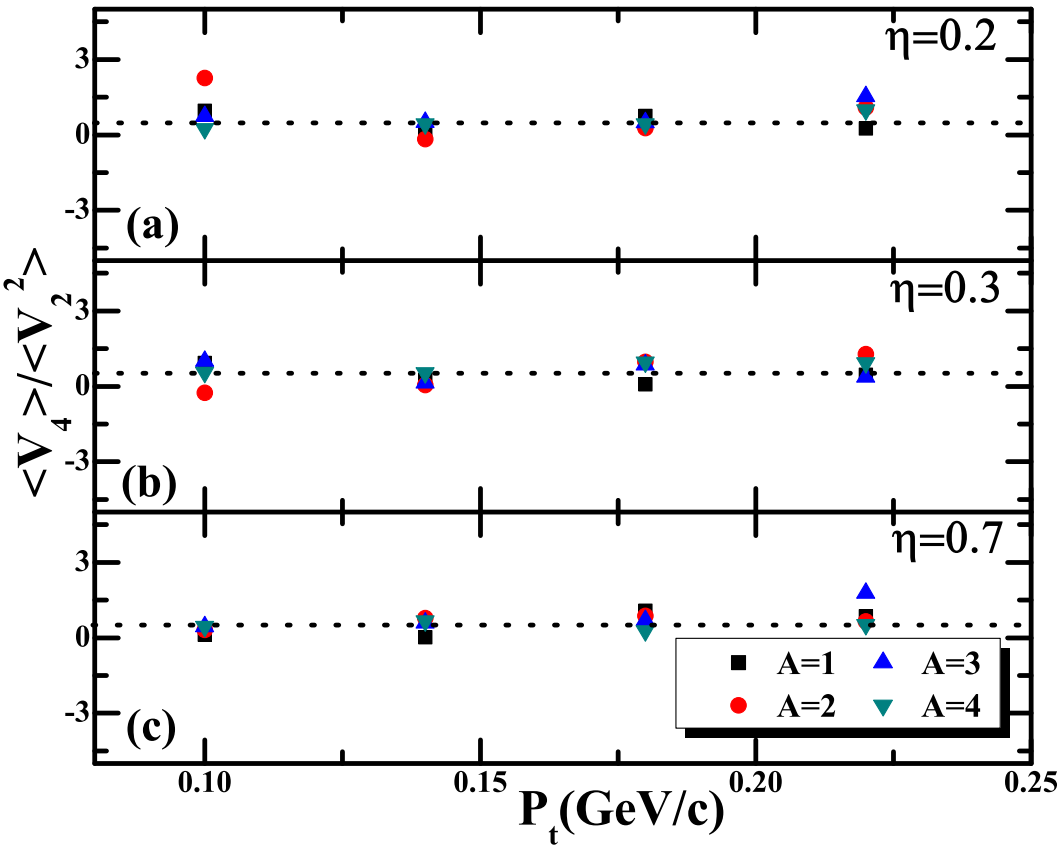

Figure 5.7: v_4/v_2^2 is shown as a function of transverse momentum(p_t) for different values of mass asymmetry of the nuclear reaction at incident energy E=50 MeV/nucleon for centrality $0.25 < b/b_{max} < 0.45$ for projectile side rapidity range.

- The scaling of fragments participating in directed and elliptic flow is affected by the mass asymmetry content of the reaction. As the value of η changes, the repulsive Coulomb interactions and isospin asymmetric nuclear matter's symmetry energy destructs the nuclear matter into heavier un-interacted spectator part(or heavier fragments) and lesser participant part(or lighter fragments). Due to this phenomenon, larger scaling factors are required in directed and elliptic flow to scale the lighter fragments (A = 1, 2 and 3) to A = 4 fragment as the mass asymmetry of reaction increases.

- Scaling of fragments in mass asymmetric nuclear reactions has been affected strongly by the rapidity zone calculated on the basis of mass asymmetry of the reaction. With an increase in mass asymmetry, the extent of the nucleons/fragments emitted from the participant or T. L. rapidity zone decreases with the enhancement of nucleons/fragments emitted from the spectator or P. L. rapidity region. Therefore, the directed flow of fragments which are participating in the P. L. rapidity zone increases and their scaling angles are also more in comparison to the T. L. rapidity zone's fragments.

- The ratio of v_4/v_2^2 of fragments which are selected from the P. L. rapidity zone has been calculated for different mass asymmetric nuclear reactions, but the ratio does not follow the constant value of 0.5 as reported in literature for the number of constituent quark (NCQ) scaling of flow for mesons and baryons.

Chapter 6

Summary and outlook

"To myself I am only a child playing on the beach, while vast oceans of truth lie undiscovered before me".....Isaac Newton

This thesis contains a detailed theoretical study of the different components of flow as a function of rapidity, incident energy and transverse momentum in intermediate energy regime. This work mainly focused on the directed and elliptic flow in various rapidity bins. Furthermore, the scaling of collective flow and rotational dynamics features in various mass asymmetric reactions have also been explored. The isospin-dependent Quantum Molecular Dynamics (IQMD) Model has been used to carry out present research work.

We have tried to explore different aspects of elliptic flow by simulating ${}^{197}_{79}Au + {}^{197}_{79}Au$, ${}^{150}_{60}Nd + {}^{150}_{60}Nd$, ${}^{124}_{50}Sn + {}^{124}_{50}Sn$, ${}^{96}_{44}Ru + {}^{96}_{44}Ru$, ${}^{78}_{36}Kr + {}^{78}_{36}Kr$, ${}^{48}_{20}Ca + {}^{48}_{20}Ca$ and ${}^{40}_{20}Ca + {}^{40}_{20}Ca$ at different impact parameters and energy span. It has been shown that the peak of Gaussian shapes formed by the nucleons participating in elliptic flow and the spread of these shapes around the mid-rapidity follows proportional behaviour with the mass of colliding systems. The centrality dependance has been investigated and it has been concluded that elliptic flow enhances more with the peripheral than central or semi-peripheral impact parameters. The another crux of this work is to explore the transition energy (E_t) for elliptic flow. It has been revealed that E_t strongly depends on the centrality of the reaction. The interesting part was to see the second transition from

out-of-plane to in-plane at higher energies.

Next, the role of rotational dynamics in various quantities like angular momentum, moment of inertia, angular velocity and rotational energy in the mass asymmetric nuclear reactions ${}^{122}_{49}In+{}^{126}_{50}Sn$, ${}^{114}_{48}Cs+{}^{134}_{54}In$, ${}^{100}_{40}Mo+{}^{148}_{64}Gd$, ${}^{86}_{36}Kr+{}^{162}_{67}Ho$, ${}^{71}_{31}Ga+{}^{177}_{71}Lu$, ${}^{60}_{28}Ni+{}^{188}_{76}Os$ and ${}^{50}_{24}Cr+{}^{198}_{78}Pt$. The analysis have been carried out at incident energies between 40 MeV/nucleon and 400 MeV/nucleon over centrality range $0.25 < \hat{b} < 0.45$ changing η value. The values of η for these reactions varies from 0.0 to 0.7.

The time dependence of (angular momentum)/nucleon, (moment of inertia)/nucleon, angular velocity and (rotational energy)/nucleon for different mass asymmetric reactions have been calculated. Angular momentum/nucleon shows lower values at participant rapidity zone as the nucleons are restricted to mid-rapidity, but shows higher values of angular momentum/nucleon at freeze-out stage because the nucleons are far apart in space leading to higher values of angular momentum/nucleon. (Moment of inertia)/nucleon shows a reverse trend in comparison to the angular momentum. Angular velocity and (rotational energy)/nucleon are closely related to each other and almost shows a similar pattern. At participant rapidity zone, both observable show a maxima at the thermalization stage. Another interesting feature that has been explored is the rotational flow for mass asymmetric nuclear reactions. The squeeze-out flow has been seen only for the symmetric case and only in-plane/rotational flow has been observed for higher mass asymmetric nuclear reactions.

Finally, we investigate the scaling between the various harmonics of flow and their fragments for mass asymmetric reactions. To study scaling, we have simulated the reactions of ${}^{122}_{49}In+{}^{126}_{50}Sn$, ${}^{114}_{48}Cs+{}^{134}_{54}In$, ${}^{100}_{40}Mo+{}^{148}_{64}Gd$, ${}^{86}_{36}Kr+{}^{162}_{67}Ho$, ${}^{71}_{31}Ga+{}^{177}_{71}Lu$, ${}^{60}_{28}Ni+{}^{188}_{76}Os$, ${}^{50}_{24}Cr+{}^{198}_{78}Pt$ and ${}^{40}_{20}Ca+{}^{208}_{82}Pb$. The analysis have been carried out at incident energies between 50 MeV/nucleon and 400 MeV/ nucleon over centrality range $0.25 < \hat{b} < 0.45$.

Attempts have been made to study the scaling in directed (first harmonic) and elliptic flow in mass asymmetric reactions. Scaling has been studied for $< v_1 >$ and $< v_2 >$ for different mass fragments. It has been concluded that this type of scaling is best suited for directed than for elliptic flow, as directed flow is itself a asymmetric quantity. In

addition to this, the ratio of $< v_4/v_2^2 >$ has also been checked with p_t for different η values.

One can elaborate this work by studying the effect of isospin as well as rapidity dependence in higher harmonics of flow using the IQMD model. Pressure, density, temperature calculations of nucleons can be co-related with the hydro-dynamical calculations in celestial systems. The dependance of rotational quantities on the various model ingredients like isospin, equation of state, momentum dependent interactions etc. will also be a worth investigation. Moreover, rotational dynamics study will be helpful to probe the phenomenon of rotating galaxies by calculating their angular momentum and angular velocity etc. It will become interesting to study the role of scaling in symmetric masses for higher harmonics of flow. Scaling of fragments will be helpful for the experimentalists to locate the detectors in the forward and backward direction.

Bibliography

[1] H. Becquerel, Comptes Rendus **122**, 420421 (1896).

[2] E. Rutherford, Philosophical Magazine **21**, pp. 669-688 (1911).

[3] E. Rutherford, Philosophical Magazine **24**, 669 (1912).

[4] *see*, *http* : *//www2.lbl.gov/abc/wallchart/chapters/01/4.html*

[5] P. Danielewicz and M. Gyulassy, Phys. Rev. D **31**, 53 (1985).

[6] *see*, *http* : *//www.astro.cornell.edu/academics/courses/astro201/galaxies/evol.html*.

[7] *see*, *http* : *//www.sciencetechworld.com/category/science/physics/nuclearphysics*.

[8] K. Kaur and S. Kumar, Nucl. Phys. A **973**, 149 (2018).

[9] S. S. Malik and R. K. Gupta, Phys. Rev. C **39**, 1992 (1989).

[10] P. K. Rath, Phys. Rev. C **79**, 051601(R) (2007).

[11] A. Bharti and S. K. Khosa, Nucl. Phys. A **572**, 317 (1994).

[12] M. Balasubramaniam, R. Kumar, R. K. Gupta, C. Beck and W. Scheid, J. Phys. G: Nucl. Part. Phys. **29**, 2703 (2003).

[13] G. Mohanto, N. Madhavan, S. Nath, J. Gehlot, I. Mukul, A. Jhingan, T. Varughese, A. Roy, R. K. Bhowmik, I. Mazumdar, D. A. Gothe, P. B. Chavan, J. Sadhukhan, S. Pal, M. Kaur, V. Singh, A. K. Sinha, V. S. Ramamurthy, Phys. Rev. C **88**, 034606 (2013).

[14] B. P. Singh et al, Int. J. Mod. Phys. E **01**, 823 (1992).

[15] A. Bonasera, Phys. Rev. C **60**, 065212 (1999).

[16] S. Terranova and A. Bonasera, Phys. Rev. C **70**, 024906 (2004).

[17] R. Raniwalaa, S. Raniwalaa, Y. P. Viyogi, Physics Letters B **489**, 9 (2000).

[18] B. Kardan (HADES Collaboration), Nucl. Phys. A, **967**, 812 (2017).

[19] C. Hartnack, R. K. Puri, J. Aichelin, J. Konopka, S. A. Bass, H. Stöcker and W. Greiner, Eur. Phys. J. A **1**, 151 (1998).

[20] P. Danielewicz, AIP Conference Proceedings **597**, 24 (2001).

[21] M. Di Toro, V. Baran, M. Colonna, V. Greco, S. Maccarone, and M. Cabibbo, Eur. Phys. J. A **13**, 155 (2002).

[22] J. Aichelin, Phys. Rep. **202**, 233 (1991).

[23] C. Sfienti *et al.*, Nucl. Phys. A **749**, 83 (2005).

[24] V. Kaur and S. Kumar, Phys. Rev. C **81**, 064610 (2010).

[25] N. Herrmann, J. P. Wessels, T. Wienold, Annu. Rev. Nucl. Part. Sci. **49**, 581 (1999).

[26] R. Donangelo and S. R. Souza, Phys. Rev. C **52**, 326 (1995).

[27] H. Stöcker, J. A. Maruhn and W. Greiner, Phys. Rev. Lett. **44**, 725 (1980).

[28] H. Sorge, Phys. Rev. Lett. **78**, 2309 (1997).

[29] K. Aamodt *et al.*, Phys. Rev. Lett. **107**, 032301 (2011).

[30] K. Aamodt *et al.*, Phys. Lett. B **708**, 249 (2012).

[31] E. Sanz, C. Vega, J. L. F. Abascal, and L. G. MacDowell, Phys. Rev. Lett. **92**, 255701 (2004).

[32] Y. Aoki, G. Endrodi, Z. Fodor, S. D. Katz, K. K. Szabo, Nature **443**, 675 (2006).

[33] S. A. Bass, M. Gyulassy, H. Stöcker and W. Greiner, Jour. Phys. G: Nucl. Part. Phys. **25**, R1 (1999) and references therein.

[34] S. W. Hawking and W. Israel, *Three Hundred Years of Gravitation (1st ed.)*, Cambridge: Cambridge University Press; ISBN 0-521-37976-8 (1989).

[35] H. Shen, H. Toki, K. Oyamatsu and K. Sumiyoshi, Prog. of Theoret. Phys. **100**, 1013 (1998).

[36] H. Shen, H. Toki, K. Oyamatsu and K. Sumiyoshi, Nucl. Phys. A **637**, 435 (1998).

[37] R. B. Jacobsen, C. A. Z. Vasconcellos, B. E. J. Bodmann and F. Fernandez, Astronomy and Relativistic Astrophysics:pp. 55-59, Proceedings of the Third Workshop (IWARA07), Joo Pessoa, Paraba, Brazil, 3-6 October (2007).

[38] P. Danielewicz, Nucl. Phys. A **661**, 82c (1999).

[39] R. Chatterjee and D. K. Srivastava, DAE Symposium Nucl. Phy., **54**, 556 (2009).

[40] T. K. Nayak, Phases of matter, CURRENT SCIENCE, **103**, NO. 8, (2012) and references therein.

[41] Nuclear Science:A Guide to the Nuclear Science Wall Chart, Chapter-9, Contemporary Physics Education Project (CPEP) (2004).

[42] B. A. Li, C. M. Ko, and W. Bauer, Int. J. of Mod. Phys. E **7**, 147 (1998).

[43] B. K. Sharma and S. Pal, Phys. Rev. C **82**, 055802 (2010).

[44] M. Di Toro, S. J. Yennello, and B. A. Li, Eur. Phys. J. A **30**, 153 (2006).

[45] M. Di Toro, V. Baran, M. Colonna and V. Greco, J. Phys. G: Nucl. Part. Phys. **37**, 083101 (2010).

[46] Y. Gao, G. C. Yong, L. Zhang and W. Zuo, Phys. Rev. C **97**, 014609 (2018).

[47] A. Kaur and S. Kumar, *Ind. Jour. of Phys.* **91**, 1095 (2017).

[48] B. K. Agrawal, Phys. Rev. C **81**, 034323 (2010).

[49] B. A. Li, L. W. Chen and C. M. Ko, Phys. Rep. **464**, 113 (2008).

[50] M. B. Tsang, Y. Zhang, P. Danielewicz, M. Famiano, Z. Li, W. G. Lynch and A.W. Steiner, Phys. Rev. C **102**, 122701 (2009).

[51] M. B. Tsang *et al.*, Phys. Rev. Lett. **92**, 062701 (2004).

[52] C. Y. Wong, Introduction to high-energy heavy-ion collisions, World Scientific, Singapore, (1994).

[53] $see, http://www.hep.shef.ac.uk/edaw/PHY206/Site/2012_course_files/phy206rlec7.pdf$.

[54] J. D. Bowman, W. J. Swiatecki and C. F. Tsang, Lawrence Berkeley Laboratory, **Report No. LBL-2908**, (1973).

[55] G. Westfall, J. Gosset, P. J. Johansen, A. M. Poskanzer, W. G. Meyer, H. H. Gutbrod, A. Sandoval, and R. Stock, Phys. Rev. Lett. **18**, 1202 (1976).

[56] D. Beavis *et al.*, Phys. Rev. C **45**, 299 (1992).

[57] A. Andronic *et al.*, Nucl. Phys. A **679**, 765 (2001).

[58] A. Andronic *et al.*, Phys. Lett. B **612**, 173 (2005).

[59] Y. Zhang and Z. Li, Phys. Rev. C **74**, 014602 (2006).

[60] W. Reisdorf *et al.*, Nucl. Phys. A **876**, 1 (2012).

[61] A. D. Sood and R. K. Puri, Phys. Rev. C **69**, 054612 (2004).

[62] A. Jain, S. Kumar and R. K. Puri, Phys. Rev. C **85**, 064608 (2012).

[63] S. Kumar, V. Kaur and S. Kumar, Cent. Eur. Jour. of Phys. **9(4)**, 986 (2011).

[64] K. Vinayak and S. Kumar, Phys. of Atom. Nucl. **76**, 286 (2013).

[65] G. Torrieri, Phys. Rev. C **82**, 054906 (2010).

[66] L. Ma, G. L. Ma and Y. G. Ma, Phys. Rev. C **89**, 044907 (2014).

[67] H. Heiselberg and A. M. Levy, Phys. Rev. C **59**, 2716 (1999).

[68] P. Danielewicz, Nucl. Phys. A **673**, 375 (2000).

[69] S. Voloshin , Y. Zhang , Z. Phys. C **70**, 665 (1996).

[70] M. B. Tsang, D. R. Bowman, N. Carlin, P. Danielewicz, C. K. Gelbke, W. G. Gong, Y. D. Kim, W. G. Lynch, L. Phair, R. T. de Souza and F. Zhu, Phys. Rev. C **47**, 2717 (1993).

[71] H. A. Gustafsson, H. H. Gutbrod, B. Kolb, H. Lhner, B. Ludewigt, A. M. Poskanzer, T. Renner, H. Riedesel, H. G. Ritter, A. Warwick, F. Weik and H. Wieman, Phys. Rev. Lett. **52**, 1590 (1984).

[72] G. D. Westfall *et al.*, Phys. Rev. Lett. **71**, 1983 (1993).

[73] P. Danielewicz, arXiv preprint nucl-th/9704009 (1997).

[74] S. Goel, Eur. Phys. J. A **49**, 153 (2013).

[75] G. Peilert, H. Stöcker, W. Greiner, A. Rosenhauer, A. Bohnet and J. Aichelin, Phys. Rev. C **39**, 1402 (1989).

[76] C. Gale, G. M. Welke, M. Prakash, S. J. Lee and S. Das Gupta, Phys. Rev. C **41**, 1545 (1990).

[77] D. Krofcheck *et al.*, Phys. Rev. Lett. **63**, 2028 (1989).

[78] V. de la Mota, F. Sebille, M. Farine, B. Remaud and P. Schuck, Phys. Rev. C **46**, 677 (1992).

[79] H. Zhou, Z. Li, Y. Zhou and G. Mao, Nucl. Phys. A **580**, 627 (1994).

[80] D. J. Majestro, W. Bauer, O. Bjarki, J. D. Crispin, M. L. Miller, M. B. Tonjes, A. M. Vander Molen, G. D. Westfall, R. Pak, and E. Norbeck, Phys. Rev. C **61**, 021602(R) (2000).

[81] D. J. Majestro, W. Bauer and G. D. Westfall, Phys. Rev. C **62**, 041603(R) (2000).

[82] A. Buta *et al.*, Nucl. Phys. A **584**, 397 (1995).

[83] J. Lukasik *et al.*, Phys. Lett. B **608**, 223 (2005).

[84] A. Jain, K. S. Vinayak and S. Kumar, Annu. of Phys. **334**, 334 (2013).

[85] S. A. Voloshin, A. M. Poskanzer and R. Snellings, arxiv: 0809.2949[nucl-ex].

[86] J. Y. Ollitrault, Phys. Rev. D **46**, 229 (1992).

[87] Md. Nasim and B. Mohanty, Int. J. Mod. Phys. E **24**, 1550027 (2015).

[88] K. Kaur and S. Kumar, Mod. Phys. Lett. A **32**, 1750001 (2017).

[89] B. A. Li, Phys. Rev. C **60**, 011901 (1999).

[90] M. B. Tsang, W. G. Lynch, C. B. Chitwood, D. J. Fields, D. R. Klesch, C. K. Gelbkea, G. R. Young, T. C. Awes, R. L. Ferguson, F. E. Obenshain, F. Plasil and R. L. Robinson, Phys. Lett. B **148**, 265 (1984).

[91] C. B. Chitwood, D. J. Fields, C. K. Gelbke, D. R. Klesch, W. G. Lynch, M. B. Tsang, T. C. Awes, R. L. Ferguson, F. E. Obenshain, F. Plasil, R. L. Robinson, and G. R. Young, Phys. Rev. C **34**, 858 (1986).

[92] M. Demoulins *et al.*, Phys. Lett. B **241**, 476 (1990).

[93] S. Wang *et al.*, Phys. Rev. Lett. **76**, 3911 (1996).

[94] D. Brill *et al.*, Z. Phys. A **355**, 61 (1996).

[95] M. B. Tsang *et al.*, Phys. Rev. C **53**, 1959 (1996).

[96] H. Appelsh*äuser et al.*, Nucl. Phys. A **698**, 253c (2002).

[97] C. Alt *et al.*, Phys. Rev. C **68**, 034903 (2003).

[98] H. H. Gutbrod, K. H.Kampert, B. W. Kolb, A. M. Poskanzer and H. R. Schmidt, Phys. Lett. B **216**, 267 (1989).

[99] H. H. Gutbrod, K. H. Kampert, B. Kolb, A. M. Poskanzer, H. G. Ritter, R. Schicker, and H. R. Schmidt, Phys. Rev. C **42**, 640 (1990).

[100] K. H. Ackermann *et al.*, Phys. Rev. Lett. **86**, 402 (2001).

[101] C. Pinkenburg *et al.*, Phys. Rev. Lett. **83**, 1295 (1999).

[102] P. Braun-Munzinger and J. Stachel, Nucl. Phys. A **638**, 3c (1998).

[103] C. Adler *et al.*, Phys. Rev. Lett. **90**, 032301 (2003).

[104] C. Adler *et al.*, Phys. Rev. Lett. **91**, 182301 (2003).

[105] S. Zhang, Y. G. Ma, J. H. Chen, W. B. He, and C. Zhong, Phys. Rev. C **95**, 064904 (2017).

[106] B. H. Alver, C. Gombeaud, M. Luzum and J. Y. Ollitrault, Phys. Rev. C **82**, 034913 (2010).

[107] J. S. Bagla, Reson **14**, 216 (2009).

[108] S. Hawkings, Mon. Not. R. astr. Soc. **142**, 129 (1969).

[109] *see, https* : *//www.nobelprize.org/nobel*$_p$*rizes/physics/laureates/2006/mather* − *slides.pdf*.

[110] B. J. T. Jones and G. Efstathiou, Monthly Notices of the Royal Astronomical Society **189**, 27 (1979).

[111] P. J. E. Peebles, The Astrophysical Journal, **155**, 393 (1969).

[112] Y. G. Ma and W. Q. Sen, Phys. Rev. C **48**, R1492 (1993).

[113] Y. G. Ma and W. Q. Sen, Phys. Rev. C **51**, 3256 (1995).

[114] W. Q. Shen, *et. al.*, Phys. Rev. C **56**, 1996 (1997).

[115] W. Q. Shen, *et al.*, Phys. Rev. C **57**, 1508 (1998).

[116] L. W. Chen, F. S. Zhang and Z. Y. Zhu, Phys. Rev. C **61**, 067601 (2000).

[117] A. Ghatak and S. Lokanathan, *Quantum Mechanics: Theory and Applications*, ISBN:9789350591970, Edition:1, Macmillan Publishers, 2004.

[118] R J Fries, B. M*ü*ller, C Nonaka and S A Bass *Phys. Rev. Lett.* **90**, 202303 (2003).

[119] T. Z. Yan *et al.*, Phys. Lett. B **638**, 50 (2006).

[120] T. Z. Yan *et al.*, Chin. Phys. **16**, 2676 (2007).

[121] Y. G. Ma *et al.*, Nucl. Phys. A **787**, 611c (2007).

[122] T. Z. Yan *et al.*, Chin. Phys. Lett. **26**, No. 11, 112501(2009).

[123] L. Zheng, H. Li, H. Qin, Q. Ye Shou and Z. B. Yin, Eur. Phys. J. A **53**, 124 (2017).

[124] J Adams *et al.*(STAR Collaboration) Nucl. Phys. A **757**, 102 (2005).

[125] K. Adcox *et al.*(PHENIX Collaboration), Nucl. Phys. A **757**, 184 (2005).

[126] C. Q. Guo, C. J. Zhang and J. Xu, Eur. Phys. J. A **53**, 233 (2017).

[127] J. Adams *et al.* (STAR Collaboration), Phys. Rev. C **92**, 062301 (2004).

[128] P. F. Kolb, L. W. Chen, V. Greco and C. M. Ko, Phys. Rev. C **69**, 051901 (2004).

[129] L. W. Chen, C. M. Ko and Z. W. Lin, Phys. Rev. C. **69**, 031901 (2004).

[130] J. J. Molitoris and H. St*ö*cker, Phys. Lett. B **162**, 47 (1985).

[131] P. Danielewicz and G. Odyniec, Phys. Lett. B **157**, 146 (1985).

[132] G. F. Bertsch, W. G. Lynch and M. B. Tsang, Phys. Lett. B **189**, 384 (1987).

[133] J. Aichelin, A. Rosenhauer, G. Peilert, H. St*ö*cker, and W. Greiner, Phys. Rev. Lett. **58**, 1926 (1987).

[134] A. Bonasera and L. P. Csernai, Phys. Rev. Lett. **59**, 630 (1987).

[135] B. Bl*ä*ttel, V. Koch, A. Lang, K. Weber, W. Cassing and U. Mosel, Phys. Rev. C **43**, 2728 (1991).

[136] H. Sorge, Phys. Rev. C **52**, 3291 (1995).

[137] R. J. M. Snellings, H. Sorge, S. A. Voloshin, F. Q. Wang, and N. Xu, Phys. Rev. Lett. **84**, 2803 (2000).

[138] Y. Wang, C. Guo, Q. Li, H. Zhang, Z. Li and W. Trautmann, Phys. Rev. C **89**, 034606 (2014).

[139] D. Krofcheck, W. Bauer, G. M. Crawley, C. Djalali, S. Howden, C. A. Ogilvie, A. V. Molen, G. D. Westfall, W. K. Wilson, R. S. Tickle, and C. Gale, Phys. Rev. Lett. **63**, 2028 (1989).

[140] B. A. Li, Phys. Rev. C **48**, 2415 (1993).

[141] A. Bohnet, N. Ohtsuka, J. Aichelin, R. Linden, A. Faessler, Nucl. Phys. A **494**, 349 (1989).

[142] R. K. Puri, N. Ohtsuka, E. Lehmann, A. Faessler, M. A. Matin, D. T. Khoa, G. Batko and S. W. Huang, Nucl. Phys. A **575**, 733 (1994).

[143] A. D. Sood and R. K. Puri, Eur. Phys. J. A **30**, 571 (2006).

[144] S. Gautam, Journal of Physics: Conference Series **282**, 012022 (2011).

[145] P. Danielewicz *et al.*, Phys. Rev. C **38**, 120 (1988).

[146] C. A. Ogilvie *et al.*, Phys. Rev. C **40**, 2592 (1989).

[147] H. M. Xu, W. G. Lynch, P. Danielewicz and G. F. Bertsch, Phys. Rev. Lett. **65**, 843 (1990).

[148] A. Lang, B. Bl*ä*ttel, W. Cassing, V. Koch, U. Mosel and K. Weber, Z. Phys. A **340**, 287 (1991).

[149] J. Jaenicke, J. Aichelin, H. Ohtsuka, R. Linden and A. Faessler, Nucl. Phys. A **536**, 201 (1992).

[150] Q. Pan and P. Danielewicz, Phys. Rev. Lett. **70**, 2062 (1993).

[151] Q. Pan and P. Danielewicz, Phys. Rev. Lett. **70**, 3523 (1993).

[152] A. Ono, H. Horiuchi and T. Maruyama, Phys. Rev. C **48**, 2946 (1993).

[153] A. Insolia, U. Lombardo, N. G. Sandulescu and A. Bonasera, Phys. Lett. B **334**, 12 (1994).

[154] S. Soff, S. A. Bass, C. Hartnack, H. Stöcker and W. Greiner, Phys. Rev. C **51**, 3320 (1995).

[155] C. Fuchs, T. Gaitanos and H. H. Wolter, Phys. Lett. B **381**, 23 (1996).

[156] P. K. Sahu, A. Hombach, W. Cassing, M. Effenberger and U. Mosel, Nucl. Phys. A **640**, 493 (1998).

[157] A. Insolia, U. Lombardo and N. Sandulescu, Phys. Rev. C **61**, 067902 (2000).

[158] R. Pak, O. Bjarki, S. A. Hannuschke, R. A. Lacey, J. Lauret, W. J. Llope, A. Nadasen, N. T. B. Stone, A. M. Vander Molen and G. D. Westfall, Phys. Rev. C **54**, 2457 (1996).

[159] R. Pak, O. Bjarki, S. A. Hannuschke, R. A. Lacey, J. Lauret, W. J. Llope, A. Nadasen, N. T. B. Stone, A. M. Vander Molen and G. D. Westfall, Phys. Rev. Lett. **78**, 1026 (1997).

[160] S. Voloshin, Phys. Rev. C **55**, R1630 (1997).

[161] H. Stöcker, Phys. Rev. C **25**, 1873 (1982).

[162] B. A. Li and C. M. Ko, Nucl. Phys. A **601**, 457 (1996).

[163] P. Danielewicz, R. A. Lacey, P.-B. Gossiaux, C. Pinkenburg, P. Chung, J. M. Alexander and R. L. McGrath, Phys. Rev. Lett. **81**, 2438 (1998).

[164] A. M. Poskanzer and S. A. Voloshin, Phys. Rev. C **58**, 1671 (1998).

[165] Y. M. Zheng, C. M. Ko, B. A. Li and B. Zhang, Phys. Rev. Lett. **83**, 2534 (1999).

[166] H. Liu, S. Panitkin and N. Xu, Phys. Rev. C. **59**, 348 (1999).

[167] P. K. Sahu, N. Otuka, A. Ohnishi and M. Baldo, Pramana Journal of Physics **60**, 1107 (2003).

[168] R. A. Lacey, Nucl. Phys. A **774**, 199 (2006).

[169] S. Kumar, S. Kumar and R. K. Puri, Phys. Rev. C **81**, 014611 (2010).

[170] J. Wang, Y. G. Ma, G. Q. Zhang and W. Q. Shen, Phys. Rev. C **90**, 054601 (2014).

[171] H. J. Xu, Z. Li and H. Song, Phys. Rev. C **93**, 064905 (2016).

[172] A. Jaiswal and P. P. Bhaduri, Phys. Rev. C **97**, 044909 (2018).

[173] J. Auvinen and H. Petersen, arXiv:1310.1764v1[nucl-th] (2013).

[174] B. Alver and G. Roland, Phys. Rev. C **81**, 054905 (2010).

[175] H. Petersen, G. Y. Qin, S. A. Bass and B. Mller, Phys. Rev. C **82**, 041901(R) (2010).

[176] D. Teaney and L. Yan, Phys. Rev. C **83**, 064904 (2011).

[177] P. F. Kolb, Phys. Rev. C **68**, 031902 (2003).

[178] J. Xu and C. M. Ko, Phys. Rev. C **83**, 021903(R) (2011).

[179] J. Xu and C. M. Ko, Phys. Rev. C **84**, 014903 (2011).

[180] L. X. Han, Phys. Rev. C **84**, 064907 (2011).

[181] S. Goyal, Phys. Rev. C **83**, 047604 (2011).

[182] V. Kaur and S. Kumar, Pramana Journal of Physics **77**, 1095 (2011).

[183] V. Kaur, S. Kumar and R. K. Puri, Phys. Lett. B **697**, 512 (2011).

[184] J. Gosset *et al.*, Phys. Rev. C **16**, 629 (1977).

[185] J. Gosset *et al.*, Phys. Rev. Lett. **62**, 1251 (1989).

[186] M. Gyulassy, K. A. Frankel and H. Stöcker, Phys. Lett. B **110**, 185 (1982).

[187] R. L. Ray (STAR Collaboration), Nucl. Phys. A **715**, 45 (2003).

[188] J. Lukasik *et al.*(INDRA AND ALADIN Collaboration), Prog. in Part. and Nucl. Phys. **53**, 77 (2004).

[189] J. Ritman (FOPI collaboration), Nuclear Physics 13 (Proc. Suppl.) **44**, 708 (1995).

[190] M. Merschmeyer, Ph.D. Thesis, University of Heidelberg, Germany, 2004.

[191] J. W. Harris *et al.*, Nucl. Phys. A **471** 241 (1987).

[192] W. M. Zhang *et al.*, Phys. Rev. C **42**, R491 (1990).

[193] V. Ramillien *et al.*(FOPI Collaboration), Nucl. Phys. A **587**, 802 (1995).

[194] H. Appelshäuser *et al.*(NA49 Collaboration), Phys. Rev. Lett. **80**, 4136 (1998).

[195] A. Andronic *et al.*(FOPI Collaboration), Phys. Rev. C. **67**, 034907 (2003).

[196] B. Hong (FOPI Collaboration), Phys. Rev. C **71**, (2005) 034902.

[197] D. Krofcheck *et al.*, Phys. Lett. C **43**, 350 (1991).

[198] M. J. Huang *et al.*, Phys. Rev. Lett. **77**, 3739 (1996).

[199] Y. H. Zhi *et al.*, Nucl. Phys. A **598**, 248 (1996).

[200] R. Popescu *et al.*, Phys. Lett. B **331**, 285 (1994).

[201] A. Andronic *et al.*, Eur. Phys. Jour. A **30**, 31 (2006).

[202] P. Chung *et al.* (E895 Collaboration), Phys. Rev. Lett. **86**, 2533 (2001).

[203] J. L. Klay *et al.* (E895 Collaboration), Phys. Rev. Lett. **88**, 102301 (2002).

[204] P. Crochet, *et al.*, Nucl. Phys. A **624**, 755 (1997).

[205] N. Bastid *et al.*, Nucl. Phys. A **622**, 573 (1997).

[206] W. Reisdorf, H. G. Ritter, Annu. Rev. Nucl. Part. Sci. **47**, 663 (1997).

[207] W. Reisdorf *et al.*, Phys. Rev. Lett. **92**, 232301 (2004).

[208] W. Reisdorf *et al.*, Phys. Lett. B **595**, 118 (2004).

[209] C. Alt *et al.*, (NA49 Collaboration), Phys. Rev. C **68**, 034903 (2003).

[210] S. Esumi (PHENIX Collaboration), Nucl. Phys. A **715**, 599 (2003).

[211] K. Filimonov *et al.*, (CERES/NA45 Collaboration), arXiv:nuclex/0109017.

[212] J. Slivova (CERES/NA45 Collaboration), Nucl. Phys. A **715**, 615 (2003).

[213] S. I. Esumi, J. Slivova, and J. Milosevic (CERES Collaboration) SFIN, year XV, Series A:77 Conferences, No. A2 (2002).

[214] S. Manly *et al.* (PHOBOS Collaboration), Nucl. Phys. A **715**, 611 (2003).

[215] J. Y. Ollitrault, Phys. Rev. D **48**, 1132 (1993).

[216] Y. Leifels *et al.*, Phys. Rev. Lett. **71**, 963 (1993).

[217] A. Kugler *et al.*, Phys. Lett. B **335**, 319 (1994).

[218] D. Brill *et al.*, Z. Phys. A **357**, 207 (1997).

[219] J. Lukasik, W. Trautmann, for the INDRA and ALADIN Collaborations, arXiv:0708.2821v1 [nucl-ex],2007.

[220] J. Lukasik, *et al.*, International workshop on multi-fragmentation and related topics, 47 Nov., IWM2007.

[221] J. Lukasik *et al.*, Acta Phys. Hung. A **25**, 229 (2006).

[222] K. Aamodt *et al.* (ALICE collaboration), Phys. Rev. Lett. **107**, 032301 (2011) and references therein.

[223] M. Krzewicki (ALICE Collaboration), J. Phys. G: Nucl. Part. Phys. **38**, 124047 (2011).

[224] ALICE collaboration, Phys. Lett. B **708**, 249 (2012).

[225] Y. Bai (STAR collaboration, J. Phys. G: Nucl. Part. Phys. **34**, S903 (2007).

[226] P. Soren, J. Phys. G: Nucl. Part. Phys. **38**, 124029 (2011).

[227] B. A. Li and S. J. Yennello, Phys. Rev. C **52**, R1746 (1995).

[228] B. A. Li, Z. Ren, C. M. Ko, and S. J. Yennello, Phys. Rev. Lett. **76**, 4492 (1996).

[229] H. Feldmeier, Nucl. Phys. A **515**, 147 (1990).

[230] H. Feldmeier, K. Bieler and J. Schnack, Nucl. Phys. A **586**, 493 (1995).

[231] H. Feldmeier and J. Schnack, Prog. Part. Nucl. Phys. **39**, 393 (1997).

[232] *see*, *http* : *//www.int.washington.edu/PROGRAMS/frib10/talks/Neff.pdf*.

[233] H. Horiuchi, Nucl. Phys. A 522, 257c (1991).

[234] H. Horiuchi, T. Maruyama, A. Ohnishi and S. Yamaguchi, Preprint, KUNS **1028**, Kyoto University.

[235] C. Coriano, R. Parwani and H. Yamagishi, Nucl. Phys. A **522**, 591 (1991).

[236] N. Wang, Z. Li and X. Wu, Phys. Rev. C **65**, 064608 (2002).

[237] Z. Kohley, G. Christian, T. Baumann, P. A. DeYoung, J. E. Finck, N. Frank, M. Jones, J. K. Smith, J. Snyder, A. Spyrou and M. Thoennessen, Phys. Rev. C **88**, 041601(R) (2013).

[238] G. F. Bertsch, H. Kruse and S. D. Gupta, Phys. Rev. C **29**, R673 (1984).

[239] L. Wilet, E. M. Henley, M. Kraft, A. D. Mackellar, Nucl. Phys. A **282**, 341 (1977).

[240] A. Ono, H. Horiuchi, T. Maruyama, and A. Ohnishi, Phys. Rev. Lett. **68**, 2898 (1992).

[241] A. Ono, H. Horiuchi, T. Maruyama, A. Ohnishi, Prog. Theo. Phys. **87**, 1185 (1992).

[242] A. Ono and H. Horiuchi, Phys. Rev. C. **51**, 299 (1995).

[243] A. Ono and H. Horiuchi, Prog. in Part. and Nucl. Phys. **53**, 501 (2004).

[244] N. Wang, Z. Li, X. Wu, J. Tian, Y. Zhang and M. Liu, Phys. Rev. C **69**, 034608 (2004).

[245] J. Bartel, P. Quentin, M. Brack, C. Guet and H. B. Hkansson, Nucl. Phys. A **386**, 79 (1982).

[246] E. Chabanat, P. Bonche, P. Haensel, J. Meyer and R. Schaeffer, Nucl. Phys. A **627**, 710 (1997).

[247] E. Chabanat, P. Bonche, P. Haensel, J. Meyer and R. Schaeffer, Nucl. Phys. A **635**, 231 (1998).

[248] Y. Zhang, P. Danielewicz, M. Famiano, Z. Li, W. G. Lynch and M. B. Tsang, Phys. Lett. B **664**, 145 (2008).

[249] L. W. Chen and C. M. Ko, Phys. Lett. B **634**, 205 (2006).

[250] S. Das Gupta et. al., Phys. Rep. **160**, 189 (1988).

[251] W. D. Tian et. al., Int. Jour. of Mod. Phys. E **17**, 1705 (2008).

[252] J. Aichelin, Phys. Rep. **202**, 233 (1991).

[253] C. Hartnack, H. Oeschler, J. Aichelin, Phys. Rev. Lett. **96**, 012302 (2006).

[254] C. Fuchs, A. Faessler, E. Zabrodin, Y.M. Zheng, Phys. Rev. Lett. **86**, 1974 (2001).

[255] H. Yukawa, Phys. Rev. **76**, 300 (1949).

[256] H. Yukawa, Nobel Lecture, Dec. 12 (1949).

[257] L. G. Arnold *et al.*, Phys. Rev. C **25**, 936 (1982).

[258] G. Passatore, Nucl. Phys. A **95**, 694 (1967).

[259] P. Bonche, S. Koonin, and J. W. Negele, Phys. Rev. C **13**, 1226 (1976).

[260] R. Cusson and J. Maruhn, Phys. Rev. Lett. **36**, 1166 (1976).

[261] S. A. Bass, C. Hartnack, H. Stöcker, and W. Greiner, Phys. Rev. C **51**, 3343 (1995).

[262] B. J. VerWest and R. A. Arndt, Phys. Rev. C **25**, 1979 (1982).

[263] H. Kruse, B. V. Jacak, and H. Stöcker, Phys. Rev. Lett. **54**, 289 (1985).

[264] J. J. Molitoris and H. Stöcker, Phys. Rev. C **32**, R346 (1985).

[265] P. Danielewicz and G. F. Bertsch, Nucl. Phys. A **533**, 712 (1991).

[266] S. Huber and J. Aichelin, Nucl. Phys. A **573**, 587 (1994).

[267] S. R. Souza, L. de Paula, S. Leray, J. Nemeth, C. Ngo and H. Ngo, Nucl. Phys. A **571**, 159 (1994).

[268] R. K. Puri and J. Aichelin, Journal of Computational Physics **162**, 245 (2000).

[269] S. Kumar and R. K. Puri, Phys. Rev. C **58**, 320 (1998).

[270] M. B. Tsang *et al.*, Phys. Rev. Lett. **57**, 559 (1986).

[271] A. D. Sood, R. K. Puri, J. Aichelin, Phys. Lett. B **594**, 260 (2004).

[272] Y. Zhang, Z. Li, C. Zhou and M. B. Tsang, Phys. Rev. C **85**, 051602(R) (2012).

[273] S. Kaur and R. K. Puri, Phys. Rev. C **87**, 014620 (2013).

[274] R. Bansal, S. Gautam, R. K. Puri, and J. Aichelin, Phys. Rev. C. **87**, 061602(R) (2013).

[275] R. Bansal, S. Gautam and R. K. Puri, Jour. Phys. G **41**, 035103 (2014).

[276] J. Ollitrault, Phys. Rev. D **46**, 229 (1992).

[277] G. Peilert, H. Stöcker and W. Greiner, Rep. Prog. Phys. **57**, 533(1994).

[278] K. S. Vinayak and S. Kumar, Eur. Phys. J. A **47**, 144 (2012).

[279] A. Jain and S. Kumar, Phys. Scrp. **89**, 035301 (2014).

[280] P. Rossotto, M. D. Cozma, A. Le Fvre, Y. Leifels, R. Lemmon, Q. Li, J. ukasik and W. Trautmann, Eur. Phys. J. A **50**, 38 (2014).

[281] P. Rossotto, P. Z. Wu, M. Zoric, M. Chartier, Y. Leifels, R. C. Lemmon, Q. Li, J. ukasik, A. Pagano, P. Pawowski, W. Trautmann, Phys. Lett. B. **697**, 471 (2011).

[282] H. G. Ritter *et al.*, J. Phys. G **41**, 124002 (2014).

[283] A. Sharma, A. Bharti, S. Gautam and R. K. Puri, Nucl. Phys. A **945**, 95 (2016).

[284] R. K. Puri, C. Hartnack and J. Aichelin, Phys. Rev. C **54**, R28 (1996).

[285] Y. K. Vermani and R. K. Puri, Eur. Lett. **85**, 62001 (2009).

[286] Y. K. Vermani and R. K. Puri, J. Phys. G **37**, 015105 (2010)

[287] A. D. Sood and R. K. Puri, Phys. Rev. C **79**, 064618 (2009).

[288] H. Y. Zhang *et al.*, J. Phys. G **28**, 2397 (2002).

[289] C. Pinkenburg, *et al.*, Phys. Rev. Lett. **83**, 77 (1999).

[290] H. Y. Zhang, W. Q. Shen, Y. G. Ma, X. Z. Cai, D. Q. Fang, L. P. Yu, C. Zhong and Y. B. Wei, Eur. Phys. J. A. **15**, 399 (2002).

[291] C. Hartnack, H. Oeschler, Y. Leifels, E. L. Bratkovskaya and J. Aichelin, Phys. Rep. **510**, 119 (2012).

[292] *see*, *http* : *//www.astro.cz/apod/ap080721.html* : *GeminiObservatory*.

[293] G. Kaur, N. Grover, K. Sandhu and M. K. Sharma, Nucl. Phys. A **927**, 232 (2014).

[294] A. Jain and S. Kumar, Nucl. Phys. A **876**, 109 (2012).

[295] C. Hartnack, H. Oeschler and J. Aichelin, Phys. Rev. Lett. **90**, 102302 (2003).

[296] C. Hartnack, H. Oeschler and J. Aichelin, Jour. Phys. G **35**, 044021 (2008).

[297] H. Stöcker and W. Greiner, Phys. Rep. **137**, 277 (1986).

[298] J. Pan, S. Das Gupta and M. Grant, Phys. Rev. Lett. **80**, 1182(1998).

[299] C. Hartnack, H. Oeschler, Y. Leifels, E. L. Bratkovskaya and J. Aichelin *Nucl. Phys. A* **914** 392 (2013).

[300] J. Aichelin *et al. Relativistic Heavy Ion Physics* **23** (Germany:Springer) *Edition 1*(2010).

[301] S. A. Bass *et al.*, Prog. Part. Nucl. Phys. **41**, 225 (1998).

[302] R. Chatterjee, E. S. Frodermann, U. W. Heinz, and D. K. Srivastava, Phys. Rev. Lett. **96**, 202302 (2006).

[303] D. Molnar and S. Voloshin, Phys. Rev. Lett. **91**, 092301 (2003).

[304] A. K. Chaudhary, Phys. Rev. C **81**, 044905 (2010).

[305] V. P. Konchakovski *et al.*, Phys. Rev. C **83**, 044922 (2012).

[306] L. Ma *et al.*, Phys. Rev. C **89**, 044907 (2014).

[307] J. Tian *et al.*, Phys. Rev. C **79**, 067901 (2009).

[308] M. He, R. J. Fries and R. Rapp, Phys. Rev. C. **82**, 034907 (2010).